AD A137 047 FRACTURE LONGEVITY (FATIGUE) DYNAMICS AND AEROELASTICITY OF COMPOSITE STR..(U) MASSACHUSETTS INST OF TECH CAMBRIDGE TECHNOLOGY LAB FOR ADVAN..

1/2

UNCLASSIFIED P A LAGACE ET AL. JUN 83 TELAC-83-11 F/G 11/4 NL

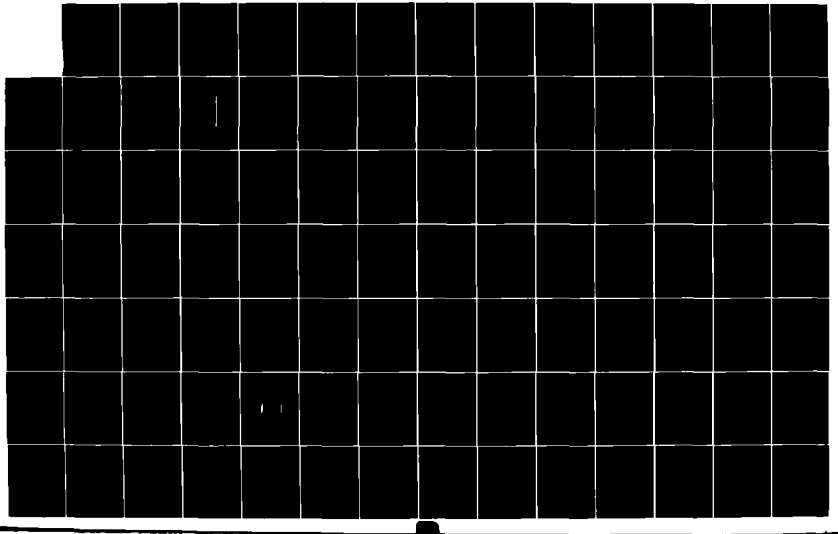

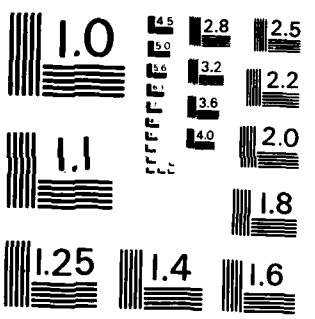

(12)

AFOSR-TR- 84-0001

AD A137047

FRACTURE, LONGEVITY (FATIGUE), DYNAMICS, AND AEROELASTICITY OF COMPOSITE STRUCTURES

Paul A. Lagace, James W. Mar, and John Dugundji

Technology Laboratory for Advanced Composites
Massachusetts Institute of Technology
77 Massachusetts Avenue
Cambridge, Massachusetts 02139

JUNE 1983

Final Report for Period January 1982 - December 1982

Grant No. AFOSR 82-0071

UNCLASSIFIED

SECURITY CLASSIFICATION OF THIS PAGE (When Data Entered)

REPORT DOCUMENTATION PAGE		READ INSTRUCTIONS BEFORE COMPLETING FORM
1. REPORT NUMBER AFOSR-TR- 84-0001	2. GOVT ACCESSION NO.	3. RECIPIENT'S CATALOG NUMBER
4. TITLE (and Subtitle) FRACTURE, LONGEVITY (FATIGUE), DYNAMICS, AND AEROELASTICITY OF COMPOSITE STRUCTURES		5. TYPE OF REPORT & PERIOD COVERED FINAL: 01 JAN 1982-31 DEC 1982 6. PERFORMING ORG. REPORT NUMBER TELAC 83-11
7. AUTHOR(s) Paul A Lagace, James W Mar, and John Dugundji		8. CONTRACT OR GRANT NUMBER(s) AFOSR-82-0071
9. PERFORMING ORGANIZATION NAME AND ADDRESS Technology Laboratory for Advanced Composites Massachusetts Institute of Technology Cambridge, Massachusetts 02139		10. PROGRAM ELEMENT, PROJECT, TASK AREA & WORK UNIT NUMBERS 61102F 2307/B1
11. CONTROLLING OFFICE NAME AND ADDRESS AFOSR/NA Bolling AFB DC 20332		12. REPORT DATE June 1983 13. NUMBER OF PAGES 150
14. MONITORING AGENCY NAME & ADDRESS(if different from Controlling Office)		15. SECURITY CLASS. (of this report) UNCLASSIFIED 15a. DECLASSIFICATION/DOWNGRADING SCHEDULE

16. DISTRIBUTION STATEMENT (of this Report)

Approved for public release; distribution unlimited

17. DISTRIBUTION STATEMENT (of the abstract entered in Block 20, if different from Report)

18. SUPPLEMENTARY NOTES

19. KEY WORDS (Continue on reverse side if necessary and identify by block number)

graphite/epoxy	damage growth	cyclic loads
fabric	delamination	flutter
fracture	splitting	divergence
notch sensitivity	tension	
nonlinear stress-strain	compression	

20. ABSTRACT (Continue on reverse side if necessary and identify by block number)

The results of several investigations into the fracture, longevity (fatigue), dynamics, and aeroelasticity of composite materials are reported. The experimental work was conducted using Hercules graphite/epoxy prepreg in two forms: AS1/3501-6 unidirectional tape and A370-5H/3501-6 fabric. The topics discussed include unnotched tensile fracture, sensitivity to notches under tensile loading, nonlinear stress-strain behavior, compression specimen development, damage growth under cyclic load, and the flutter and divergence of graphite/epoxy wings.

DD FORM 1 JAN 73 1473 EDITION OF 1 NOV 65 IS OBSOLETE

UNCLASSIFIED

SECURITY CLASSIFICATION OF THIS PAGE (When Data Entered)

FOREWORD

This report describes work done at the Technology Laboratory for Advanced Composites (TELAC) at the Massachusetts Institute of Technology for the Air Force Office of Scientific Research under contract AFOSR 82-0071. Dr. Anthony Amos was the contract monitor.

The work reported herein was performed during the period 1 January 1982 to 31 December 1982. The work represents the efforts of several graduate and undergraduate students under the direction of the faculty in the laboratory and is reported as such.

TABLE OF CONTENTS

NOMENCLATURE

a	half-notch length
A	1. parameter in Mar-Lin equation 2. parameter in split growth equation
B	parameter in split growth equation
E_L	longitudinal modulus
E_T	transverse modulus
F_c^L	longitudinal compressive ultimate strength
F_c^T	transverse compressive ultimate strength
F_t^L	longitudinal tensile ultimate strength
F_t^T	transverse tensile ultimate strength
ft/sec	foot per second
G_{LT}	shear modulus
GPa	Giga (10^9) pascal
H_c	parameter in Mar-Lin equation--composite fracture toughness
Hz	hertz
in	inch
ksi	thousand pounds per square inch
m	parameter in Mar-Lin equation equal to singularity at bimaterial interface
m/s	meter/second
mm	millimeter
MPa	Mega (10^6) pascal
N	cycles
N_o	cycle for split initiation

NOMENCLATURE

P	applied load
R	correlation coefficient
w	width
$\frac{da}{dn}$	split growth rate
ϵ	strain
Λ	sweep angle
σ	stress
σ_f	fracture stress
σ_o	unnotched fracture stress
σ_{zz}	interlaminar normal stress
θ	ply angle
ν_{LT}	major Poisson's ratio
ν_{TL}	minor Poisson's ratio
"	inch
°	degrees

LIST OF FIGURES

LIST OF FIGURES

LIST OF FIGURES

LIST OF TABLES

LIST OF TABLES

1. INTRODUCTION

The Technology Laboratory for Advanced Composites (TELAC) of the Department of Aeronautics and Astronautics at M.I.T. has developed facilities in recent years, with significant support from the Air Force Office of Scientific Research (AFOSR) to examine the properties of composite materials and their structures. During the past year, the students and faculty of TELAC have conducted research in a number of problem areas in a continuing effort to understand the fracture, longevity, dynamics and aeroelasticity of composite structures. Both graduate and undergraduate students have been involved in this work which involves the manufacture and testing of specimens in the facilities of the laboratory as well as the use of analytical tools in reviewing the experimental data.

This work has been supported on a continuing basis by the Air Force Office of Scientific Research. The present report will describe work which has been concluded during the past year, work which has been conducted during the past year, and work which was initiated during the past year and is continuing under AFOSR contract #F49620-83-K-0015 during the current year. Several of the projects which have been completed are fully reported in student theses which are referenced here. A summary of these activites are presented and interested personnel may refer to the individual thesis for a more thorough

description. In addition, a list of all reports generated under this contract during the contract year are listed in Appendix B.

2. FRACTURE

The work in fracture at TELAC has been directed at finding methods by which the fracture stress of an arbitrary layup may be predicted for various loading conditions. As a step in the process, the great majority of work has looked at the behavior of the Hercules AS1/3501-6 graphite/epoxy material system. Hundreds of specimens, both unnotched and with holes, have been tested under static tension to observe fracture modes and stresses. The conclusion of a large sector of this program is reported herein. The work on notched specimens has also branched out to include the case of slits in specimens and the sensitivity of the composite to these notches. During the past year, work was also begun on examining a woven fabric graphite/epoxy prepreg also manufactured by Hercules: A370-5H/3501-6. A comparison of the behavior of the fabric system with the unidirectional prepreg tape is being made and is also reported here.

2.1 Fracture of Unnotched Tensile Coupons

A considerable amount of work has been conducted at TELAC examining the fracture modes and stresses of coupons loaded in uniaxial tension. This work has been conducted on laminates consisting of four to eight plies. These experiments have con-

sidered the effects which lamination angle and stacking sequence have on the fracture characteristics of composites. In these experiments, the material investigated was Hercules AS1/3501-6 graphite/epoxy unidirectional tape. Some of this work was earlier reported by Garcia [1,2], McManus [3], and Soderquist [4]. However the great majority of this data has been accumulated by Lagace and is summarized and analyzed in his doctoral thesis [5].

The overriding objective of this work is to establish the methodology by which the fracture stress of an arbitrary laminate can be predicted. It is therefore necessary to understand the phenomena involved. In this investigation, five different laminate "families" (or stacking arrangements) were used: [θx8]*, [+-θ]s, [+-θ/0]s, [0/+-θ]s, and [+θ/0/-θ]s. The lamination angle was varied in each family to include the values of 0°, 15°, 30°, 45°, 60°, 75°, and 90°. Additional laminates tested by the previously mentioned authors are also included in this discussion. These laminates are [+-5/0]s, [0/+-5]s, [+-10/0]s, [0/+-10]s, [+-20/0]s, [+-25/0]s, [+-35/0]s, [10x8], [20x8], and [40x8]. Five specimens of each laminate were

---

* In order to simplify the reporting process, the notation "x8" replaces a subscript 8 to show number of plies. Thus [θx8] is the same as [θ_8].

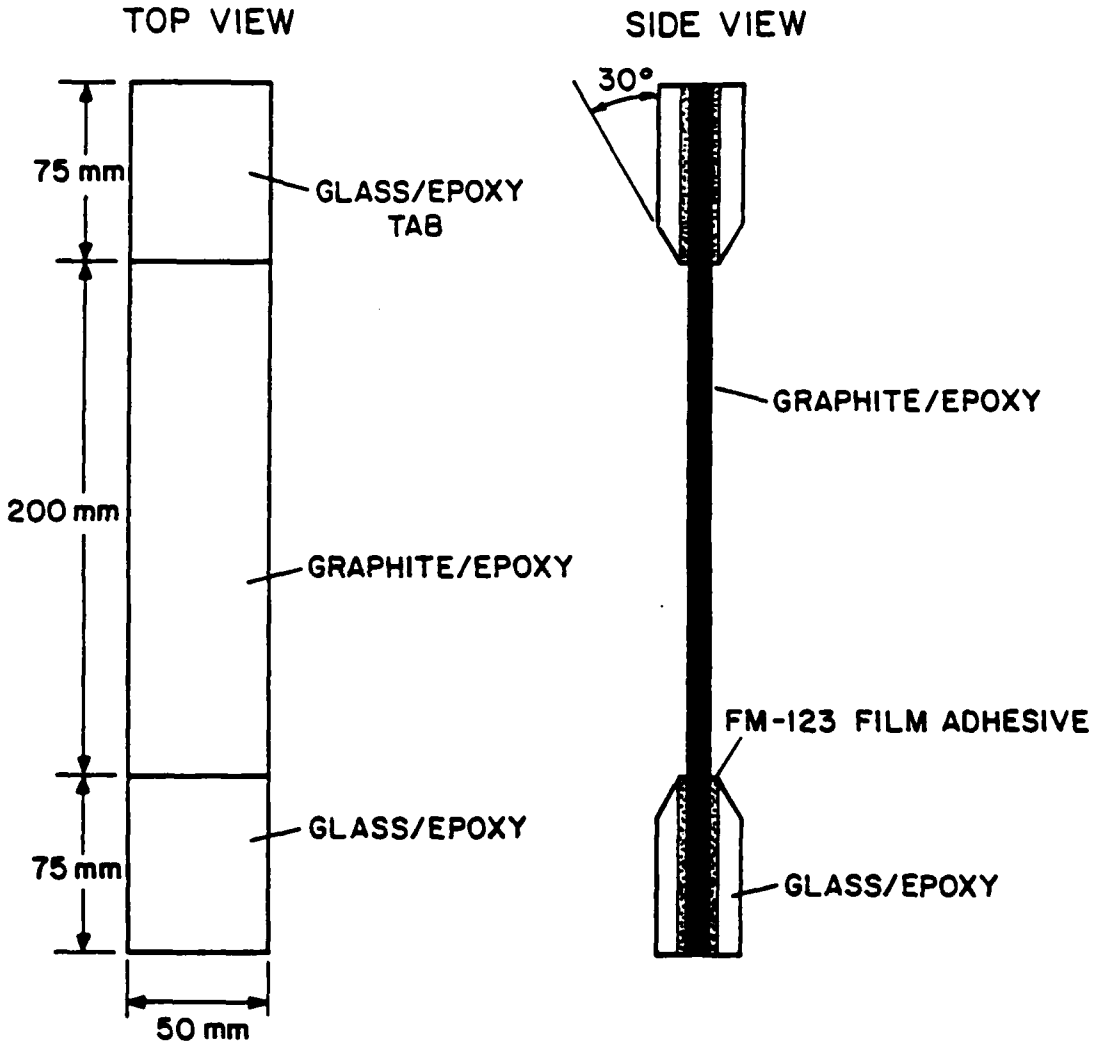

FIGURE 1 PHYSICAL CHARACTERISTICS OF THE COUPON SPECIMEN

TABLE 1

LAMINATES TESTED IN UNNOTCHED CONDITION

Laminate Family:	$[\theta_8]$	$[\pm\theta]_s$	$[\pm\theta/0]_s$	$[0/\pm\theta]_s$	$[+\theta/0/-\theta]_s$
			$[\pm5/0]_s$	$[0/\pm5]_s$	
	$[10_8]$		$[\pm10/0]_s$	$[0/+10]_s$	
	$[15_8]$	$[\pm15_s]$	$[\pm15/0]_s$	$[0/\pm15]_s$	$[+15/0/-15]_s$
	$[20_8]$		$[\pm20/0]_s$		
			$[\pm25/0]_s$		
	$[30_8]$	$[\pm30]_s$	$[\pm30/0]_s$	$[0/\pm30]_s$	$[+30/0/-30]_s$
			$[\pm35/0]_s$		
	$[40_8]$				
	$[45_8]$	$[\pm45]_s$	$[\pm45/0]_s$	$[0/\pm45]_s$	$[+45/0/-45]_s$
	$[60_8]$	$[\pm60]_s$	$[\pm60/0]_s$	$[0/\pm60]_s$	$[+60/0/-60]_s$
	$[75_8]$	$[\pm75]_s$	$[\pm75/0]_s$	$[0/\pm75]_s$	$[+75/0/-75]_s$
	$[90_8]$	$[90_4]$	$[90_2/0]_s$	$[0/90_2]_s$	$[90/0/90]_s$

(5 specimens of each laminate)

tested. The typical specimen is shown in Figure 1. A summary of the specimens tested is given in Table 1.

All testing was accomplished on an MTS 810 Materials Test System with the aid of hydraulic grips. The specimens were loaded at a constant stroke rate of 1 mm/minute yielding a strain rate of approximately 5000 microstrain/minute. Load and strain data were taken using a PDP-11/34 computer. Strain was measured by two gages as shown in Figure 2. Fracture loads were recorded after each test and a photograph was taken of each specimen after fracture. The specimens were also monitored by ear throughout the test for any noises indicative of damage or fracture.

The stress quadratic interaction criterion proposed by Tsai and Wu [6] was used in an attempt to correlate the data. Plots of the experimental fracture stress versus the stress predicted using the interaction criterion are shown in Figure 3 for the [θx8] laminate family, in Figure 4 for the [+-θ]s laminate family, and in Figure 5 for the [+-θ/0]s, [0/+-θ]s, and [+θ/0/-θ]s laminate families. Examination of Figure 3 shows that the criterion predicts the fracture stress extremely well for the unidirectional off-axis specimens. The data in Figure 4 shows that the fracture stresses for the [+-θ]s laminates lie on the prediction for angles of 30° and greater but that the [+-15]s laminate fracture stresses fall significantly below the prediction.

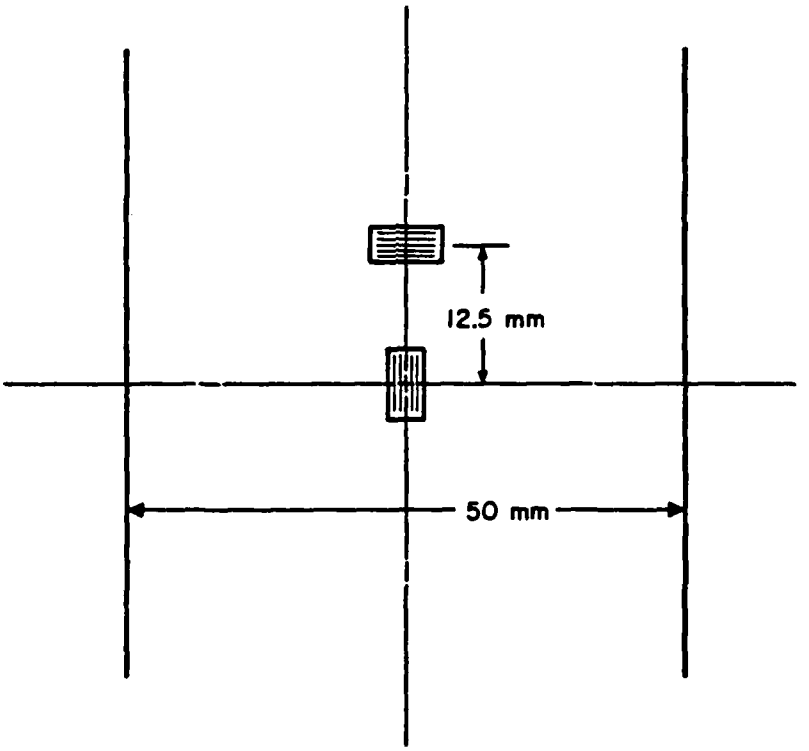

FIGURE 2 STRAIN GAGE PLACEMENT FOR UNFLAWED SPECIMENS

TABLE 2

FRACTURE STRESSES FOR UNNOTCHED SPECIMENS

(All Values in MPa)

Lamination Angle = θ	Laminate				
	$[\theta_8]$	$[\pm\theta]_s$	$[\pm\theta/0]_s$	$[0/\pm\theta]_s$	$[+\theta/0/-\theta]_s$
5°	--	--	1197 (9.8%)	1405 (5.0%)	--
10°	462 (2.5%)	--	1052 (4.5%)	1200 (3.5%)	--
15°	267 (15.2%)	889 (6.9%)	998 (7.3%)	1083 (6.1%)	999 (8.1%)
20°	213 (19.2%)	--	1064 (1.1%)	--	--
25°	--	--	1062 (3.9%)	--	--
30°	136 (13.8%)	527 (1.1%)	855 (5.1%)	945 (6.2%)	918 (2.6%)
35°	--	--	835 (5.3%)	--	--
40°	115 (11.7%)	--	--	--	--
45°	96.5 (7.7%)	148 (9.3%)	732 (7.0%)	787 (3.2%)	730 (13.6%)
60°	69.4 (5.7%)	74.6 (2.9%)	698 (3.9%)	814 (4.3%)	587 (16.2%)
75°	54.3 (6.8%)	38.0 (8.4%)	672 (4.1%)	733 (4.8%)	549 (7.0%)
90°	49.4 (18.0%)	53.9 (4.6%)	679 (8.9%)	732 (5.5%)	561 (5.2%)

Mean (Coefficient of Variation)

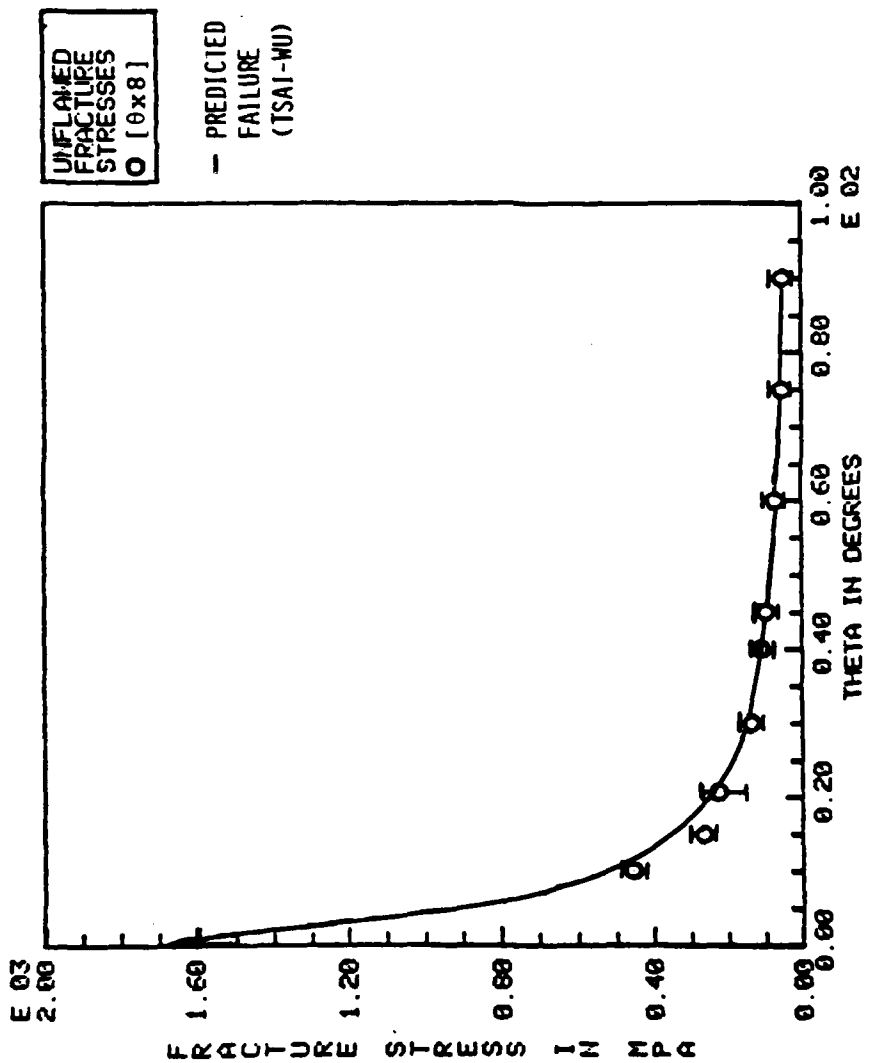

FIGURE 3 EXPERIMENTAL AND PREDICTED (VIA TSAI-WU) UNFLAWED FRACTURE STRESS VERSUS LAMINATION ANGLE FOR THE $[\theta_8]$ LAMINATE FAMILY

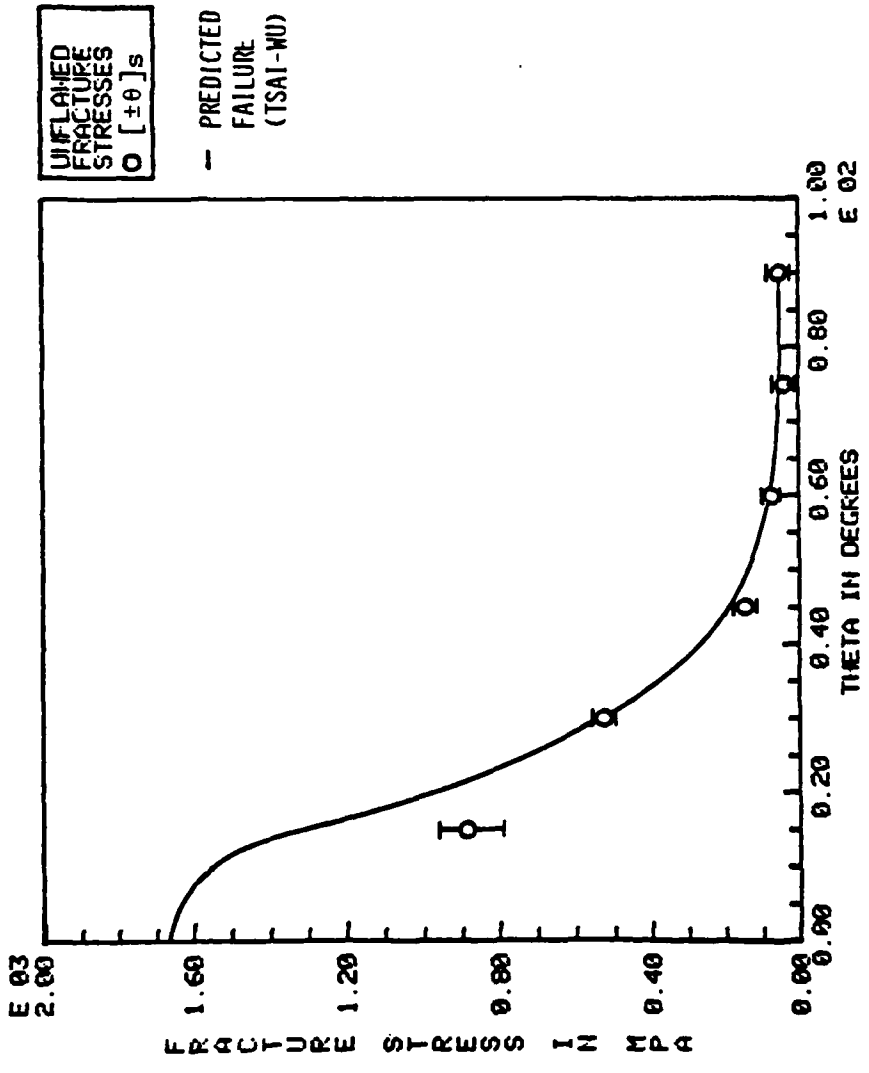

FIGURE 4 EXPERIMENTAL AND PREDICTED (VIA TSAI-WU) UNFLAWED FRACTURE STRESS VERSUS LAMINATION ANGLE FOR THE $[\pm\theta]_s$ LAMINATE FAMILY

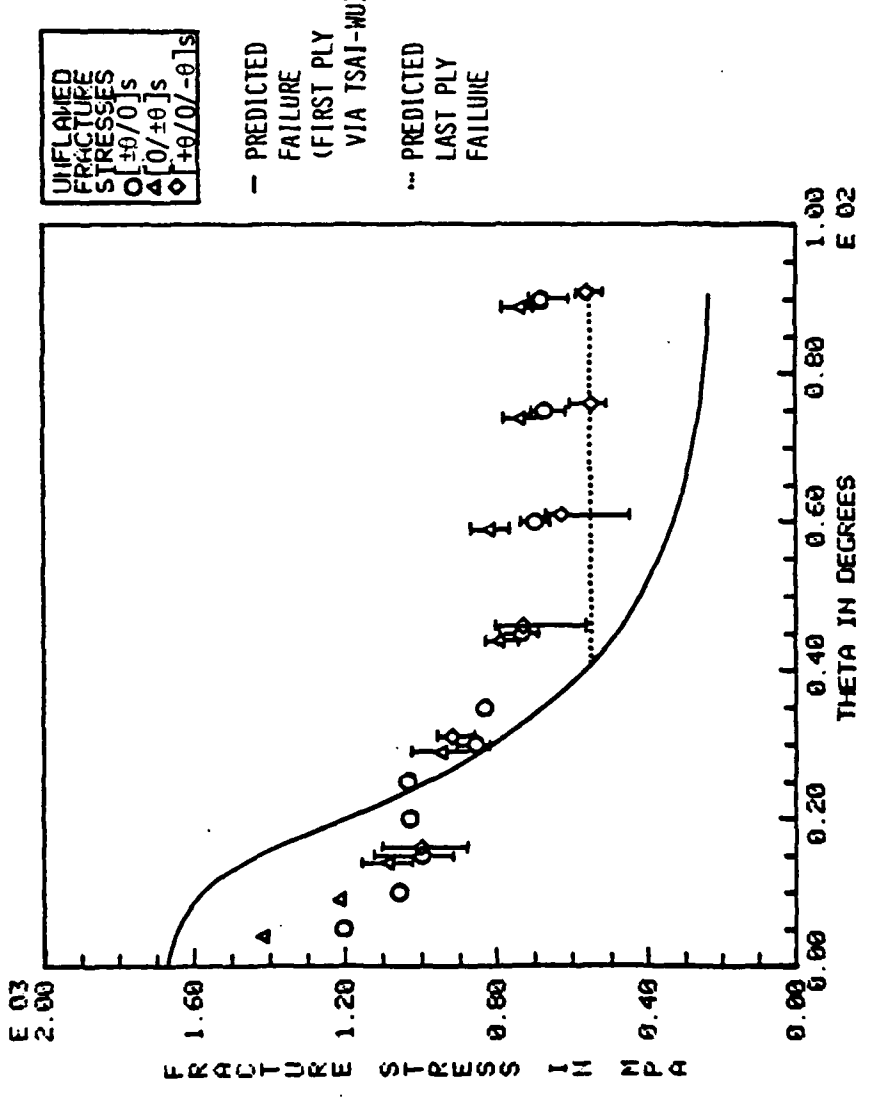

FIGURE 5 EXPERIMENTAL AND PREDICTED (VIA TSAI-WU) UNFLAWED FRACTURE STRESS VERSUS LAMINATION ANGLE FOR THE $[\pm\theta/0]_s$, $[0/\pm\theta]_s$ AND $[+\theta/0/-\theta]_s$ LAMINATE FAMILIES

The data in Figure 5 for the three different stacking sequences of the six-ply laminates can be broken into two subgroups for purposes of discussion. One group consists of laminates with lamination angles of 45° and lower, the other group consists of the laminates with lamination angles greater than 45°.

For the first group of laminates, the stress-strain curve is virtually linear-to-failure and any audible clicks emanating from the specimen during the test were confined to a short period just before final failure. For these laminates, the data does not follow the prediction of the Tsai-Wu criterion and there is a distinct difference in fracture stresses for changes in stacking sequence. For all the cases of θ less than 45°, the [0/+-θ]s stacking sequence yields the highest fracture stress. The [+-θ/0]s and [+θ/0/-θ]s laminates have fracture stresses which are 7% to 15% below that of the corresponding [0/+-θ]s laminates. These differences in fracture stresses decrease as the lamination angle θ increases.

Close consideration of the observed post-mortem fracture modes show that all the specimens of the [0/+-θ]s family (with θ of 45° or less) fail in an "in-plane" fashion. That is there is virtually no delamination. Any delamination in these laminates is limited to delamination and splitting of the top unidirectional ply in the immediate vicinity of the fracture and can be classified as "secondary". This is in marked con-

trast to the post-mortem fracture modes of the specimens of the [+-θ/0]s and [+θ/0/-θ]s laminate families. These specimens show delamination as a "primary" fracture modes.

It is known that the delaminations which occur in laminated materials are caused by interlaminar stresses which arise at free edges due to Poisson's mismatch. Therefore, calculations of the interlaminar stress states at the free edges of the laminates used in this investigation were performed using the solution procedure developed by Bar-Yoseph and Pian [7]. This solution method is based on a combination of the Rayleigh-Ritz method and matched asymptotic expansion.

These calculations were used to determine the ply interfaces where a tensile through-the-thickness interlaminar stress, σ_{zz}, occurred at the free edge. It is such a stress which can cause delamination of the plies under tensile loading as illustrated in Figure 6. Results of these calculations are reported in Tables 3-6. The interfaces with calculated normal interlaminar stress values which are positive (tensile) are identified as possible interfaces for delamination. These interfaces are also listed in Tables 3-6 along with the actual observed post-mortem fracture modes of the laminates. The results show that the laminates with a calculated compressive value of interlaminar normal stress at the free edge of a ply interface do not delaminate and therefore fracture "in-plane". The laminates with tensile values of these stresses generally

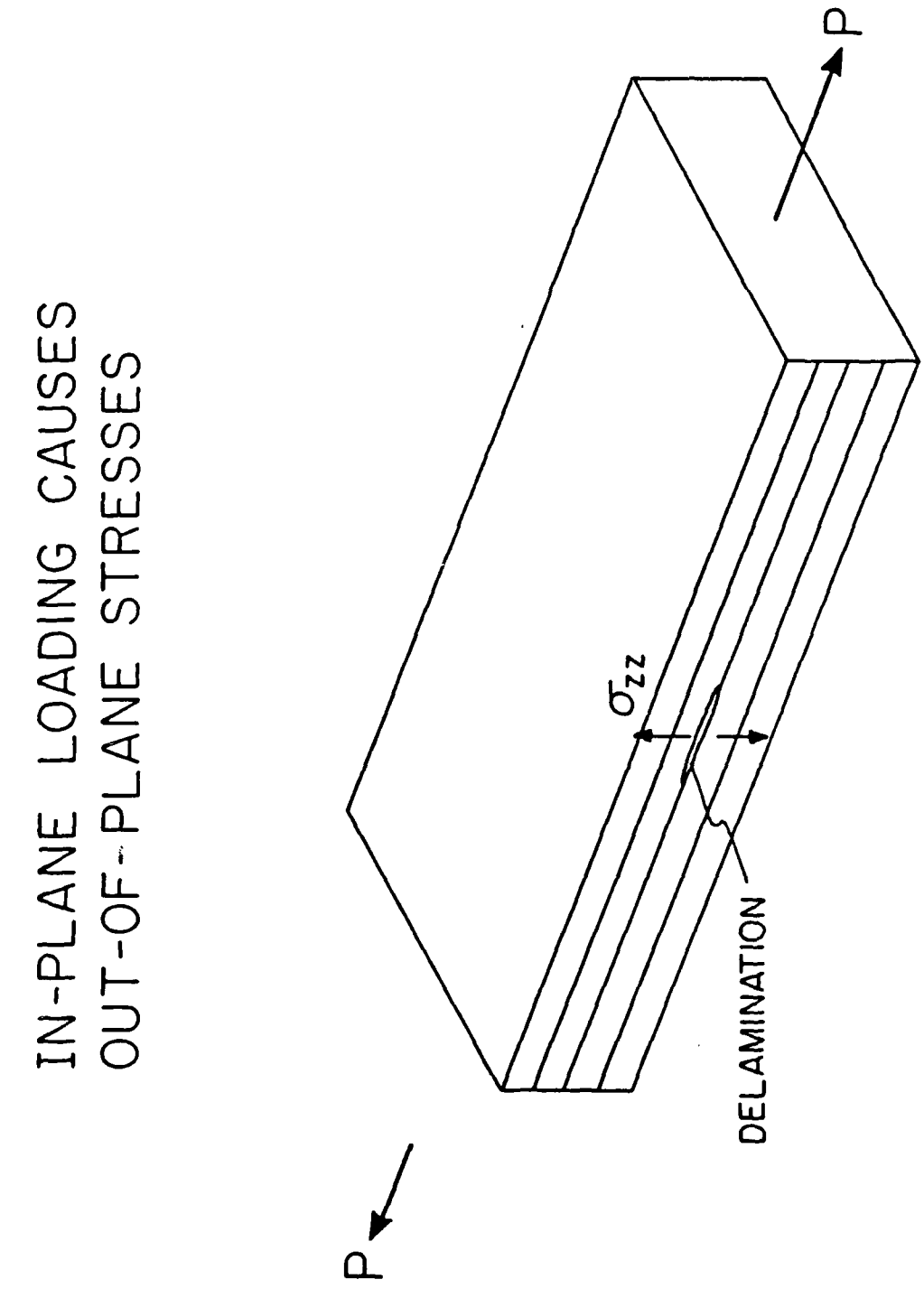

FIGURE 6 ILLUSTRATION OF TENSILE INTERLAMINAR NORMAL STRESS CAUSING DELAMINATION

TABLE 3

OBSERVED FRACTURE MODES AND PREDICTED MODES FROM INTERLAMINAR STRESS CALCULATIONS FOR $[\pm\theta]_s$ LAMINATE FAMILY

Laminate	Ply Interface	Sign of σ_{zz} at Free Edge	Predicted Fracture Mode	Observed Fracture Mode
$[\pm 15]_s$	+15/-15 midplane	- -	No delamination	In-plane/No delamination
$[\pm 30]_s$	+30/-30 midplane	- -	No delamination	In plane/No delamination
$[\pm 45]_s$	+45/-45 midplane	- -	No delamination	In plane/No delamination
$[\pm 60]_s$	+60/-60 midplane	- -	No delamination	In plane/No delamination
$[\pm 75]_s$	+75/-75 midplane	- -	No delamination	In plane/No delamination
$[90_4]$	90/90 midplane	0 0	No delamination	In plane/No delamination

TABLE 4

OBSERVED FRACTURE MODES AND PREDICTED MODES FROM INTERLAMINAR STRESS CALCULATIONS FOR $[\pm\theta/0]_s$ LAMINATE FAMILY

Laminate	Ply Interface	Sign of σ_{zz} at free edge	Predicted Fracture Mode	Observed Fracture Mode
$[\pm 5/0]_s$	+5/-5 -5/0 midplane*	- + +	Delamination at midplane with some delamination at -5/0 interface	Some delamination of midplane away from fracture surface
$[\pm 10/0]_s$	+10/-10 -10/0 midplane*	- + +	Delamination at midplane with some delamination at -10/0 interface	Some delamination of midplane away from fracture surface
$[\pm 15/0]_s$	+15/-15 -15/0 midplane*	- + +	Delamination at midplane with some delamination at -15/0 interface	Some delamination of midplane and angled plies away from fracture surface
$[\pm 30/0]_s$	+30/-30 -30/0* midplane	- + -	Delamination at -30/0 interface	Delamination at -30/0 interface with some at +30/-30 interface
$[\pm 45/0]_s$	+45/-45 -45/0* midplane	- + -	Delamination at -45/0 interface	Delamination of angle plies away from fracture surface
$[\pm 60/0]_s$	+60/-60 -60/0 midplane*	+ - +	Delamination at midplane with some delamination at +60/-60 interface	Delamination of 0° plies with secondary angle ply delamination
$[\pm 75/0]_s$	+75/-75* -75/0 midplane	+ - -	Delamination at +75/-75	Significant delamination at angle ply interface
$[90_2/0]_s$	90/90* 90/0 midplane	+ - -	Delamination at 90/90 interface	Delamination at 90/90 and 90/0 interfaces

*asterisk indicates interface with largest calculated tensile interlaminar normal stress.

TABLE 5

OBSERVED FRACTURE MODES AND PREDICTED MODES FROM INTERLAMINAR STRESS CALCULATIONS FOR $[0/\pm\theta]_s$ LAMINATE FAMILY

Laminate	Ply Interface	Sign of σzz at free edge	Predicted Fracture Mode	Observed Fracture Mode
$[0/\pm5]_s$	0/+5 +5/-5 midplane	- - -	No delamination	In-plane/No delamination
$[0/\pm10]_s$	0/+10 +10/-10 midplane	- - -	No delamination	In-plane/No delamination
$[0/\pm15]_s$	0/+15 +15/-15 midplane	- - -	No delamination	In-plane/No delamination
$[0/\pm30]_s$	0/+30 +30/-30 midplane*	- - +	Delamination at midplane	Slight internal ply delamination at midplane. Outer ply secondary delamination
$[0/\pm45]_s$	0/+45 +45/-45 midplane*	- - +	Delamination at midplane	Slight delamination of inner plies at midplane
$[0/\pm60]_s$	0/+60 +60/-60 midplane*	- - +	Delamination at midplane	Severe internal delamination of angle plies at midplane
$[0/\pm75]_s$	0/+75* +75/-75 midplane	+ + +	Delamination at all interfaces	Severe internal angle ply delamination at midplane and at +75/-75 interface. Slight top ply delamination
$[0/90_2]_s$	0/90 90/90* midplane*	+ + +	Delamination at all interfaces	Extensive delamination of 90 plies at midplane and at 90/90 interface. Secondary top ply delamination

*asterisk indicates interface with largest calculated tensile interlaminar normal stress.

TABLE 6

OBSERVED FRACTURE MODES AND PREDICTED MODES FROM INTERLAMINAR STRESS CALCULATIONS FOR $[+\theta/0/-\theta]_s$ LAMINATE FAMILY

Laminate	Ply Interface	Sign of σ_{zz} at free edge	Predicted Fracture Mode	Observed Fracture Mode
$[+15/0/-15]_s$	+15/0* 0/-15 midplane	+ + -	Delamination at +15/0 and 0/-15 interfaces	Some delamination of angle plies leading away from fracture surface
$[+30/0/-30]_s$	+30/0* 0/-30 midplane	+ + -	Delamination at +30/0 and 0/-30 interfaces	Very little delamination of angle plies leading away from fracture surface
$[+45/0/-45]_s$	+45/0* 0/-45 midplane	+ + -	Delamination at +45/0 and 0/-45 interfaces	Delamination of the 45 plies but mainly the outer ones
$[+60/0/-60]_s$	+60/0 0/-60 midplane	- - -	No delamination	Very little outer ply delamination leading away from fracture surface
$[+75/0/-75]_s$	+75/0 0/-75 midplane	- - -	No delamination	Delamination of very small area of outer angle ply near fracture surface
$[90/0/90]_s$	90/0 0/90 midplane	- - +	Delamination at midplane	Midplane delamination with slight top ply delamination

*asterisk indicates interface with largest calculated tensile interlaminar normal stress.

delaminate except in a few cases such as the [0/+-30]s and [0/+-45]s laminates where there were some problems in the calculation of the interlaminar stresses.

It can therefore be concluded that the fracture of unflawed laminates can be viewed as a competition between two separate modes to cause different types of fracture. If the critical in-plane stress is reached before the critical stress for delamination, the in-plane fracture occurs. Conversely, if the necessary stress for delamination is reached before the necessary in-plane stress, then fracture via delamination occurs.

There is an additional consideration for the [+-θ/0]s, [0/+-θ]s, and [+θ/0/-θ]s laminates of the second group: those with lamination angles above 45°. In these specimens, the failure occurs at a stress above that predicted by the Tsai-Wu criterion. It is important to remember that the a ply-by-ply application of the Tsai-Wu criterion yields the stress at which "First-Ply-Failure" occurs. However, this does not represent the maximum load-carrying capacity of the laminate. The stress-strain curves of these laminates become nonlinear and erratic shortly after a point where a large number of clicking sounds begin to emanate from the specimens. This is an indication of the occurrence of first damage in the laminate. The stresses at which this behavior begins is near the First-Ply-Failure stress predicted with the use of the Tsai-Wu criterion. With continued loading, considerable damage occurs

in the laminate before final failure and this significantly complicates the stress field. Damage in the laminate will also create new free surfaces where interlaminar stresses can arise and delamination occur. This suggests that stacking sequence will have an important effect on post-first-ply-failure behavior and final fracture of the specimen. The experimental fracture stresses for these laminates, shown in Figure 5, do indeed show distinct differences in fracture stress with stacking sequence indicating the effects of interlaminar stresses in post-first-ply failure behavior. Additional work is necessary to fully understand this phenomenon.

A more in-depth treatment of these results is given by Lagace in References 5 and 8.

Work is currently being performed to further understand the mechanisms of tensile failure. At the present time there are three main areas which are being explored. The first is to fill in the current data base with additional lamination angles. The reported work has investigated lamination angles of multiples of 15 degrees. Laminates at 5° intervals are being tested to fill in this data base and better understand the various phenomena which occur. The second area is to investigate unsymmetric stacking sequences of the six-ply laminates. The investigations of these unsymmetric six-ply laminates will give further insight into the stacking sequence effects as well as to give initial data into the effect of cur-

ing stresses on the fracture stress in uniaxial tension. The third area is the investigation of thickness effects on fracture. The ply thicknesses are being effectively increased by laying up two, three, or more of the same angle plies consecutively to give laminates of twelve, eighteen, or more plies. Thus a [+15/0/-15]s laminate would become [+15x2/0x2/-15x2]s for an effective doubling of the ply thickness. Different stacking sequences and lamination angles are being investigated.

2.2 Comparison of Tapered Graphite/Epoxy Coupons with Standard TELAC Graphite/Epoxy Coupons

The fracture data of specimens with lamination angles less than 30° fall below the predicted values using accepted failure criteria as shown by the data from Lagace [5]. This data was acquired using a standard straight-edge coupon specimen shown in Figure 1. It has been suggested that this "premature" failure is due to the end constraints imposed by hydraulically gripping the coupon at the tabs. This constraint could cause adjustment of the strain field due to the Poisson effect thereby causing irregularities in the stress field [9].

An investigation was undertaken to examine the difference in behavior of standard TELAC straight-edge coupon specimens with a tapered coupon specimen designed by Boeing. This specimen is

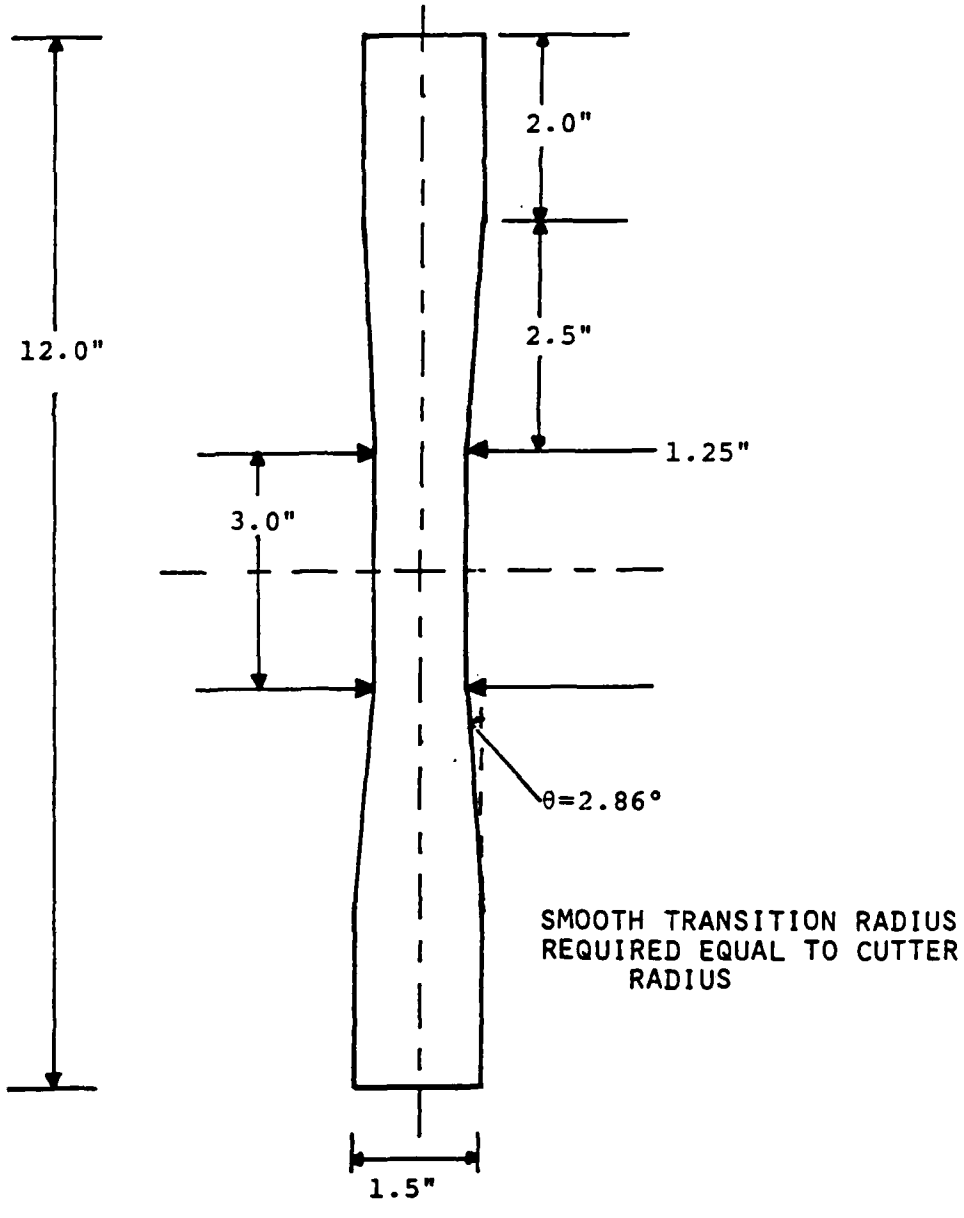

FIGURE 7 PHYSICAL CHARACTERISTICS OF BOEING TAPERED COUPON SPECIMEN

shown in Figure 7. Two different stacking sequences of a six-ply laminate were chosen for the investigation: [+-15/0]s and [0/+-15]s. All the specimens were manufactured from Hercules AS1/3501-6 graphite/epoxy using the standard TELAC methods. The tapered coupons were machined from straight edge pieces with the use of a diamond-coated grinding bit on a milling machine equipped with water cooling. Extreme care was taken to insure smooth transitions in the regions where the tapers begin.

All tests were done on an MTS 810 testing machine with the aid of hydraulic grips. Tests were conducted at a constant stroke rate of approximately 1 mm/minute to yield a constant strain rate of approximately 5000 microstrain/minute. Strain data was taken automatically, with the use of a PDP-11/34 computer, from both longitudinal and transverse gages mounted on each specimen.

The stress-strain response of the laminates was not different for the two different coupon types for the same laminate. Typical stress-strain curves for the two laminates investigated are shown in Figures 8 and 9. A summary of the elastic moduli measured (Young's Modulus and Poisson's Ratio) for the two types of specimens is in Table 7. Again, there is no difference in these values between the two specimen types.

The examination of the fracture stresses and modes of the tapered and standard coupon specimens reveals a different

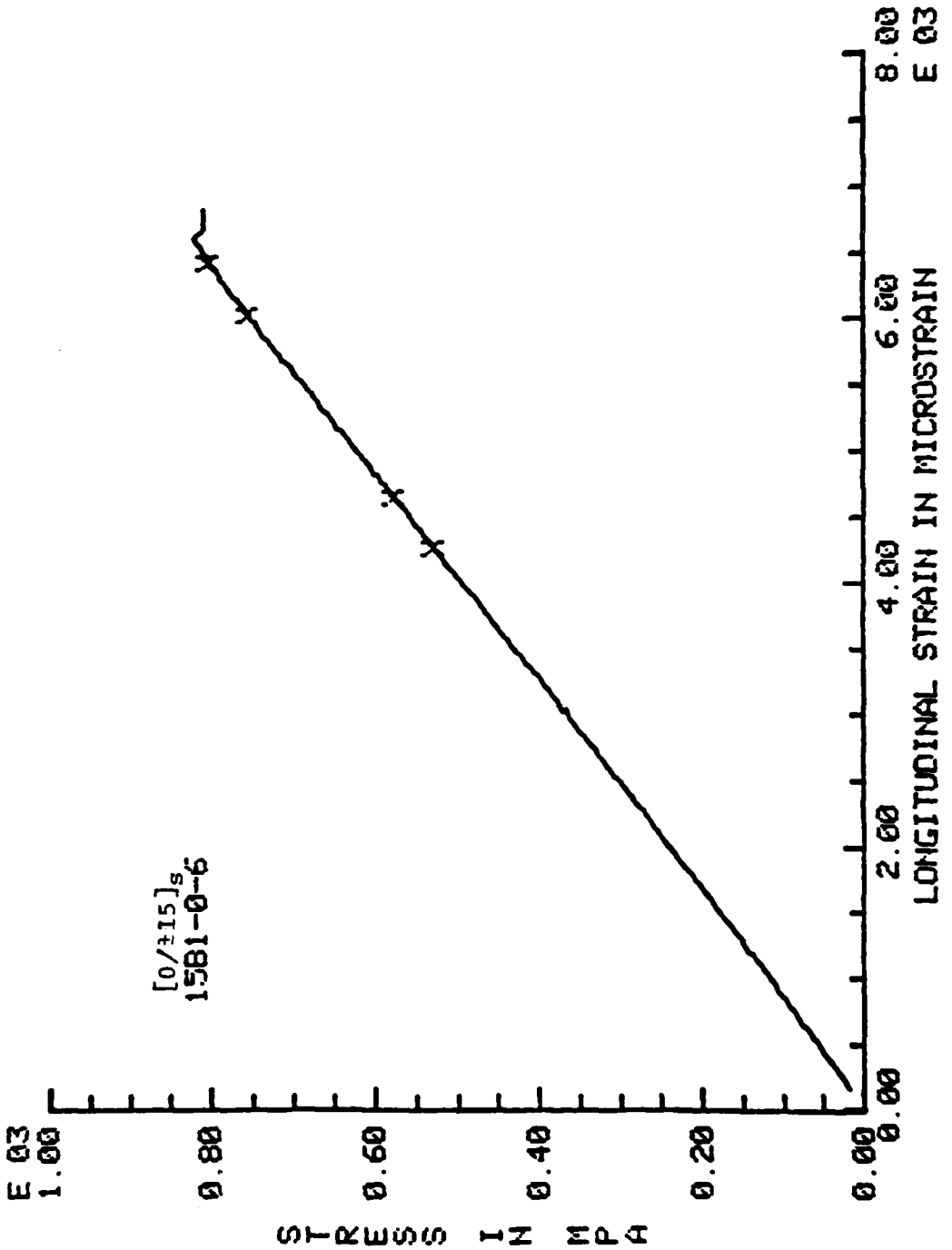

FIGURE 8 TYPICAL STRESS-STRAIN CURVE FOR $[0/\pm15]_s$ SPECIMEN

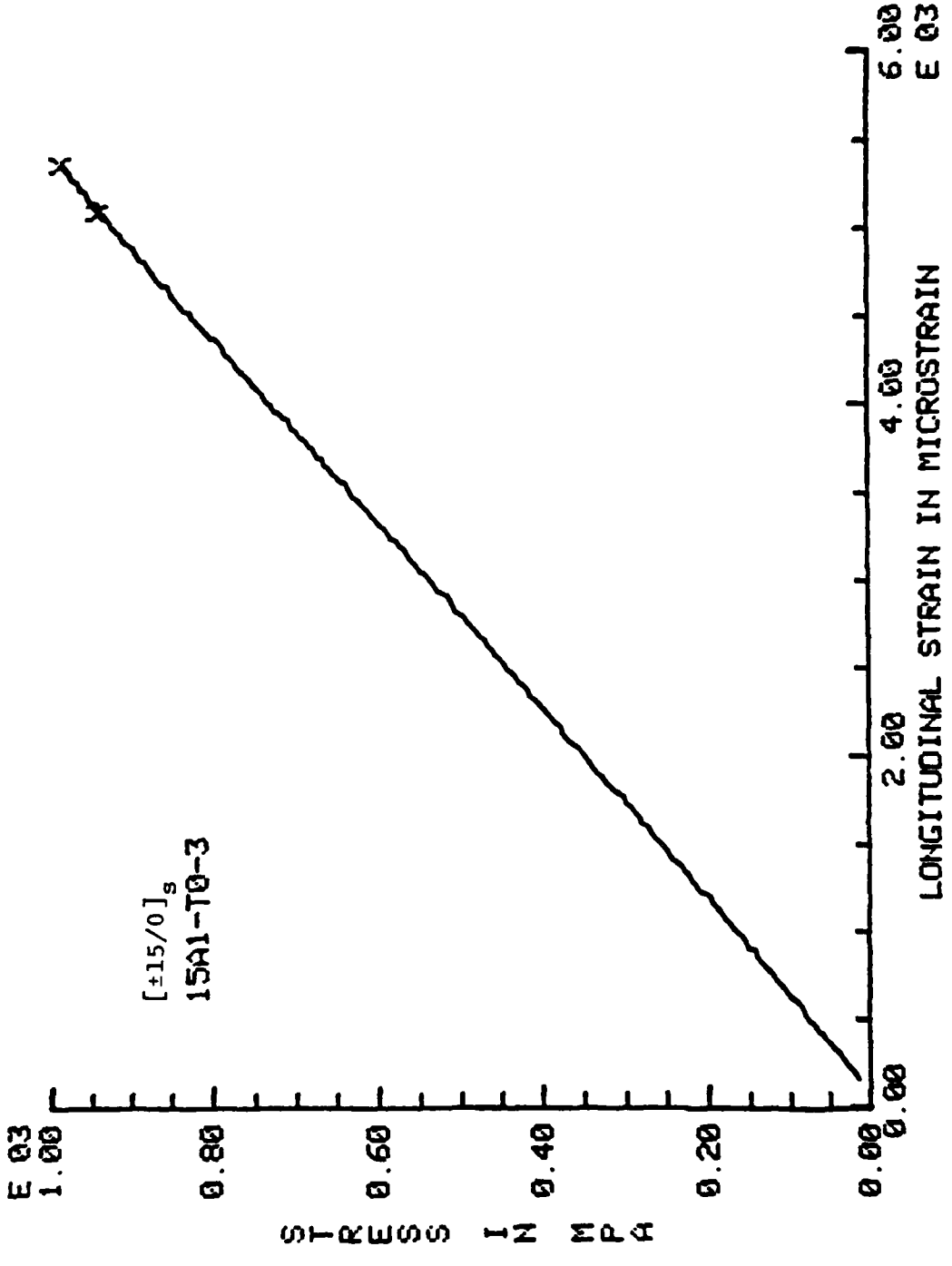

FIGURE 9 TYPICAL STRESS-STRAIN CURVE FOR $[\pm 15/0]_s$ SPECIMEN

TABLE 7

SUMMARY OF MEASURED MODULI AND FRACTURE
STRESSES FOR STANDARD AND TAPERED COUPONS

Laminate	$[\pm 15/0]_s$		$[0/\pm 15]_s$	
Coupon Type	Standard	Tapered	Standard	Tapered
Longitudinal Modulus [GPa]	124 (2.3%)	122 (3.7%)	123 (2.8%)	124 (2.1%)
Poisson's Ratio	.638 (4.2%)	.674 (9.5%)	.734 (7.6%)	.655 (10.1%)
Fracture Stress [MPa]	1080 (3.2%)	1011 (3.5%)	844 (2.7%)	770 (7.5%)
Fracture Strain [μs]	8450 (4.9%)	8016 (3.8%)	6929 (3.2%)	6322 (9.5%)

Mean (Coefficient of Variation)

story. In both the [+-15/0]s and [0/+-15]s laminates there is a small but discernible difference in the fracture stresses of the two coupon types as listed in Table 7. For both laminates, the average fracture stress of the standard straight-edge coupon specimens is higher by about 7-8% than the average fracture stress of the tapered specimens. The coefficient of variation of the fracture stresses is about 2-5%. Thus, this 7-8% difference is not very large but the trend appears consistent with the post-mortem fracture modes of the two types of specimens. The fracture modes of the two types of specimens was the same for a given laminate except for the location of initial damage. In the case of several tapered coupon specimens, the damage initiated at the point where the taper began (point A in Figure 7). This indicates that the presence of the taper may cause stress concentrations and "premature" failure of the specimen. It should again be emphasized that extreme care was taken in the manufacture of these specimens to insure a smooth transition in the region where the taper began. A fine sandpaper was used after machining to insure a smooth transition region.

It is important to note that there was some problem encountered in the manufacture of the [0/+-15]s specimens. The cured laminates had a "shiny" appearance on their surface indicating a low resin content. However, the measured laminate thicknesses were at or slightly above nominal indicating a resin deficiency existed only in the outer 0° plies making these

plies susceptible to delamination. These plies did indeed delaminate. Results from other studies [1,5] indicate no delamination for the [0/+-15]s laminate. In addition, the ultimate fracture stresses of this laminate were lower in this investigation than in the other investigations.

This problem does not, however, invalidate the comparison between the straight edge and tapered coupons. Since both types of coupons were taken from the same cured plates, they had the same resin condition. The results still suggest that the tapered coupons fail at slightly lower loads than the straight edge coupons and that this may be caused by fracture being triggered at the "shoulder" of the taper. However, as previously noted, the stress-strain results prior to fracture are the same for both types of coupons.

In addition to the investigation of coupon shape on behavior, a simpler tab type was used on one-half of the tapered coupons. On these a piece of 400C grit sandpaper glued onto two 50 mm by 75 mm pieces of thin aluminum was used as a loading tab rather than the standard bonded glass/epoxy tabs on the other half. This other tab type was placed around the top of the specimen and then inserted into the machine grips such that the grip faces were applied directly to the aluminum and the sandpaper face gripped into the graphite/epoxy surface. Although there was no difference in the stress-strain or fracture data for the specimens with these type of tabs versus the

specimens with the standard tabs, post-mortem examination of the specimens showed considerable damage to the graphite/epoxy surface where the sandpaper gripped the specimen raising questions as to the suitability of such a loading tab for general purpose use.

This work is described in detail by Brewer in Reference 10.

2.3 Nonlinear Stress-Strain Behavior of Graphite/Epoxy Laminates

Previous investigations at TELAC [1,3,5,10] and from other sources have shown that composite laminates can exhibit nonlinear stress-strain behavior. This behavior can be classified as either a softening or a stiffening with reference to the tangent modulus of the stress-strain curve at any point. This is illustrated in Figure 10. This nonlinear phenomenon is even visible in fiber-dominated laminates although the nonlinearities may occur only near the end of a monotonic test to failure.

Several experiments were performed to obtain a data base on this nonlinear behavior and to look at the consequences of unloading and reloading composite specimens with such stress-strain curves. The laminates chosen for this initial work were of the $[+-\theta]s$ family. This particular laminate family was chosen since the nonlinear stress-strain behavior is

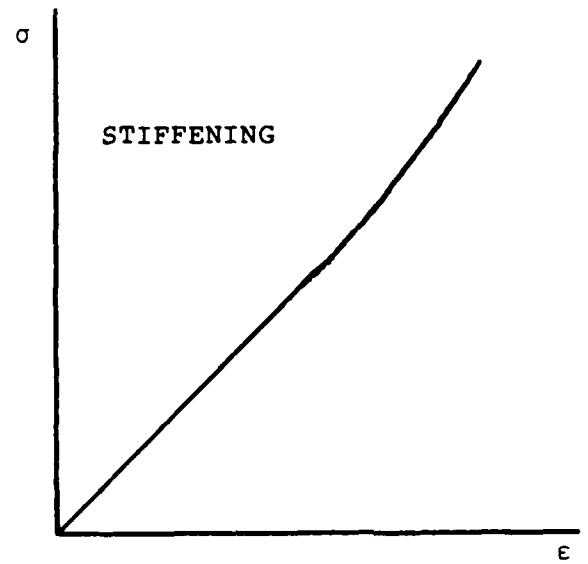

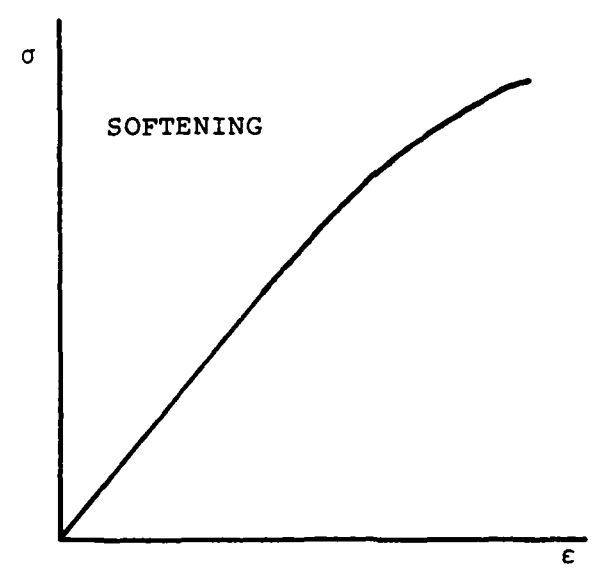

FIGURE 10 ILLUSTRATION OF "SOFTENING" AND "STIFFENING" STRESS-STRAIN BEHAVIOR

very apparent in these laminates. Seven different values of θ were chosen for the experiments: 5°, 10°, 15°, 20°, 30°, 35°, and 45°. Fifteen unnotched specimens of each of the first four lamination angles were manufactured while twenty of each of the latter three angles were built. This is summarized in Tables 8 and 9.

The standard TELAC tension coupon (See Figure 1) was used and all the specimens were tested in tension. Several different types of tests were performed on the specimens with load history being the variable. Groups of three specimens of each type were subjected to a specific load history. All tests were conducted in stroke control on an MTS 810 testing machine with hydraulic grips. Except where noted, a constant strain rate of approximately 5000 microstrain was used. Data was taken with a PDP-11/34 computer.

For each laminate type, three specimens were tested monotonically to failure to determine the stress-strain curve. The results from these tests were used to determine the "break stress" for each laminate. The "break stress" is defined as the stress level at which the laminate departs from its initial linear behavior. The break stress was determined with the aid of a program developed at TELAC called LIN6 [5,11]. This program determines linear regions of data and their slopes and endpoints.

TABLE 8

TEST PLAN FOR $[\pm 30]_s$, $[\pm 35]_s$, AND $[\pm 45]_s$ LAMINATES

Test Type \ Laminate	$[\pm 30]_s$	$[\pm 35]_s$	$[\pm 45]_s$	Load vs. Time History P_b = "Break" Load P_f = Failure Load
Monotonic to Failure	3	3	3	
Load to 1/4 Point, Unload, Load to Failure	3	3	3	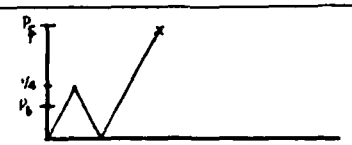
Load to 1/2 Point, Unload, Load to Failure	3	3	3	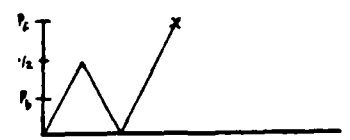
Load to 3/4 Point, Unload, Load to Failure	3	3	3	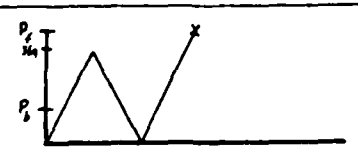
Load to 1/4 Point, Unload, Load to 1/2 Point, Unload, Load to 3/4 Point, Unload, Load to Failure	3	3	3	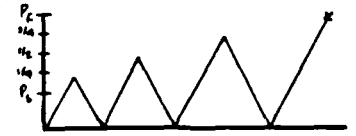

Numbers indicate number of specimens tested

TABLE 9

TEST PLAN FOR $[\pm 5]_s$, $[\pm 10]_s$, $[\pm 15]_s$, AND $[\pm 20]_s$ LAMINATES

Test Type \ Laminate	$[\pm 5]_s$	$[\pm 10]_s$	$[\pm 15]_s$	$[\pm 20]_s$	Load vs. Time History P_b = "Break" Load P_f^b = Failure Load
Monotonic to Failure	3	3	3	3	
Load to 1/3 Point, Unload, Load to Failure	3	3	3	3	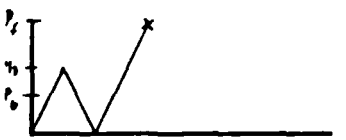
Load to 2/3 Point, Unload, Load to Failure	3	3	3	3	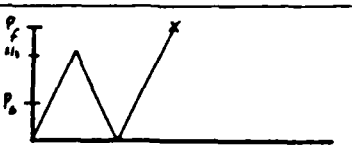
100 Load-Unload Cycles to 1/3 Point, Load to Failure	3	3	3	3	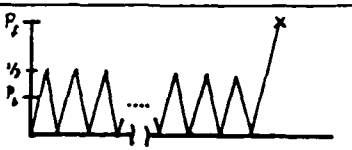
100 Load-Unload Cycles to 2/3 Point, Load to Failure	3	3	3	3	

For lamination angles of 30°, 35°, and 45°, four different load histories were used. The first involves loading the specimen to the one-quarter point, unloading to zero and then reloading to failure. The one-quarter point is defined as the stress level which is one-quarter of the way between the break stress and fracture stress which were determined experimentally from the monotonic tests to failure:

$$\text{"x point stress"} = x \cdot \begin{pmatrix}\text{fracture}\\ \text{stress}\end{pmatrix} + \begin{pmatrix}\text{break}\\ \text{stress}\end{pmatrix} \cdot (1-x) \qquad (2.1)$$

This is illustrated in Figure 11. The second load history is the same as the previous except the initial loading is to the one-half point. The third load history type involves the same scenario with the initial loading to the three-quarters point. The final load history for this group involved four load-unload repetitions: the first to the quarter point, the second to the half point, the third to the three-quarters point, and the fourth to fracture. This information is summarized in Tables 8 and 9.

Similar tests were conducted on the specimens with lamination angles of 5°, 10°, 15°, and 20°. Again, groups of three specimens were tested under each type of loading. After the initial monotonic to failure tests were conducted, a group of specimens were tested via an initial loading to the one-third point, unloading and then reloading to failure. A second group

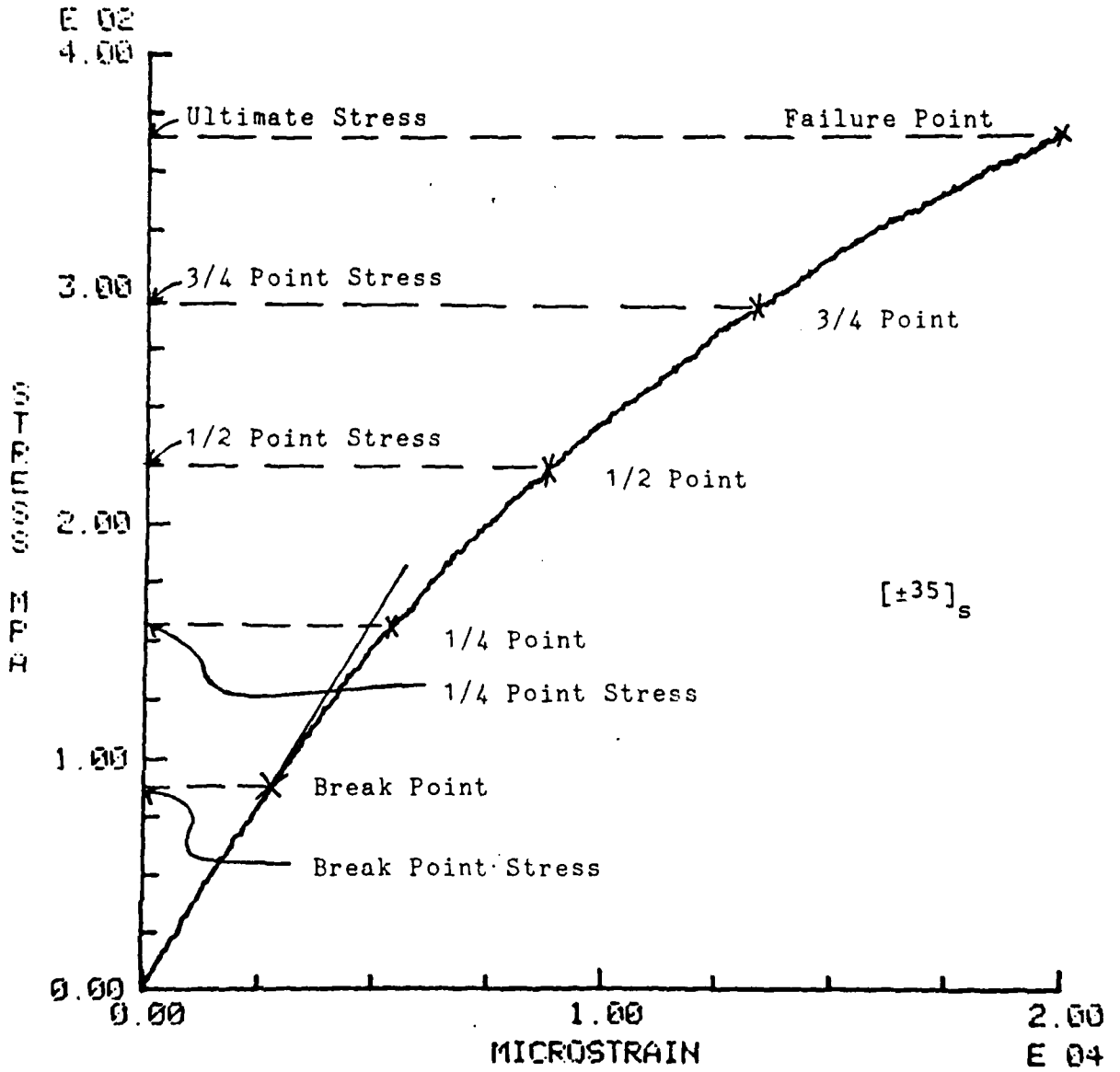

FIGURE 11 STRESS-STRAIN CURVE FOR $[\pm 35]_s$ SPECIMEN ILLUSTRATING "LOADING POINTS"

was loaded in the same manner except the initial loading was to the two-thirds point. The other two types of loading involved cyclic loads. One loading involved cycling the specimens between zero stress and the one-third point stress for 100 cycles at a frequency of 1/6 Hertz. The second type of loading was the same except the maximum stress for the cycling was the two-thirds point stress. In both cases, after the cyclic loads the specimens were then tested monotonically to failure at a stroke rate of 1 mm/minute. These tests were performed to determine if repeated loading caused any permanent setting or damage in the material.

The "break stress" does not always indicate that the specimen begins to soften with increased load, i.e. that the tangent modulus begins to decrease. For lamination angles between zero and twenty degrees, the tangent modulus increases after the break stress. This is illustrated for a [+-5]s specimen in Figure 12 where the tangent modulus at failure has increased by about 15% over the original value. This is in marked contrast to the laminates with larger lamination angles like the [+-35]s coupon whose stress-strain curve in Figure 11 shows a distinct softening as the tangent modulus at failure has decreased by about 70% from the initial value.

Several important observations and conclusions can be made from these tests. One, the initial modulus of the specimen did not change upon unloading and reloading. Two, the fracture

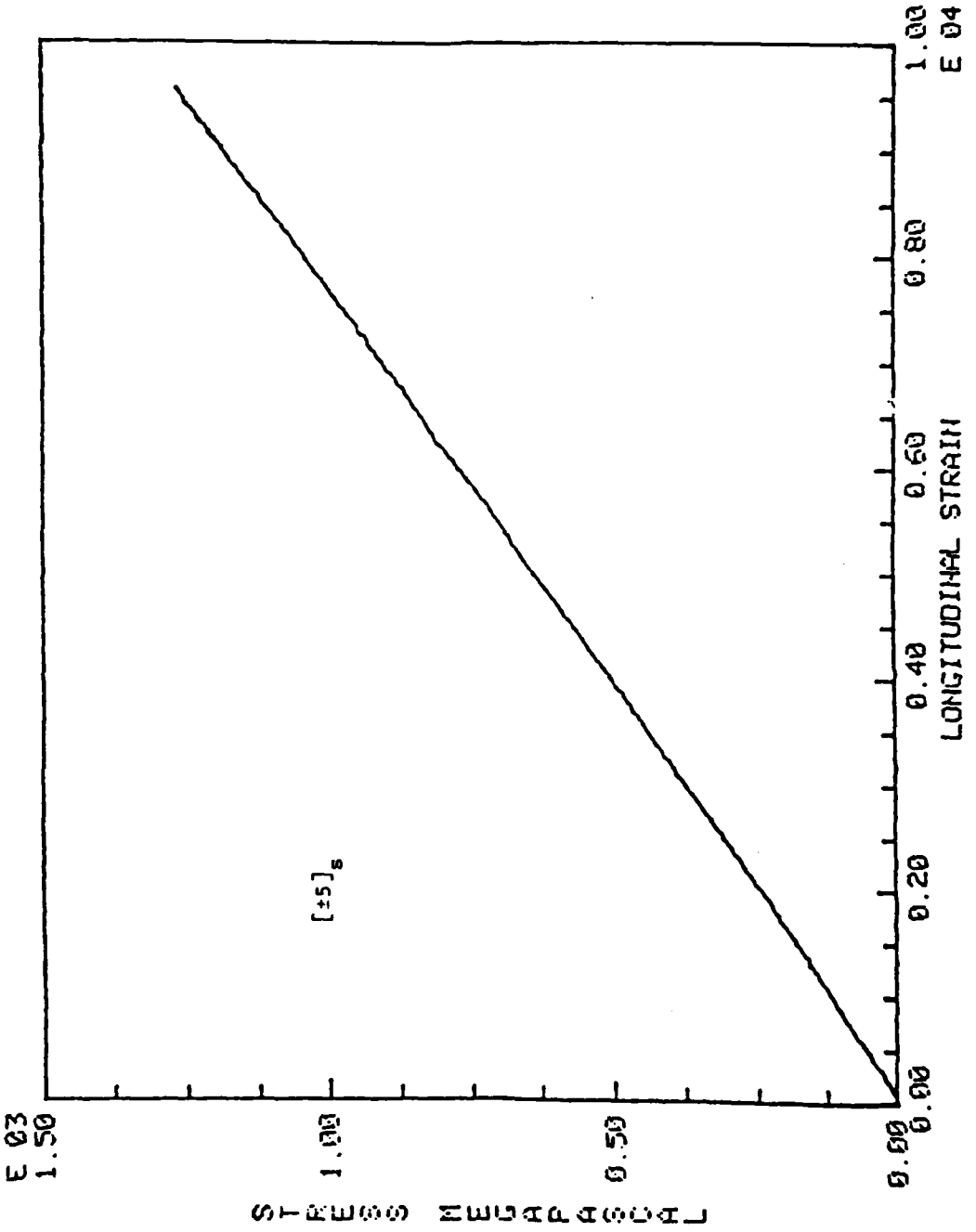

FIGURE 12 STRESS-STRAIN CURVE FOR $[\pm 5]_s$ SPECIMEN SHOWING "STIFFENING"BEHAVIOR

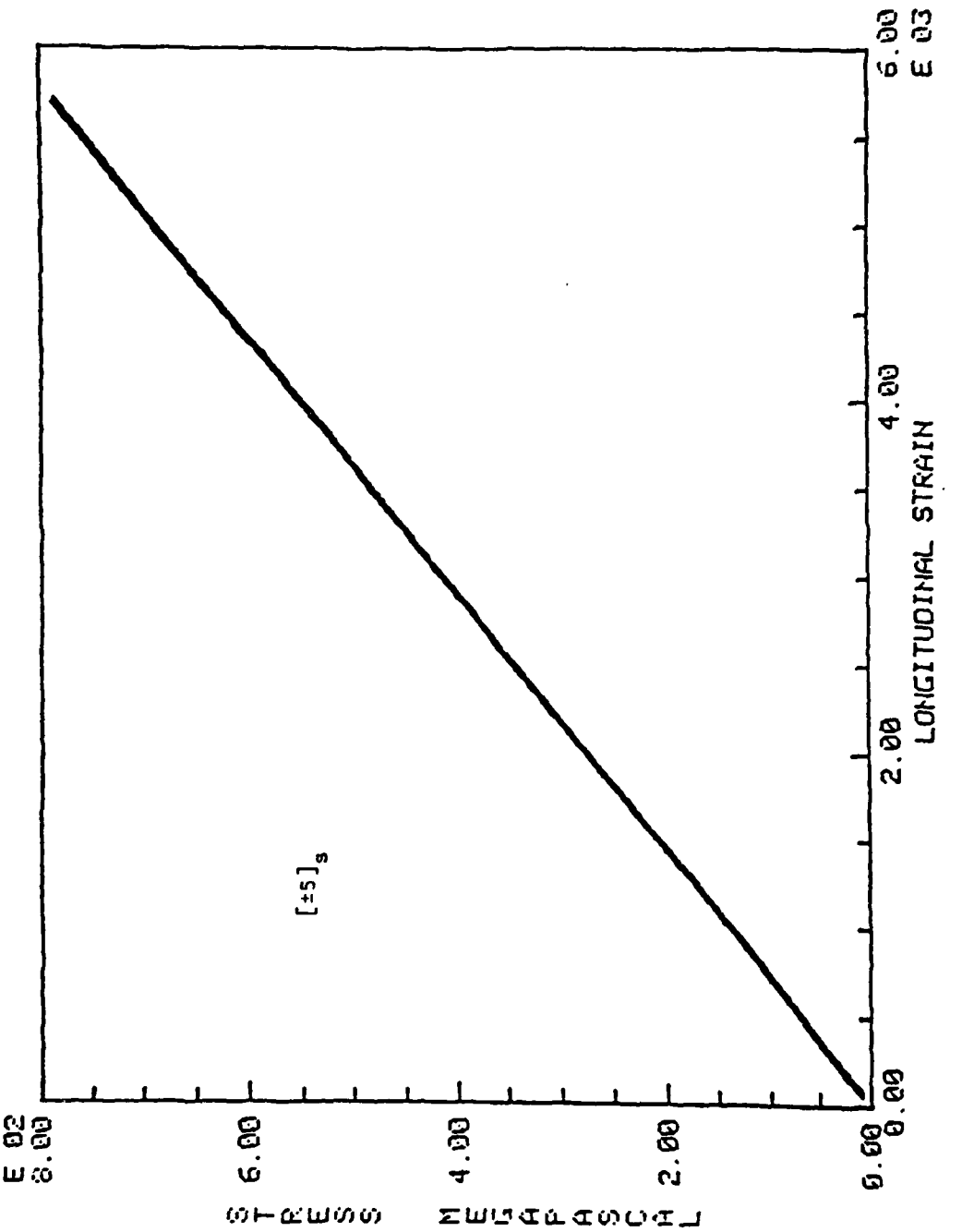

FIGURE 13 STRESS-STRAIN CURVE FOR 100 CYCLES OF LOADING FOR A $[\pm 5]_s$ SPECIMEN

stress of the specimens did not change due to the loading-unloading-loading cycle or after 100 cycles of load. Three, the tangent modulus at failure did not change due to loading-unloading cycles. These points are illustrated in Figure 13 which is a stress-strain curve for a [+-5]s specimen. The stress-strain data line is dark because the loading and unloading curves both plot on the same points. A slightly different behavior is shown for a [+-30]s specimen in Figure 14. Although the same basic conclusions can be drawn, an additional factor to note is that the load-unload curves do not follow the same path and this leaves a permanent strain in the material after an initial load-unload cycle. The amount of permament strain increased with the magnitude of the initial maximum load and also changed with lamination angle as shown in Figure 15. It is also clear from the stress-strain curve in Figure 14 that the composite does not exhibit a "memory". Although the specimen does not follow the initial stress-strain curve upon reloading, it does rejoin the original stress-strain curve at the point of original maximum load and then follows the normal stress-strain curve failure. This was observed for all tests and all lamination angles.

An important summary of this work is presented in Figure 16 where the percent change in tangent modulus from the initial value to the value at fracture is plotted versus lamination angle. The data clearly shows that a stiffening behavior is

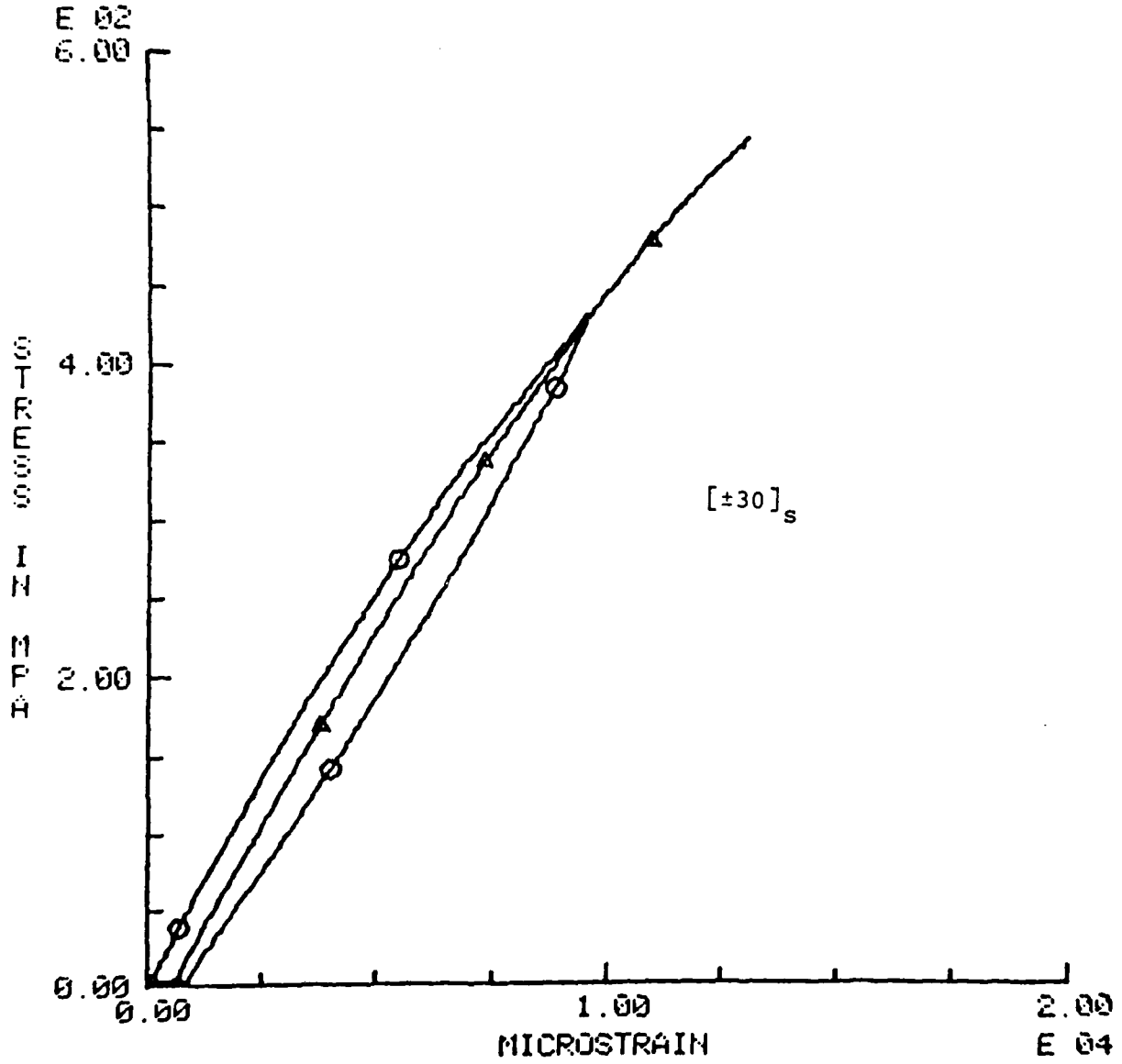

FIGURE 14 STRESS-STRAIN CURVE FOR A LOAD-UNLOAD-RELOAD CYCLE OF A $[\pm 30]_s$ SPECIMEN

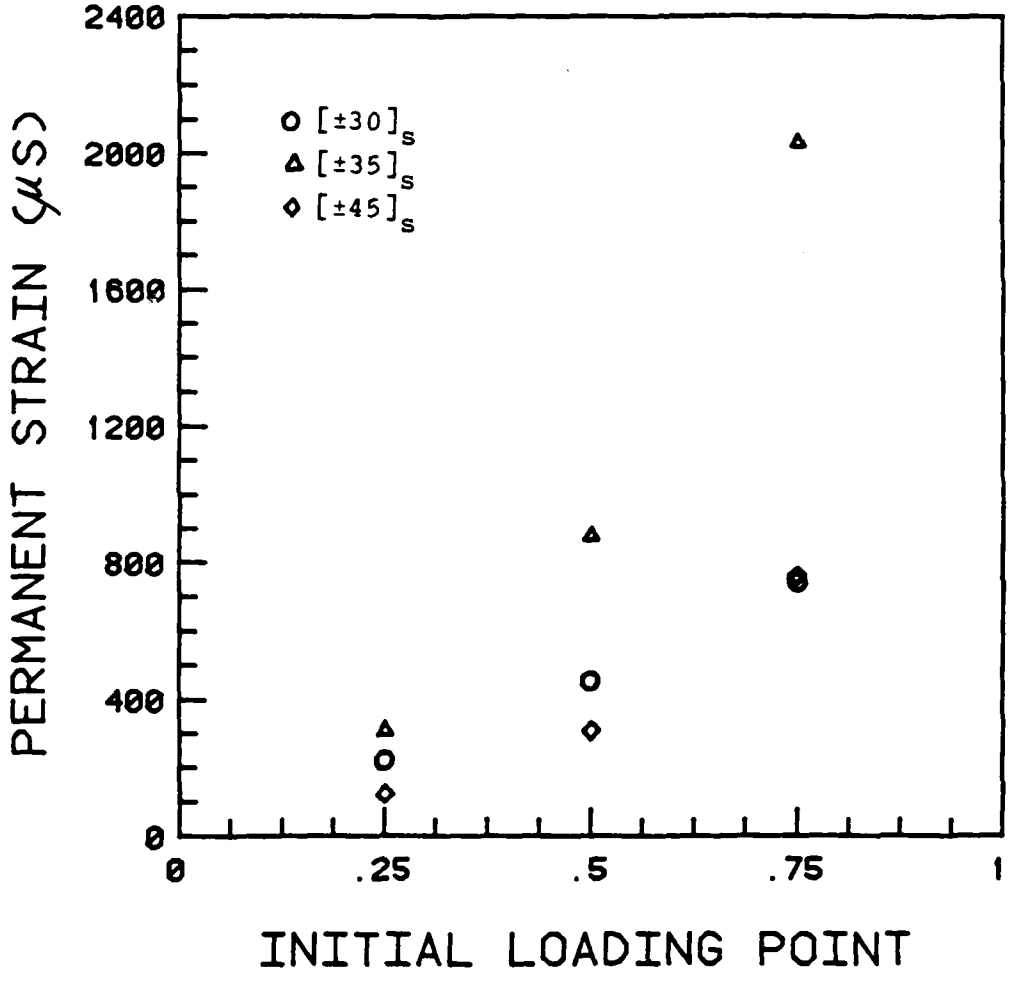

FIGURE 15 PERMANENT STRAIN AFTER LOAD-UNLOAD CYCLE VERSUS INITIAL LOADING POINT

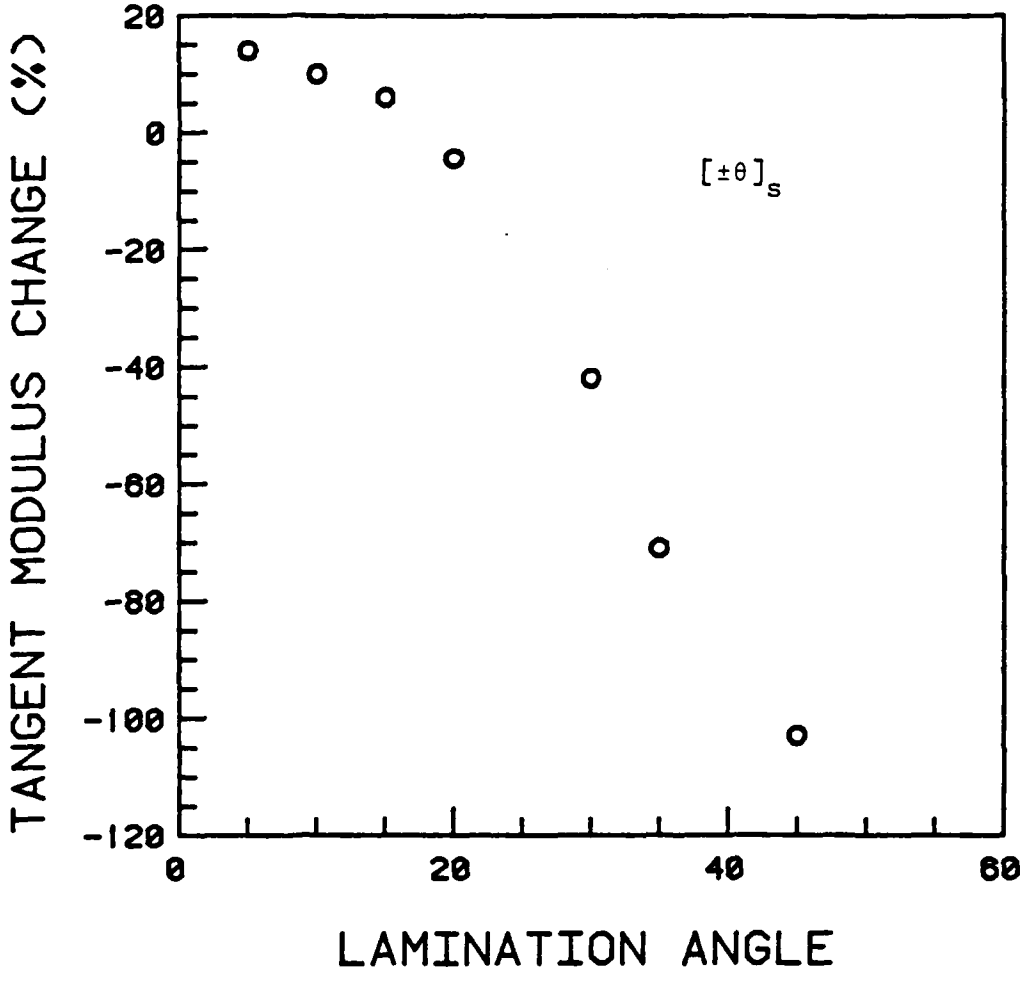

FIGURE 16 PERCENT CHANGE IN TANGENT MODULUS (INITIAL TO FINAL) VERSUS LAMINATION ANGLE

observed for lamination angles of 15 degrees or less. The amount of stiffening cannot be explained by fiber realignment as suggested by some researchers since the magnitude of the modulus change indicates realignment greater than 5° which is not possible. There also is a lamination angle between 15° and 20° where the percent change in modulus is zero indicating that the stress-strain would be perfectly linear-to-failure. The amount of softening of the modulus increases after 20° and reaches a maximum at 45° where the tangent modulus at failure is zero indicating a 100% loss of modulus.

This work is reported more fully by Dodson and Fujii in Reference 12 and Trop and Chin in Reference 13. Further research is currently being conducted on this phenomenon. First, other lamination angles will be tested. Second, cyclic tests will be conducted on the laminates which exhibited significant amounts of softening and permanent set (lamination angles greater than 20 degrees) and the number of cycles will be increased to several hundred thousand. Stress-strain behavior will be monitored during this period. This will give indication as to the effect of repeated loads on these nonlinearities and any permanent strain (sets) in the material.

2.4 Characterization of A370-5H/3501-6 Graphite/Epoxy Fabric

Fabric prepreg is seeing increased usage in aerospace applications. Most of the previous work at TELAC had been conducted on unidirectional prepreg tape. Thus, an experimental program was undertaken to study the behavior of graphite/epoxy fabric prepreg. Hercules A370-5H/3501-6 was chosen as the material. The initial investigation looked at the basic characteristics of the fabric prepreg ply.

Three laminates were used to gather the data on the fabric: [0x4] [90x4], and [+-45]s. These laminates were used so that data on the longitudinal, transverse, and shear properties of the basic ply could be determined. The basic axes of the ply are shown in Figure 17. Standard TELAC tensile coupons were used to gather tensile data (Figure 1) while a four-point-bending sandwich beam, pictured in Figure 18, was used to gather compressive data. A summary of the specimens which were tested and the data to be obtained from each is in Table 10.

The results of these tests are summarized in Table 11 and compared with the properties of unidirectional prepreg (AS1/3501-6). As expected, the longitudinal and transverse elastic properties are the same for the fabric. However, the longitudinal tensile strength is slightly higher than the

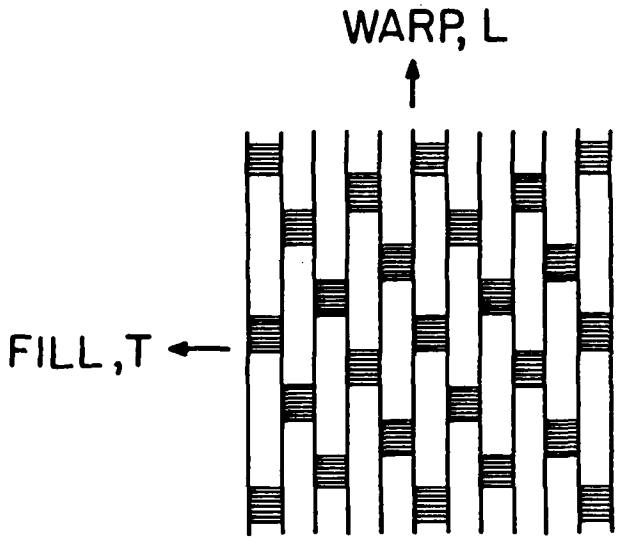

FIGURE 17 BASIC AXES FOR A PLY OF FABRIC PREPREG

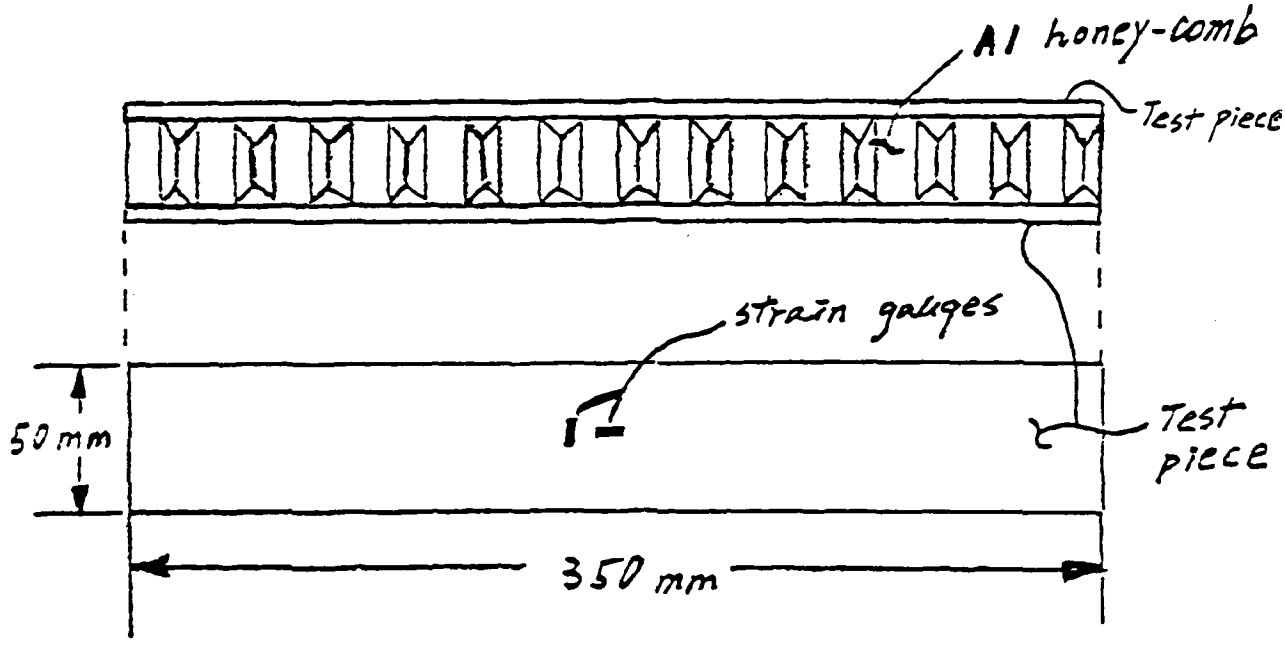

FIGURE 18 CHARACTERISTICS OF FOUR-POINT-BENDING SANDWICH BEAM SPECIMEN

TABLE 10

GRAPHITE/EPOXY FABRIC SPECIMENS TESTED

Specimen Type	Coupons (Tensile Properties)			Beams (Compressive Properties)	
Laminate	$[\ 0_4\ ]$	$[\ 90_4\ ]$	$[\ \pm 45\ ]_s$	$[\ 0_4\ ]$	$[\ 90_4\ ]$
Measured Values	Longitudinal	Transverse	Shear	Longitudinal	Transverse
	E_L	E_T	G_{LT}	E_L	E_T
	ν_{LT}	ν_{TL}		ν_{LT}	ν_{TL}
	F_t^L	F_c^T		F_c^L	F_c^T

10 specimens of each type

TABLE 11

COMPARISON OF FABRIC PROPERTIES WITH UNIDIRECTIONAL TAPE PROPERTIES

		CLOTH	TAPE
E_L	YOUNG'S MODULUS--WARP		
	TENSION	72.5 GPa	130 GPa
	COMPRESSION	66.3 GPa	130 GPa
E_T	YOUNG'S MODULUS--FILL		
	TENSION	72.6 GPa	10.5 GPa
	COMPRESSION	64.1 GPa	10.5 GPa
ν_{LT}	POISSON'S RATIO--MAJOR		
	TENSION	0.059	0.28
	COMPRESSION	0.070	0.28
ν_{TL}	POISSON'S RATIO--MINOR		
	TENSION	0.060	0.023
	COMPRESSION	0.078	0.023
G	SHEAR MODULUS		
	TENSION	4.43 GPa	6 GPa
F_U^L	ULTIMATE STRENGTH--WARP		
	TENSION	798.8 MPa	1661 MPa
	COMPRESSION	423.6 MPa	1698 MPa
F_U^T	ULTIMATE STRENGTH--FILL		
	TENSION	712.4 MPa	53.9 MPa
	COMPRESSION	423.8 MPa	221 MPa

transverse tensile strength, that is the strength along the fill fibers. This may be attributed to the fact that the fill fibers are the fibers which are woven in and their slight initial curvature may cause this slight (10%) loss in strength.

An important aspect of this investigation was to determine whether the weaving pattern of the cloth caused any imbalance or unsymmetry in these laminates. If any unsymmetry existed, there would be coupling effects (bending, shear) exhibited under uniaxial loading. Specimens were strain gaged on both the front and back faces and the results showed that these coupling effects did not exist.

This work is more thoroughly discussed by Chang and deLuis in Reference 14. They also present a discussion of the fracture modes of these specimens.

2.5 Fracture of Tensile Coupons with Holes

In addition to the work on unflawed laminates, a considerable effort has been undertaken to look at the sensitivity of composites to notches such as holes and slits. The conclusion of a large program looking at the tensile fracture of graphite/epoxy coupons with unloaded holes is summarized here. This investigation is discussed in depth by Lagace [5] and is coupled to the work reported in Section 2.1.

The standard tensile coupon as used in the other investigations was again used (Figure 1). The same laminates as reported in Section 2.1 were investigated in this part of the experiment. Twenty specimens of each laminate were tested with four different hole diameters used: 3.175 mm, 6.35 mm, 9.525 mm, and 12.7 mm. Thus five specimens of each laminate were manufactured and tested for each of the four hole sizes. The entire testing program (including the unnotched coupons) is summarized in Table 12. The same testing procedure was used as for the unnotched coupons with a constant strain rate of approximately 5000 microstrain/minute. Data was again taken using the PDP-11/34 computer system and the testing was performed on a MTS 810 Materials Test System with the aid of hydraulic grips. Fracture modes were recorded via photographs.

The theory proposed by Mar and Lin [15,16] was used to correlate the data. They have proposed that the tip of a hole or slit in a filamentary composite has the effect of a crack tip at the interface of a bimaterial in triggering rapid fracture. They proposed the following equation for the fracture stress:

$$\sigma_f = H_c(2a)^{-m} \qquad (2.2)$$

where 2a is the flaw width and H_c is known as the "composite fracture toughness". This equation is similar in form to the basic Griffith equation of Linear Elastic Fracture Mechanics

TABLE 12

TESTING PROGRAM

θ = 15°, 30°, 45°, 60°, 75°, 90°

(Numbers indicate number of specimens)

Nominal Hole Diameter	Laminate :	$[\pm\theta]_s$	$[\theta_8]$	$[\pm\theta/0]_s$	$[0/\pm\theta]_s$	$[+\theta/0/-\theta]_s$
	Shorthand Code:	A0	U8	A1	B1	C1
Unflawed	-0-	5	5	5	5	5
3.175 mm	-2-	5	5	5	5	5
6.35 mm	-4-	5	5	5	5	5
9.525 mm	-6-	5	5	5	5	5
12.7 mm	-8-	5	5	5	5	5
Total number of specimens per : laminate		25	25	25	25	25
Total number of specimens per : laminate family		150	150	150	150	150

Additional laminates: $[\pm5/0]_s$, $[\pm10/0]_s$, $[\pm20/0]_s$, $[\pm25/0]_s$, $[\pm35/0]_s$, $[0/\pm5]_s$, $[0/\pm10]_s$

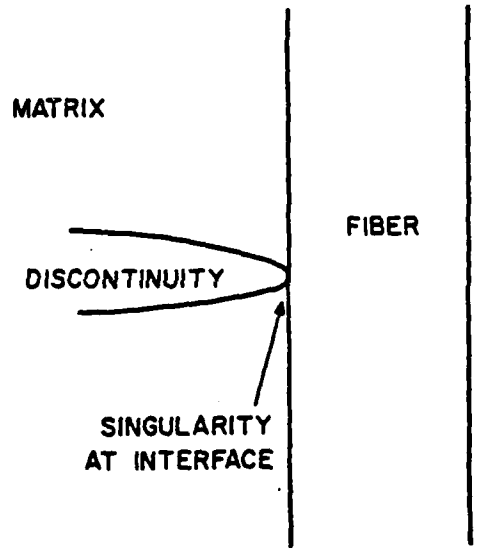

FIGURE 19 DISCONTINUITY AT FIBER/MATRIX INTERFACE

except that the value of the power m is now the value of the mathematical singularity of the stress field at a crack lying in the matrix at the interface of the matrix and filament as illustrated in Figure 19. The value of the singularity is a function of the ratio of the shear moduli of the matrix and filament and of the Poisson's ratio of these materials. This problem has been solved by Fenner [17] and the most likely value of the parameter for AS1/3501-6 graphite/epoxy is .28.

The equation is applied to experimental data by dividing both sides by the unflawed fracture stress of a laminate and then taking logarithms of both sides to yield:

$$\log \frac{\sigma_f}{\sigma_o} = \log A - m \log(2a) \qquad (2.3)$$

where the term A has been introduced and is equal to the composite fracture toughness, H_c, divided by the unflawed fracture stress σ_o. The experimental data is correlated with the above equation by performing a linear regression on the experimental data to determine experimental values of m and A.

A typical plot of experimental data and the experimental line fit are shown in Figure 20 for the [+45/0/-45]s specimens. The results of the linear regressions on the experimental data for all the laminates is summarized in Table 13 and presented graphically in Figures 21 and 22. Included in these figures

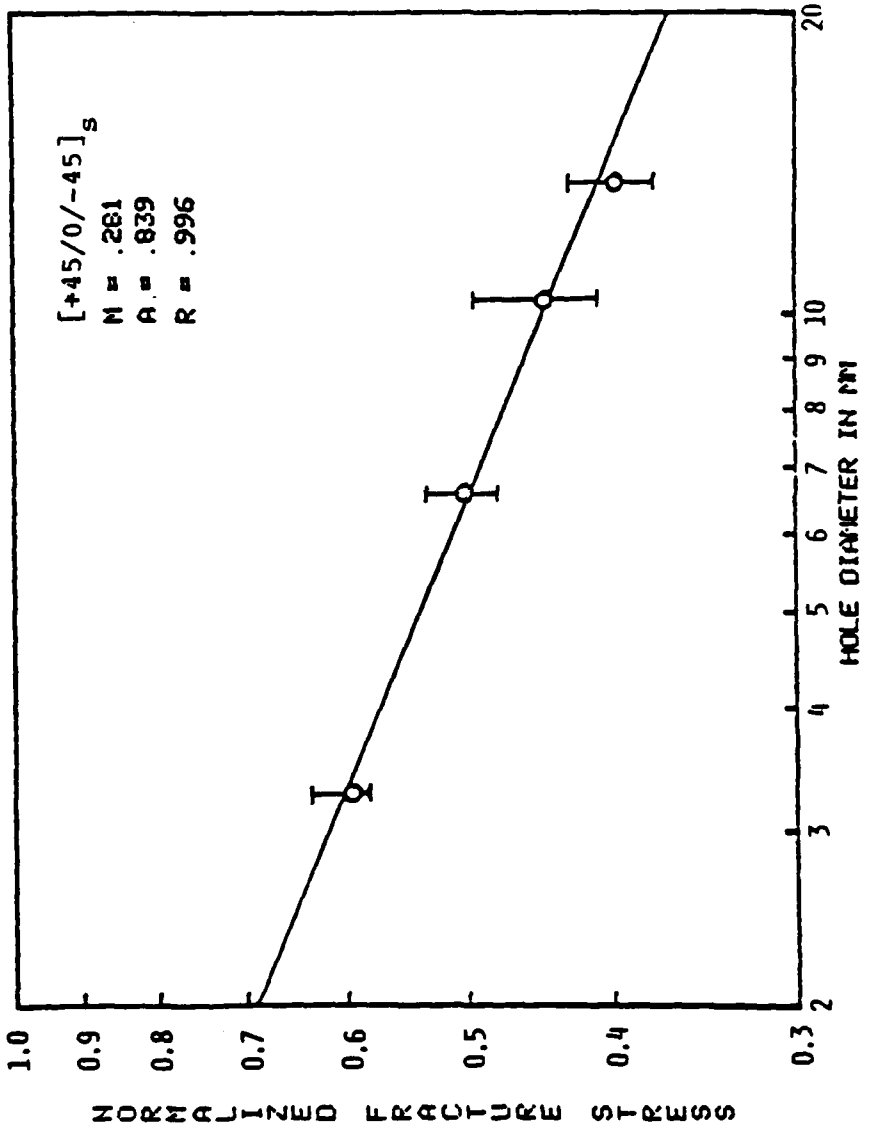

FIGURE 20 MAR-LIN PLOT FOR $[+45/0/-45]_s$

TABLE 13

SUMMARY OF PARAMETERS FOR MAR-LIN EQUATION FROM LINEAR REGRESSIONS

Laminate	Slope = m	A [mm to the m power]	Correlation Coefficient = R
$[\pm 15]_s$	.399	1.264	.997
$[\pm 30]_s$	.419	1.496	.999
$[\pm 45]_s$	.188	1.233	.932
$[\pm 60]_s$	.249	1.261	.957
$[\pm 75]_s$	.264	1.133	.909
$[90_4]$	.399	.519	.876
$[\pm 5/0]_s$	.200	1.063	.964
$[\pm 10/0]_s$	.381	1.334	.998
$[\pm 15/0]_s$	.284	1.023	.983
$[\pm 20/0]_s$	.283	1.116	.965
$[\pm 25/0]_s$	.400	1.258	.985
$[\pm 30/0]_s$	.442	1.281	.998
$[\pm 35/0]_s$	.293	1.011	.983
$[\pm 45/0]_s$	.233	.777	.974
$[\pm 60/0]_s$	.259	1.073	.960
$[\pm 75/0]_s$	.242	1.098	.936
$[90_2/0]_s$	.276	1.306	.887
$[0/\pm 5]_s$	.272	1.059	.999
$[0/\pm 10]_s$	.281	.972	.986
$[0/\pm 15]_s$	.293	.929	.965
$[0/\pm 30]_s$	.307	.807	.999
$[0/\pm 45]_s$	.292	.800	.999
$[0/\pm 60]_s$	.337	.992	.992
$[0/\pm 75]_s$	.218	.967	.995
$[0/90_2]_s$	.104	.905	.946
$[+15/0/-15]_s$	.280	1.287	.993
$[+30/0/-30]_s$	.334	1.122	.994
$[+45/0/-45]_s$	.281	.839	.996
$[+60/0/-60]_s$	.287	1.029	.992
$[+75/0/-75]_s$	.307	1.047	.999
$[90/0/90]_s$	.283	.895	.999

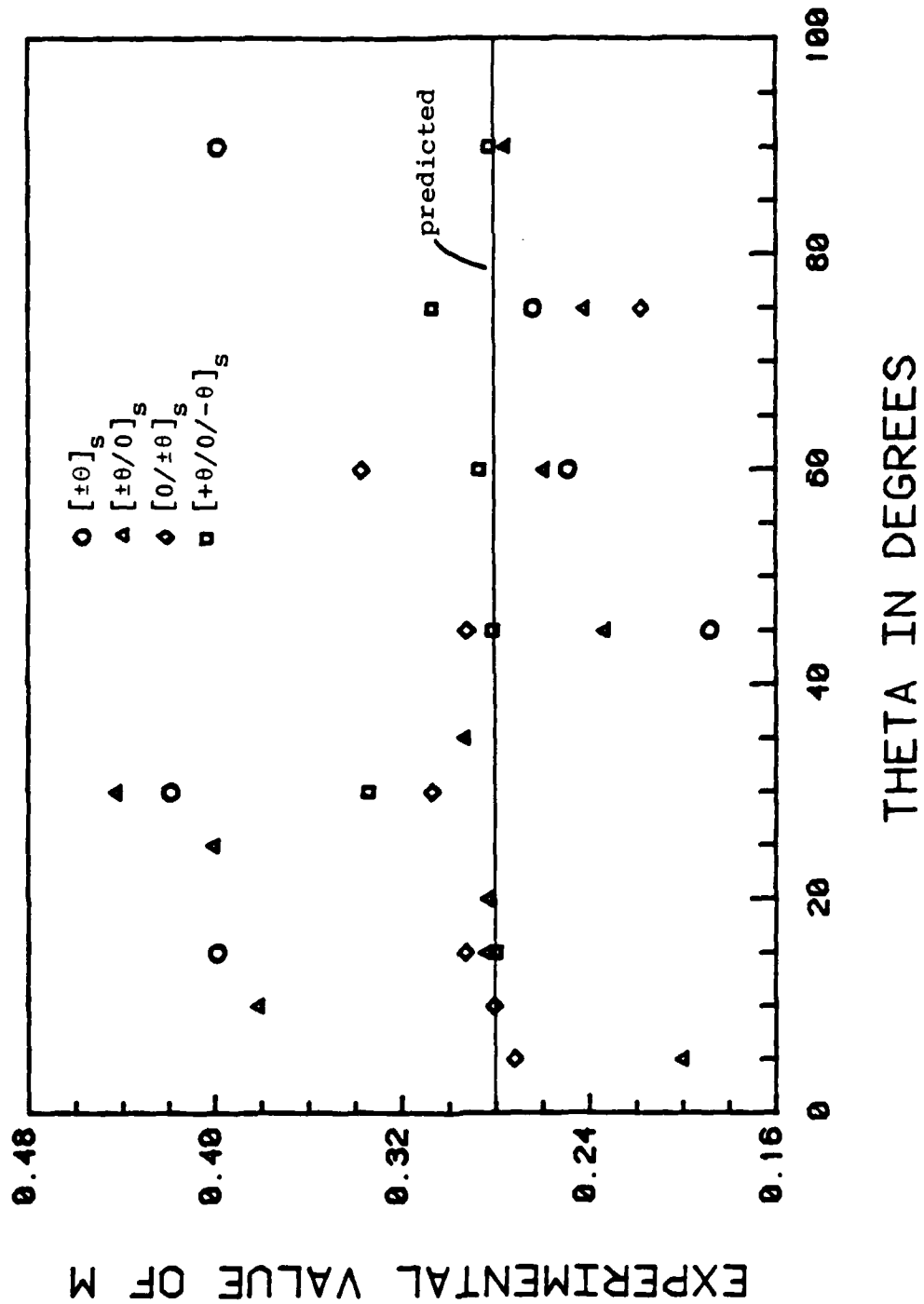

FIGURE 21 EXPERIMENTAL VALUES OF m FOR MAR-LIN EQUATION VERSUS LAMINATION ANGLE

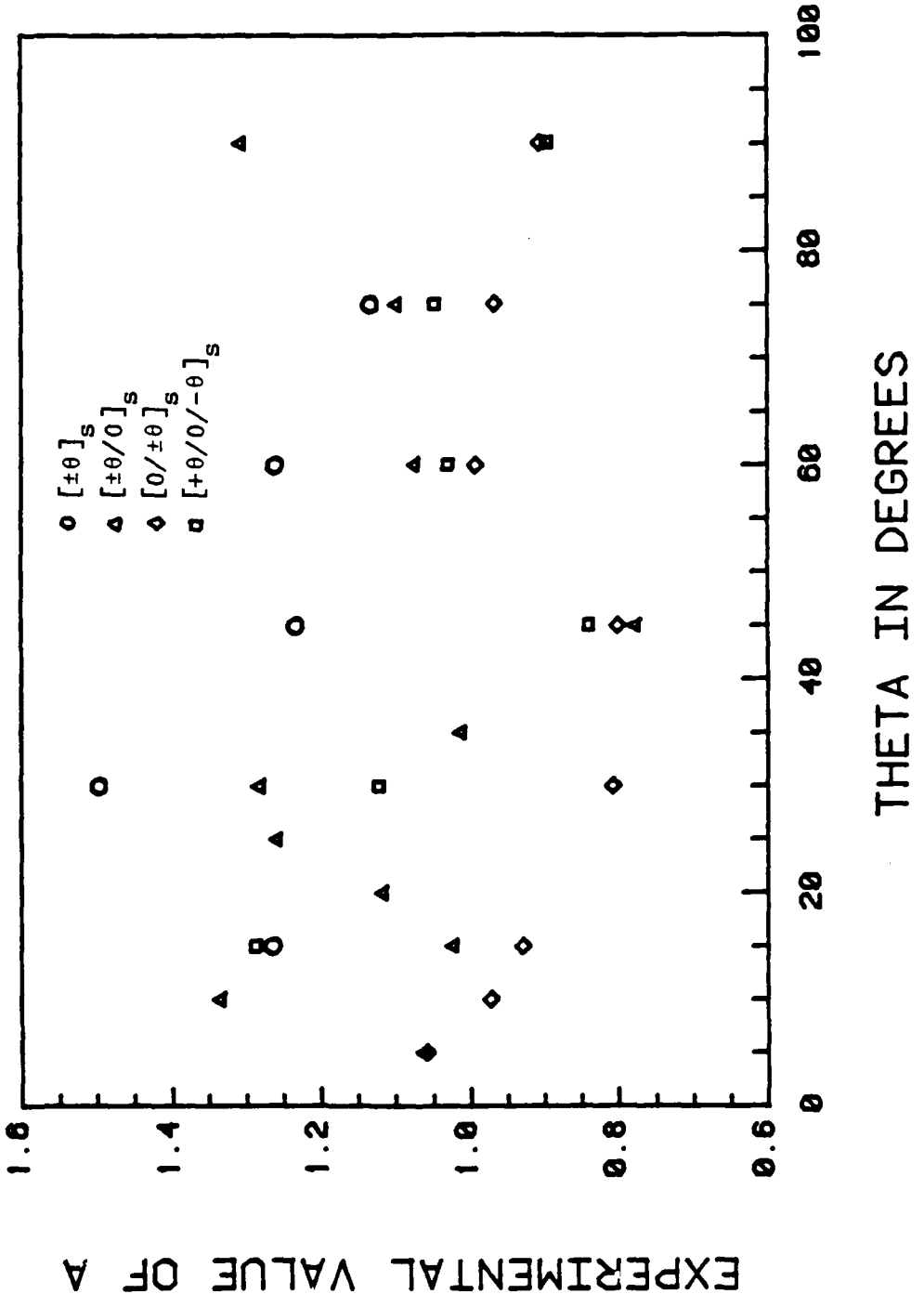

FIGURE 22 EXPERIMENTAL VALUES OF A FOR MAR-LIN EQUATION VERSUS LAMINATION ANGLE

are data from earlier investigations by Garcia and McManus [1,2,3] for the following laminates: [+-5/0]s, [0/+-5]s, [+-10/0]s, [0/+-10]s, [+-20/0]s, [+-25/0]s, and [+-35/0]s.

The results from the tests of the [θx8] specimens are not included here. These notched coupons failed at very low loads. These load levels were on the order of the accuracy of the testing machine. This was demonstrated by the high coefficient of variation for these specimens. In some cases the act of gripping the specimen caused failure. This data is therefore not useful and is not reported.

The data shows that the Mar-Lin equation generally works very well. In all cases the goodness of fit parameter for the linear regression was above .90 with many near .98. The regressions did yield experimentally-determined slopes near .28 which is the theoretical value of m as previously discussed. An important factor to consider here is the inherent scatter in the fracture stress data and thus the reproducibility of values of m. Scatter can occur for a number of reasons: variability in material lots, differences in curing, etc. Previous experiments by Mar and Lagace [18] yielded experimental values for m of .334 for the [+-30/0]s laminate and .234 for the [+-45/0]s laminate. Comparison of these values with the values obtained in the current investigation shows that the two values of m for the [+-45/0]s laminate agree quite well while the two values for the [+-30/0]s laminate (.334 and .44) are different.

A second factor to consider in examining the experimental values of m is the effect of interlaminar stresses and subsequent delamination as a fracture mode. If one considers Table 13, two laminates stand out as having extremely poor correlations with equation 2.2. The data for laminate [0/+-75]s yields a value of m of .218 while the data for the [0/90x2]s laminate yields a value of .104 for m. In order to explain this discrepancy it is necessary to consider fracture modes in the same vein as in section 2.1. Recalling that discussion, fracture can be separated into two different modes: in-plane and out-of-plane. This out-of-plane mode, known as delamination, results from interlaminar stresses which arise at a free edge. A hole is a free edge and thus will have interlaminar stresses which can cause delamination. The Mar-Lin theory is a correlation for in-plane fracture. Thus, if a laminate fails via delamination, the correlation should not apply. All the other laminates, but the two discussed here, fail via in-plane modes. Examination of the [0/+-75]s specimens show that these notched specimens fail via delamination. Since the correlation is not applicable, the experimental fit would be expected to be poor as is obtained.

The [0/90x2]s laminate is even more interesting. A post-mortem examination of the fractured specimens show that the failure is due to delamination for the two small hole sizes, 3.175 mm and 6.35 mm diameters, while specimens with the

larger holes fail via an in-plane mechanism. This can readily be seen in Figure 23 which shows photographs of the post-mortem fracture modes of a [0/90x2]s specimen with a 3.175 mm hole and one with a 12.7 mm hole. It is clearly evident in these side views of the specimens that the former specimen delaminates while the latter does not.

The plot in Figure 24 shows this in-plane versus out-of-plane phenomenon. The solid line shows the Mar-Lin correlation for the specimens with the latter two hole sizes failing in-plane giving the theoretical value of m of .28. However the two smaller holes fail by delamination so they never reach the in-plane critical stress. This can be explained by the fact that the interlaminar stress state will change as the hole size changes thereby changing the fracture mode from in-plane to out-of-plane or vice versa. More research is necessary in order to apply interlaminar stress calculation techniques to free boundaries such as holes in order to determine some criterion for out-of-plane fracture.

The other parameter in the proposed correlation, the "composite fracture toughness" H_c, has been "normalized" by the unflawed fracture stresses into the parameter A (with units of length to the m power). Referring to Table 13, it can be seen that these values fall in a band somewhere near the value of 1.0. This implies that at a certain flaw size, in this case approximately 1.0 mm, the fracture stress is equal to the

(a) (b)

FIGURE 23 SIDEVIEW PHOTOGRAPHS OF POST-MORTEM FRACTURE MODES OF $[0/90_2]_s$ SPECIMENS WITH (a) A 3.175 mm DIAMETER HOLE AND (b) A 12.7 mm DIAMETER HOLE

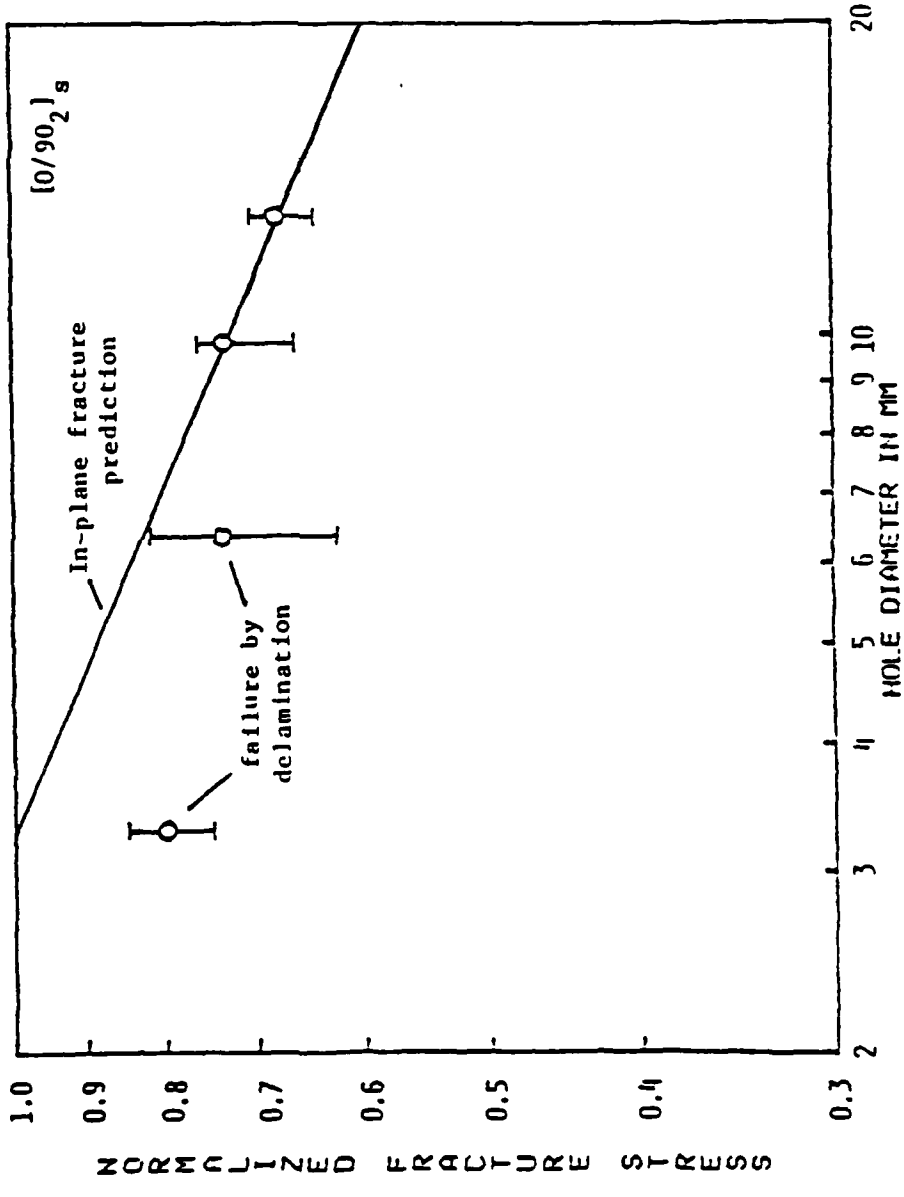

FIGURE 24 MAR-LIN PLOT FOR $[0/90_2]_s$ LAMINATE SHOWING IN-PLANE VERSUS OUT-OF-PLANE FAILURES

unflawed fracture stress. Thus, the correlation does not hold for smaller notch sizes and the unnotched in-plane mechanics of failure dominate for flaw sizes below this critical notch size. Drawing an analogy to Linear Elastic Fracture Mechanics, there is a similar initial flaw size in metals below which metals are "insensitive" to the flaw and fail at the virgin ultimate stress. This size is also a function of the fracture toughness divided by virgin ultimate strength. Thus, the current data indicates that there is some flaw size below which the composite material behaves as if it were unflawed (in the macroscopic sense). The indication is that this flaw size is most likely material dependent. This has important implications in the inspection of composite structures for damage tolerance. Identifying such a "critical flaw size" would give a threshold of flaw size below which a structure would be considered undamaged.

Further work is currently being performed to better understand the phenomena discussed here. This work is coupled with the ongoing work reported in Section 2.1. There are two basic directions which this research is taking and they both deal with thicker laminates. The first direction isolates the thickness phenomena and laminates are being tested with "effectively-increased" ply thicknesses. That is, a specimen with a [+15/0/-15]s stacking arrangment has the ply thickness "effectively-increased" by having several plies of each layer

adjacent to each other. That is the new stacking sequence is [+15xn/0xn/-15xn]s where n can be any integer.

The second direction involves laminates which have an additional pair of angled plies where the lamination angle of these plies are not equal to the lamination angle of the other pair. Thus laminates of the form [+-θ/+-α/0]s are being investigated. Stacking sequence will also be changed to investigate the effect of stacking sequence on both types of thicker laminates.

2.6 Fracture of Graphite/Epoxy Coupons with Slits

Implicit in the Mar-Lin theory discussed in Section 2.5 is that the flaw size and not its shape determines the fracture stress for in-plane fracture. Previous work at TELAC on boron/aluminum and graphite/epoxy has indicated this fact [19]. An investigation was undertaken to examine this for two different laminates of graphite/epoxy: [+-30/0]s and [+-45/0]s. Experiments were conducted on standard TELAC tensile coupons, as in Figure 1, with a machined slit in place of a drilled hole. The slits were manufactured using a jeweler's blade. Three different slit sizes were used: 3.175 mm, 6.35 mm, and 12.7 mm.

The coupons were tested at a constant strain rate of 5000 microstrain/minute directly to failure. Fracture load was recorded and fracture modes were noted. Five specimens of each

TABLE 14

FRACTURE DATA FOR [±30/0]$_s$ AND [±45/0]$_s$
LAMINATES WITH SLITS AND HOLES

all values in [MPa]

Laminate	[±30/0]$_s$		[±45/0]$_s$	
Notch Type / Nominal Notch Size	Slit	Hole*	Slit	Hole*
3.175 mm	684 (4.2%)	624 (3.1%)	475 (4.1%)	473 (4.8%)
6.35 mm	598 (5.9%)	475 (2.9%)	404 (4.8%)	405 (6.8%)
12.7 mm	465 (2.3%)	382 (6.5%)	311 (3.2%)	341 (7.1%)

Mean (Coefficient of Variation)
5 Specimens of each type

*Data from Reference 18

type were tested as summarized in Table 14. Included in this table are the average values for the fracture stresses of these specimens and a comparison with the fracture stresses for similar specimens with holes as reported by Mar and Lagace [18]. It can readily be seen that the specimens with holes and slits of the same size fail at very nearly the same stress for the [+-45/0]s laminates while those of the [+-30/0]s laminates have a greater discrepancy.

More importantly, the data was correlated using the Mar-Lin equation in the same manner discussed in section 2.5. The data yields a value of m of .306 and a value of A of .939 for the [+-45/0]s laminate and a value of m of.278 and a value of A of 1.125 for the [+-30/0]s laminate. These values of m are approximately the same as the value of .28 expected from the Fenner solution.

In addition to the fracture data and the fracture modes, the strain intensity in the vicinity of the crack was investigated by using strain gages placed on a line away from the crack. This data and the previous data is discussed in depth in a report by Hoehn [20].

2.7 Tensile Fracture of Graphite/Epoxy with Angled Slits

Since the assumption behind the Mar-Lin theory says that the flaw size and not the shape is important in fracture, an inves-

tigation was undertaken to look at the fracture behavior of standard tensile coupons with angled slits. That is, the slits were fabricated at different angles to the applied load. The important parameter in this case would thus be the projection of the slit in the direction of the applied load, 2a, as illustrated in Figure 25. A slit length of 12.7 mm (1/2 inch) was chosen for this experiment. Five different slit angles were chosen to give five different "effective widths". These are summarized and represented in Figure 26. The previous investigation by Hoehn [20] only investigated slits with slit angles of 90°.

These coupons were tested using standard procedures and a constant strain rate of 5000 microstrain/minute. Again, data was recorded automatically using a PDP-11/34 computer. Fracture load was recorded and photographs taken of the post-mortem fracture mode. The fracture stress data is summarized in Table 15. Two important observations can be made. The first is that for the same "effective" notch size the fracture stresses are approximately the same for the two different stacking sequences used: [+-30/0]s and [0/+-30]s. The second observation is that a coupon is insensitive to a very narrow slit which is parallel to the applied load. In this case, the slit angle of 0° gives an "effective width" of very near zero. Since this notch size is smaller than the critical flaw size of approximately 1 mm discussed in section 2.5, it is expected that the fracture

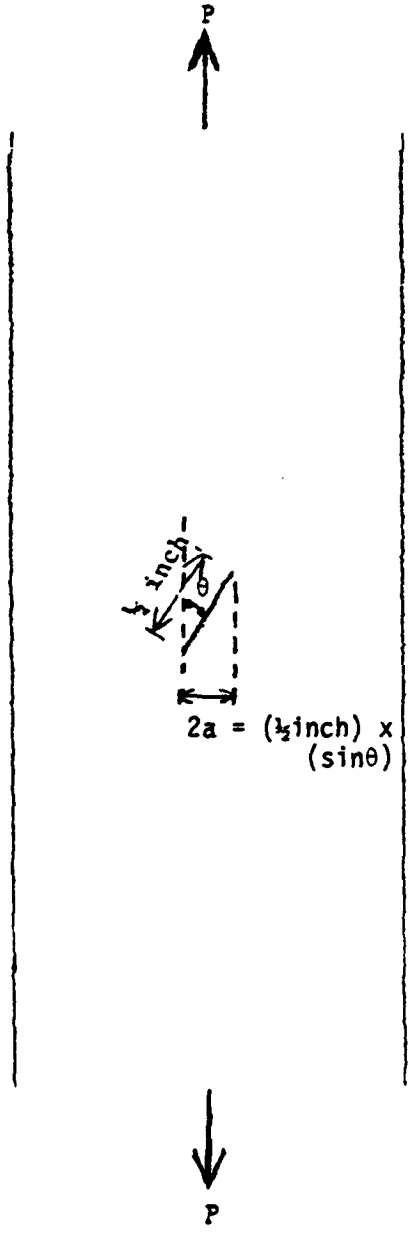

FIGURE 25 ANGLED SLIT IN A COUPON AND THE "EFFECTIVE WIDTH"

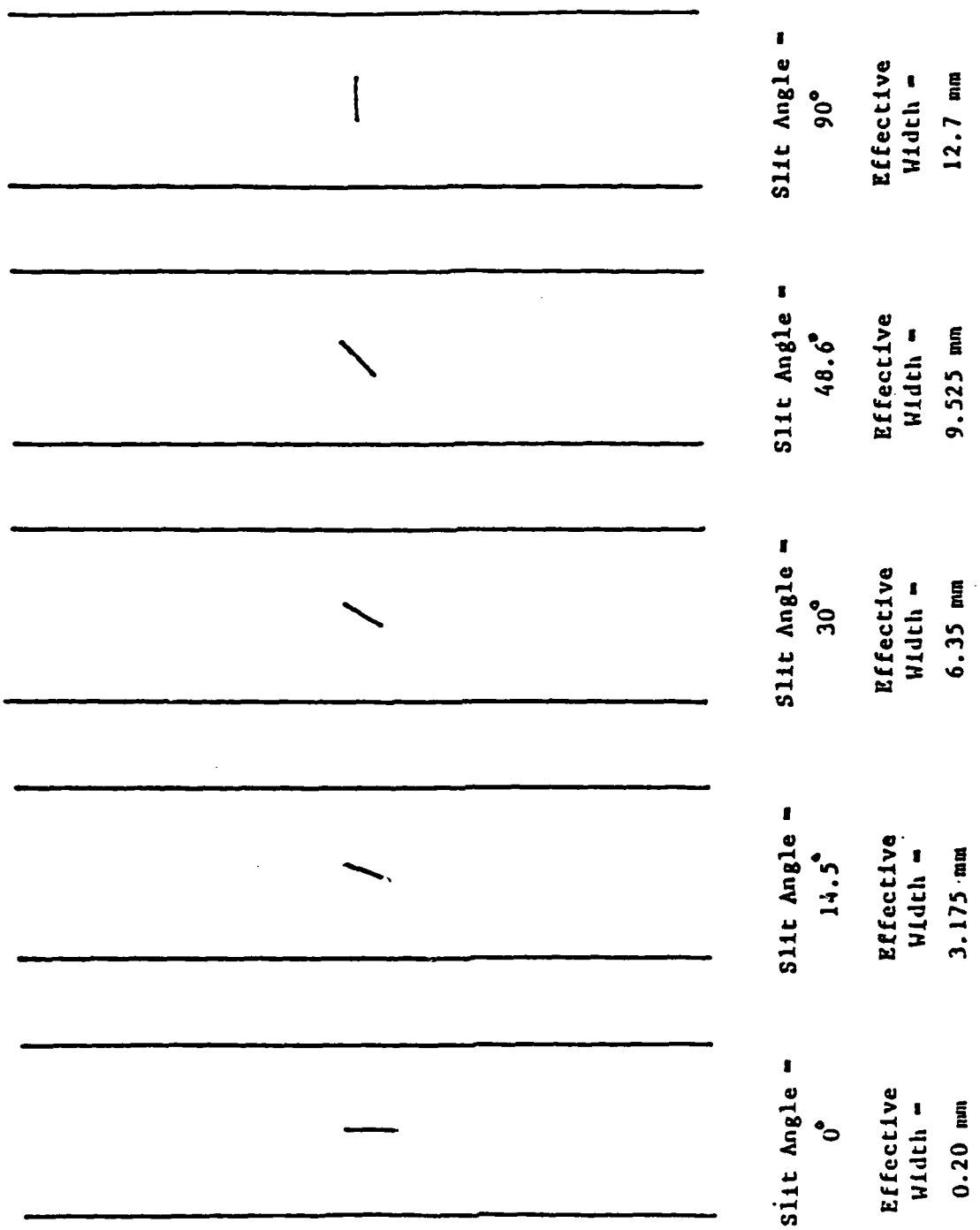

FIGURE 26 "EFFECTIVE WIDTHS" AND SLIT ANGLES USED IN INVESTIGATION

TABLE 15

FRACTURE STRESSES OF SPECIMENS WITH ANGLED SLITS

all values in [MPa]

Slit Angle	Nominal Effective Width	Laminate	
		$[\pm 30/0]_s$	$[0/\pm 30]_s$
0°	0.20 mm	845 (6.8%)	846 (3.8%)
14.5°	3.175 mm	551 (3.4%)	550 (6.3%)
30°	6.35 mm	520 (12.9%)	493 (4.0%)
48.6°	9.525 mm	421 (7.8%)	419 (11.1%)
90°	12.7 mm	382 (7.4%)	362 (7.9%)

Mean (Coefficient of Variation)
4 specimens of each type

All slit lengths = 12.7 mm

stress should be the same as the unflawed fracture stress. In fact, data from Lagace [5] for the [+-30/0]s laminates gives an unflawed fracture stress of 855 MPa. The current investigation yielded a fracture stress of 845 MPa for such a specimen with a slit angled at 0°. Thus this specimen is insensitive to a parallel slit. Data from Lagace for a [0/+-30]s unflawed laminate gives an unflawed fracture stress of 945 MPa. This is about 10% higher than the fracture stress of 846 MPa found for the [0/+-30]s specimens with a the slit parallel to the applied load. A possible explanation for this fact is that delamination was observed in the post-mortem fracture mode at the edge of the slit. This could lower the fracture stress.

The data was correlated with equation 2.2 by using the effective width for 2a. The correlations are presented in Figures 27 and 28. These correlations yield an experimental value of m of .270 for the [+-30/0]s laminate and .293 for the [0/+-30]s laminate. These are very close to the predicted value of .28. The results are also similar to those obtained by Hoehn for different slit widths but slit angles always at 90°. It is interesting to note, however, that in the current investigation the specimens with slit angles which correspond to the lamination angle, 30°, giving an effective width of 6.35 mm, have average fracture stresses which fall above the regression line. Whether or not this is attributable to scatter or is a

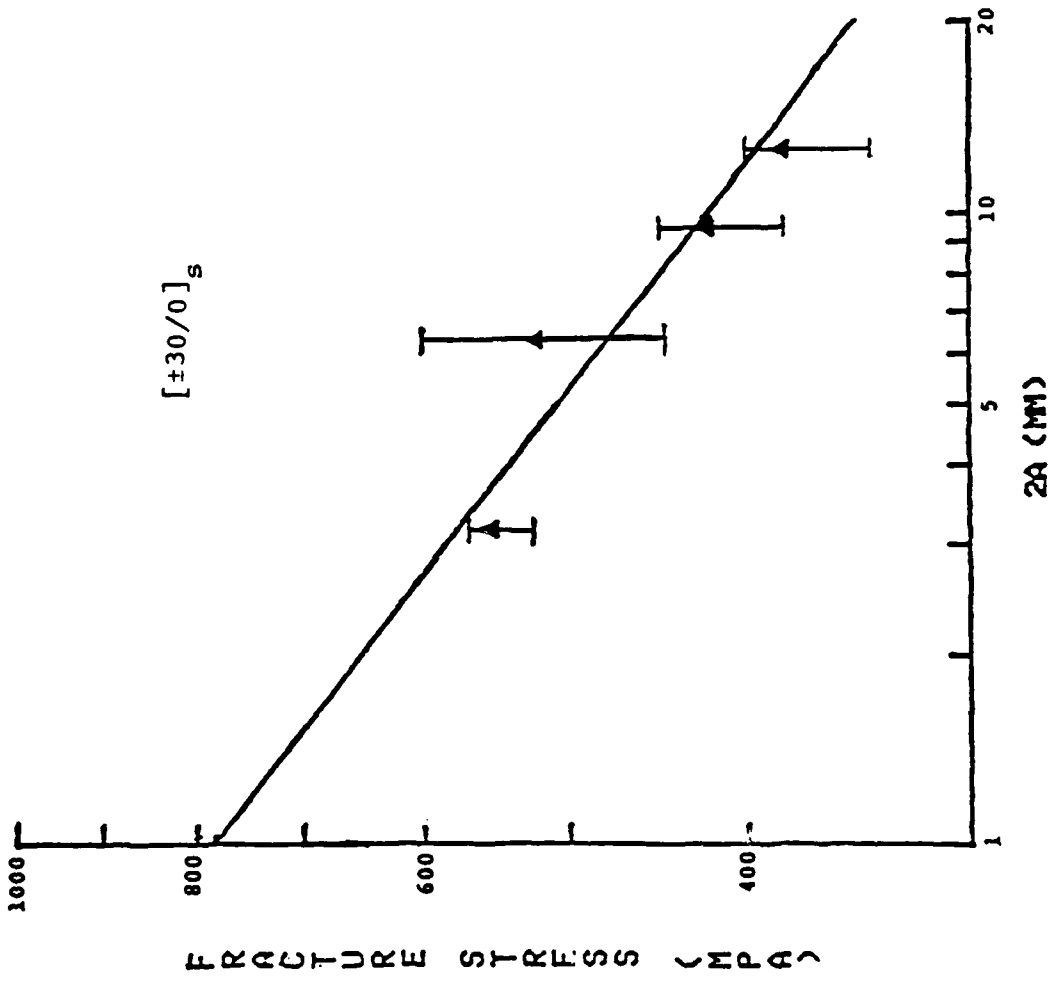

FIGURE 27 MAR-LIN CORRELATION FOR $[\pm 30/0]_s$ LAMINATE USING "EFFECTIVE WIDTH" AS 2a

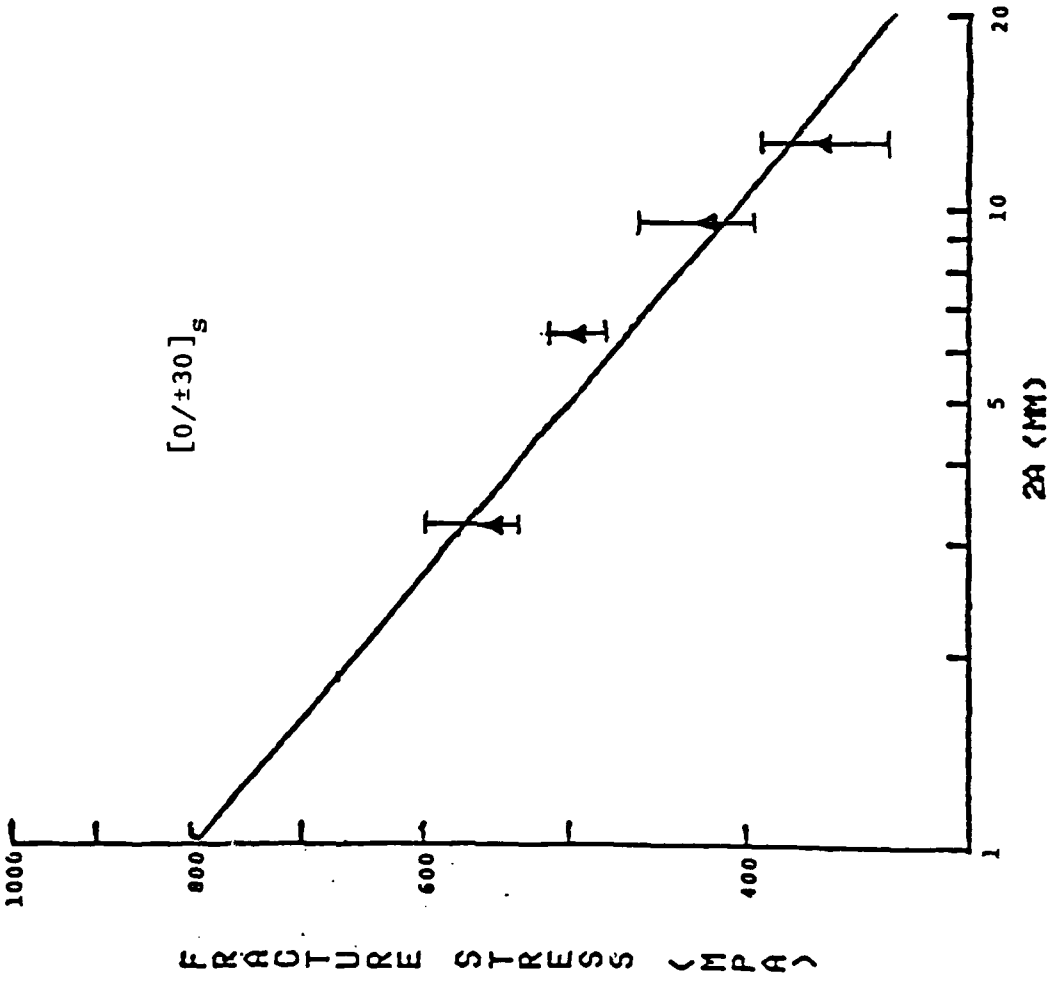

FIGURE 28 MAR-LIN CORRELATION FOR $[0/\pm30]_s$ LAMINATE USING "EFFECTIVE WIDTH" AS 2a

real effect due to the slit angle corresponding to the ply angle is still in question.

This work is reported by Brewer in Reference 21.

2.8 Tensile Fracture of Notched Graphite/Epoxy Fabric

Tensile coupons manufactured from Hercules A370-5H/3501-6 fabric were tested with notches to check for the validity of the Mar-Lin correlation for graphite/epoxy fabric. In an initial investigation conducted by Graves [22], a total of 90 coupons were manufactured and tested. Half of these were of the (0,45)s laminate and the other half of the (45,0)s laminate. For fabric, the ply angle refers to the angle which the warp fiber makes with the laminate axes. Thus, the fill fibers are at a 90° angle to the reported ply angle. The coupons were tested at 5000 microstrain/minute on an MTS 810 testing machine using the standard procedure.

Specimens with both holes and slits were tested with nominal hole diameters and slit lengths of 3.175 mm, 6.35 mm, and 12.7 mm. In addition, unnotched specimens were tested as controls. Five specimens of each flaw type, size, and laminate type were tested. The fracture stresses of the majority of these specimens are reported in Table 16. The log-log plot of the data is shown in Figures 29 and 30 using equation 2.2. The data yields an experimental exponent m of .28. Although the fabric is dif-

TABLE 16

FRACTURE STRESSES OF $(0, 45)_s$ AND $(45, 0)_s$
GRAPHITE/EPOXY FABRIC COUPONS

all values in [MPa]

Laminate	$(0, 45)_s$		$(45, 0)_s$	
Nominal Notch Size \ Notch Type	Hole	Slit	Hole	Slit
Unnotched	626 (2.2%)		615 (1.4%)	
3.175 mm	525 (3.1%)	550 (1.9%)	520 (1.7%)	534 (3.7%)
6.35 mm	453 (4.5%)	469 (3.1%)	453 (4.4%)	469 (4.2%)
I -6.35 mm	--	469 (2.3%)	--	447 (4.6%)
12.7 mm	361 (2.9%)	377 (3.8%)	331 (4.6%)	387 (4.4%)

Mean (Coefficient of Variation)
5 specimens of each type

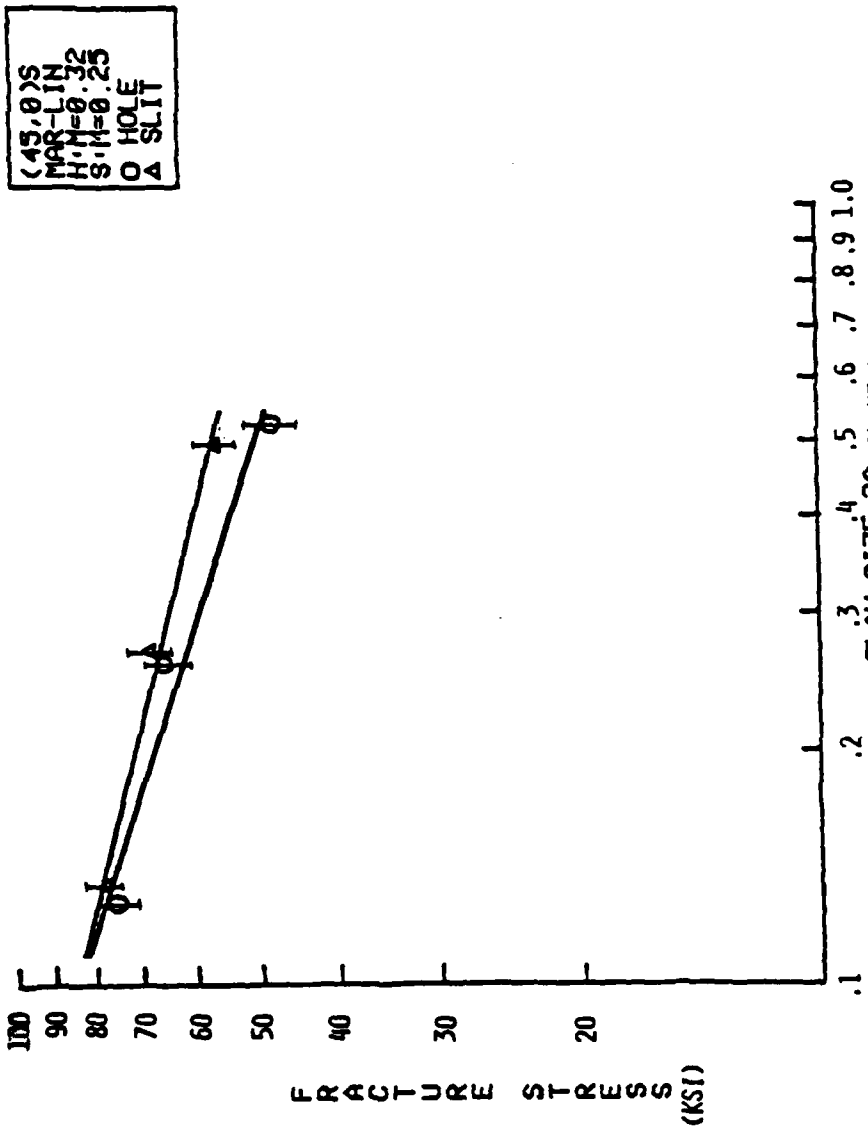

FIGURE 3 MAR-LIN CORRELATION FOR $(45,0)_S$ COUPONS

FIGURE 29 MAR-LIN CORRELATION FOR $(45,0)_s$ FABRIC LAMINATE

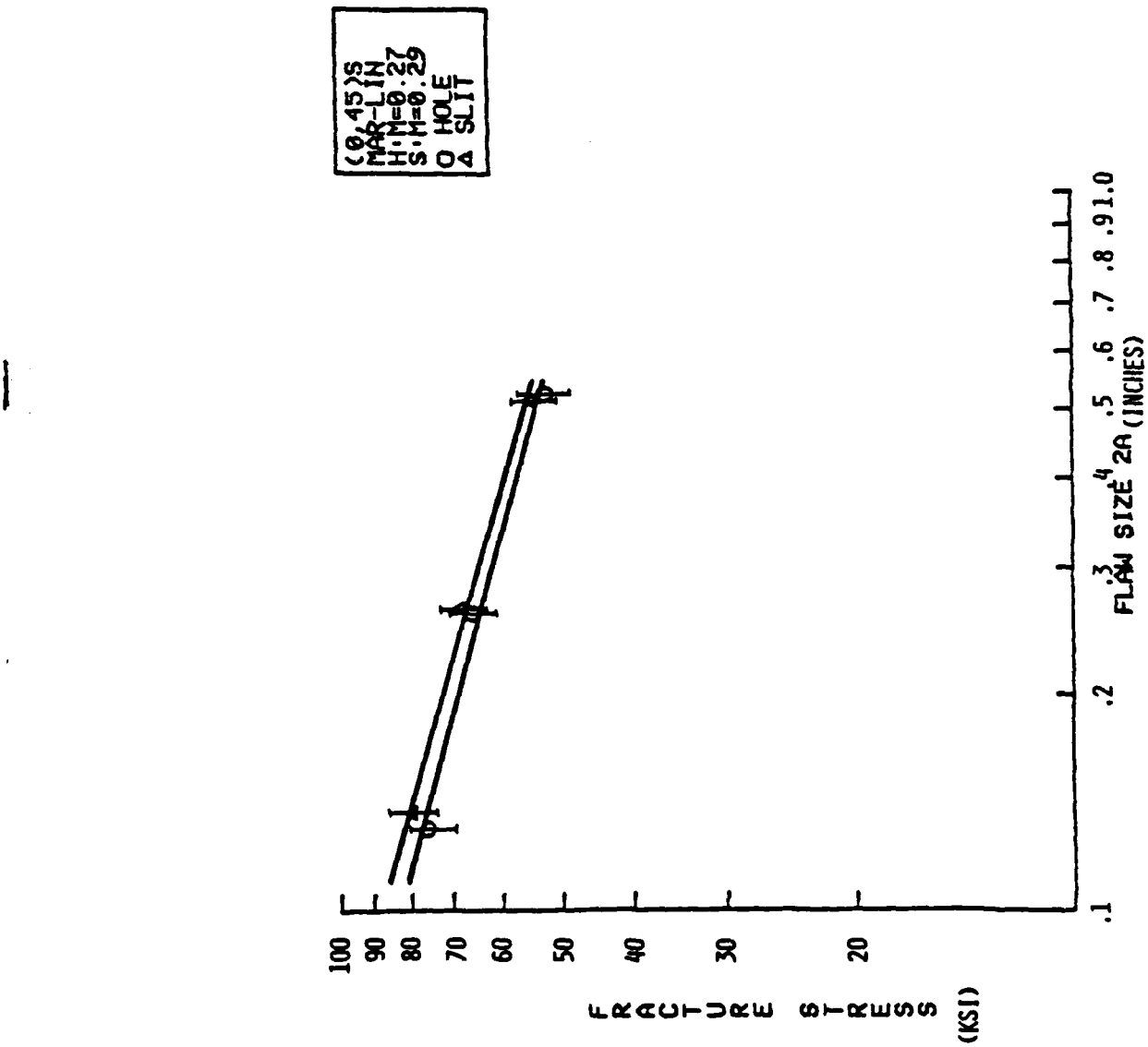

FIGURE 30 MAR-LIN CORRELATION FOR $(0,45)_s$ FABRIC LAMINATE

ferent from the tape, the theoretical value of m is still .28 since this is derived by considering the stress singularity as discussed in section 2.5. This basic situation does not change when using a fabric over a tape. Thus the exponent remains the same.

The second important fact which this data shows is that, again, the notch size and not shape controls the fracture stress. This is shown by the fact that coupons with holes or slits of the same size fail at the same fracture stress. In addition, several coupons had slits which were made using an guillotine-type impact mechanism. These are identified by the I before the notch size in Table 16. These slits did have some delamination on the backsides and were not of the perfect shape as the handmade slits using the jeweler's blade. However, the fracture stresses were the same as those specimens with the handmade slits of the same size. This gives further evidence as to the fact that notch size and not shape is the important factor in determining in-plane fracture stress.

The remaining ten specimens which were tested had "special" slits in them. In these cases the slits were either parallel to the load (slit angle equals 0°) or with a slit angle of 45°. These tests are similar to the ones reported in Section 2.7 on laminates fabricated from tape. The fracture stresses of these specimens are reported in Table 17. The fracture stresses of the specimens with slits parallel to the applied load were the

TABLE 17

FRACTURE STRESSES OF GRAPHITE/EPOXY
FABRIC SPECIMENS WITH "SPECIAL" SLITS

Slit Angle	Nominal Effective Width	Number of Specimens	Laminate	
			$(0, 45)_s$	$(45, 0)_s$
0°	0.20 mm	2	626 MPa (0.1%)	587 MPa (3.7%)
45°	4.49 mm	3	515 MPa (4.3%)	507 MPa (8.2%)

Mean (Coefficient of Variation)

All slit lengths = 6.35 mm

same as the unnotched fracture stress for that laminate as reported in Table 16. The laminates with slit angles of 45° had an "effective width" of about 4.7 mm. This fracture data correlated well with the other data if the effective flaw width was used. This is exactly as Brewer [21] found as reported in Section 2.7.

Work is continuing in this area of the sensitivity of graphite/epoxy laminates manufactured from cloth to various notches. A number of different four-ply laminates are being investigated. Each laminate will have unnotched specimens and specimens with four different hole sizes. Some initial results from this program indicate that delamination at holes is very important in graphite/epoxy fabric and must be considered in aplying in-plane fracture criteria as discussed by Lagace [8].

2.9 Development of a Compression Specimen for Composites

It is also important to investigate the behavior of composites in compression. This is true for all the fracture work described previously as well as for the fatigue work described in Section 3. Various specimens have been used and continue to be used to obtain compressive data on composite materials. These include 4-point bending sandwich beams, axial honeycomb-reinforced columns, thick and squat coupons, and coupons with restraining jigs. A project was undertaken to

investigate a means by which to test thin laminates (4 to 20 plies) under compressive loads. Sandwich beams have been used successfully in the past at TELAC [23] especially to monitor damage accumulation in fatigue. However, sandwich beams are more expensive to manufacture than simple coupon specimens. It is therefore desirable to develop a means by which to test standard coupon specimens, such as that in Figure 1, under compressive uniaxial load.

When a significant compressive load is applied to a standard coupon specimen, the specimen will buckle. A conservative estimate of this buckling load can be obtained by calculating the classical Euler column buckling load for a coupon. If this critical load is compared to the load necessary for in-plane fracture as calculated by the Tsai-Wu stress interaction criterion [24], a laminate thickness to specimen length ratio can be determined where the buckling load would equal the in-plane fracture mode. This is plotted for various values of the ply angle for six-ply laminates of the form $[+-\theta/0]s$, $[0/+-\theta]s$, and $[+\theta/0/-\theta]s$ in Figure 31. In order to insure that buckling would not occur, thickness/length ratios greater than the reported critical ratio would be necessary. Figure 31 indicates that these ratios would be on the order of .2. Thus for a six-ply specimen with a thickness of .81 mm, the specimen length could be no greater than 4 mm. This would make the proper introduction of load difficult if not impossible.

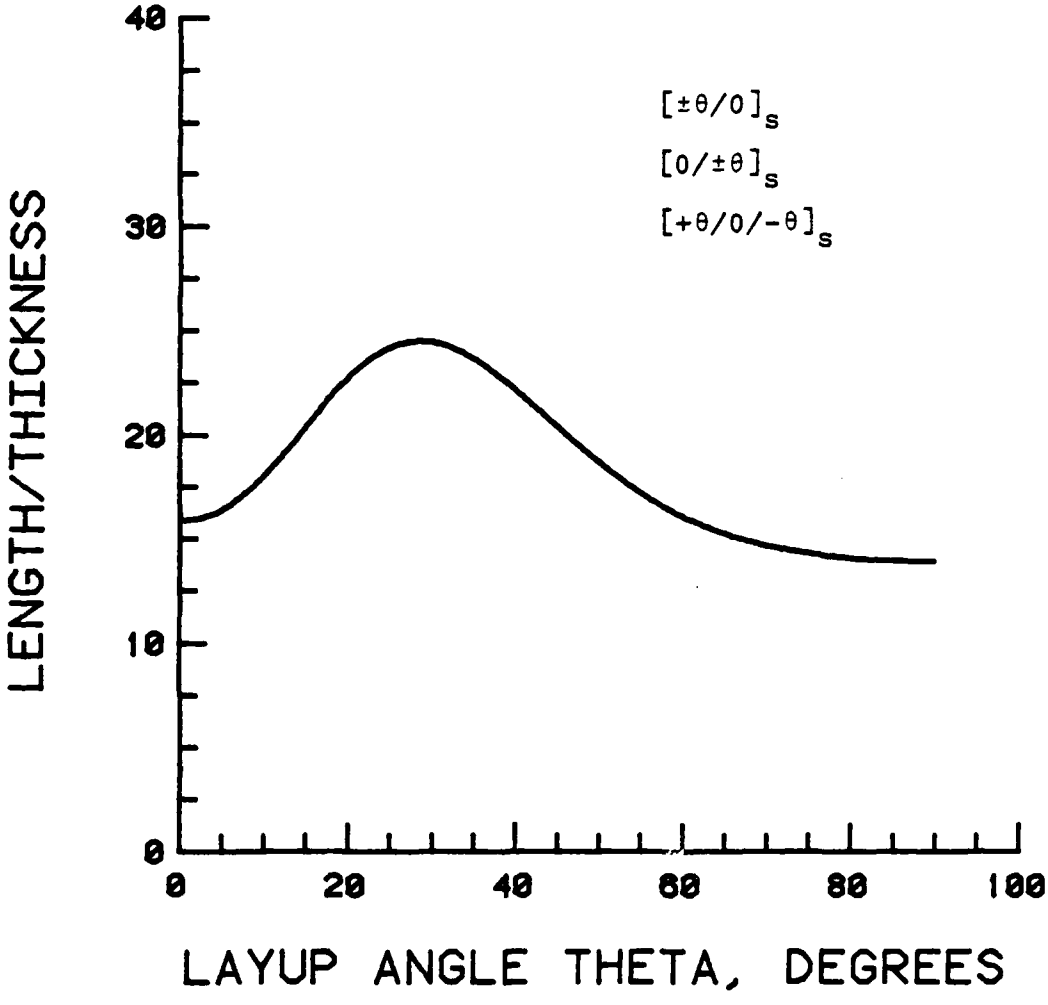

FIGURE 31 CRITICAL LENGTH-TO-THICKNESS RATIO SO THAT EULER BUCKLING LOAD EQUALS IN-PLANE FRACTURE LOAD FOR A SIX-PLY SYMMETRIC LAMINATE OF THE FORM ±θ, 0

It is therefore necessary to find some way to prevent a standard coupon from buckling. The bonded honeycomb sandwich structure is one method. However, that method is costly. Another method is to develop a restraining jig. This jig must meet several criteria in order to be useful for fracture and damage growth experiments:

1. The jig must prevent instability failures (buckling).
2. The jig must not prevent delamination failures nor alter the interlaminar stress state of the specimens.
3. The jig must not alter the coupons measured compressive strength by carrying load via coupon/jig friction, for example.
4. The jig must not cause failure at the tab/test section or the coupon/jig interfaces.
5. In notched specimens, the jig must be sure to cause failures at the notched area.

A number of jigs have been proposed and used as reported in the available literature. Some of these were fabricated and tried but did not yield acceptable fracture results. These jigs did produce acceptable stress-strain curves initially, but with increased loading, buckling occurred in local sections ultimately affecting the fracture stress of the specimen. A secession of jigs were then tried with each iteration eliminating problems encountered with the previous jig. The final

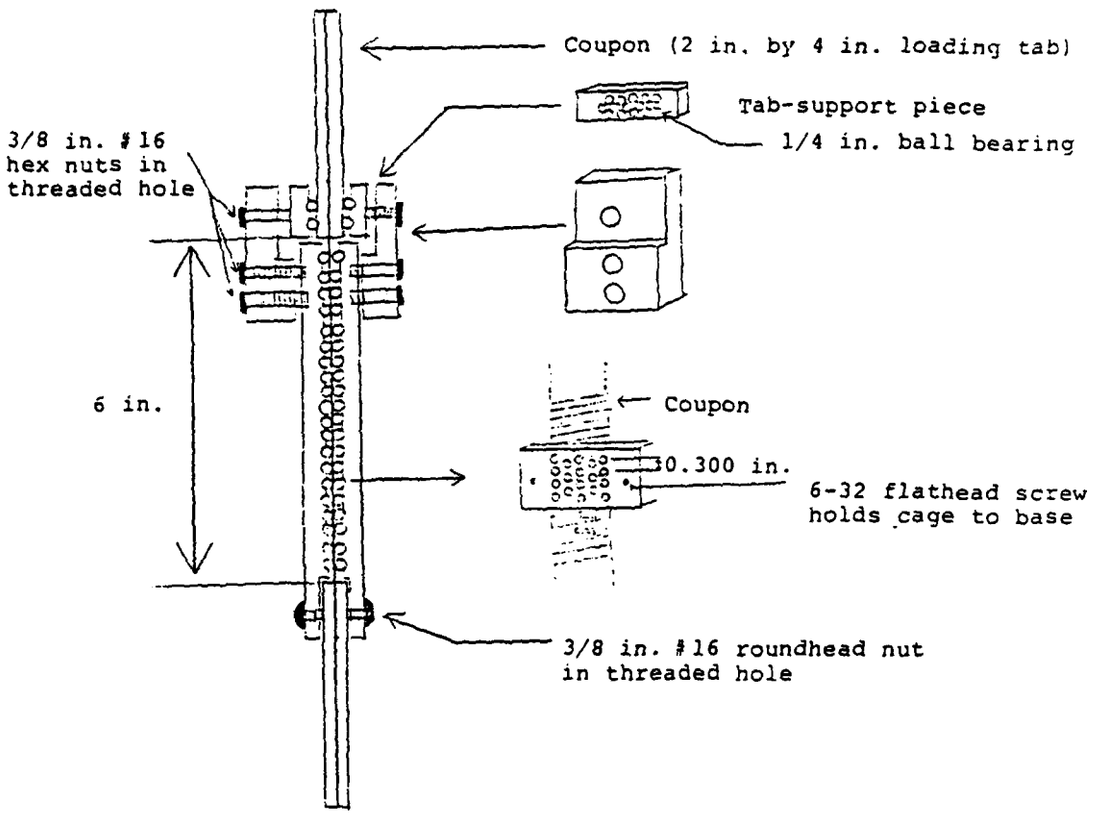

FIGURE 32 FINAL DESIGN OF TWO-PART BALL BEARING COMPRESSION JIG

AD A137 047 FRACTURE LONGEVITY (FATIGUE) DYNAMICS AND AEROELASTICITY OF COMPOSITE STR..(U) MASSACHUSETTS INST OF TECH CAMBRIDGE TECHNOLOGY LAB FOR ADVAN..

2/2

UNCLASSIFIED P A LAGACE ET AL. JUN 83 TELAC-83-11 F/G 11/4 NL

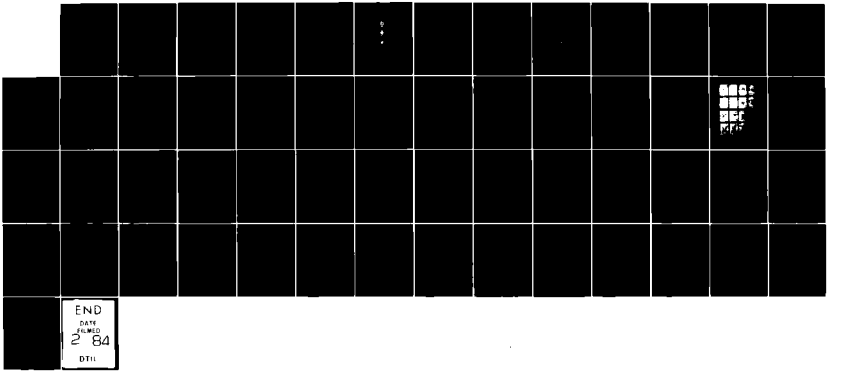

END

DATE FILMED

2 84

DTIC

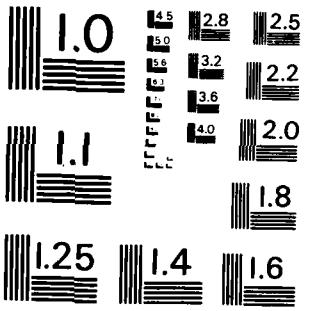

design is pictured in Figure 32. The jig consists of two steel plates each with one hundred steel balls that extend above a steel housing to support the coupon. These steel balls are free to roll insuring that little load is transferred to the jig by the coupon through friction. Since these balls are in contact with the coupon, the coupon is restricted from buckling by the force exerted by the steel balls. In addition, an arrangement was made to clamp the part of the loading tabs on the specimen which extended beyond the hydraulic grips of the machine as pictured in Figure 32.

Initial tests on standard coupon specimens using this jig yielded apparently good results. A small strain gage "window" was machined into the upper right hand section of the jig so that strain gages could be applied and the lead wires led out. Strain gages were applied on each side on the specimens and tests conducted. The results of a typical test are shown in Figure 33. Local buckling at the strain gage cutout "window" caused bending strains to occur as indicated in that Figure.

These results indicate that local buckling can occur at any unsupported area. This would include the area around a notch where damage accumulation measurements would be made or at any free edge which was left unsupported. However, if free edges are totally supported, the interlaminar stress state at the free edge would be altered since the boundary condition is

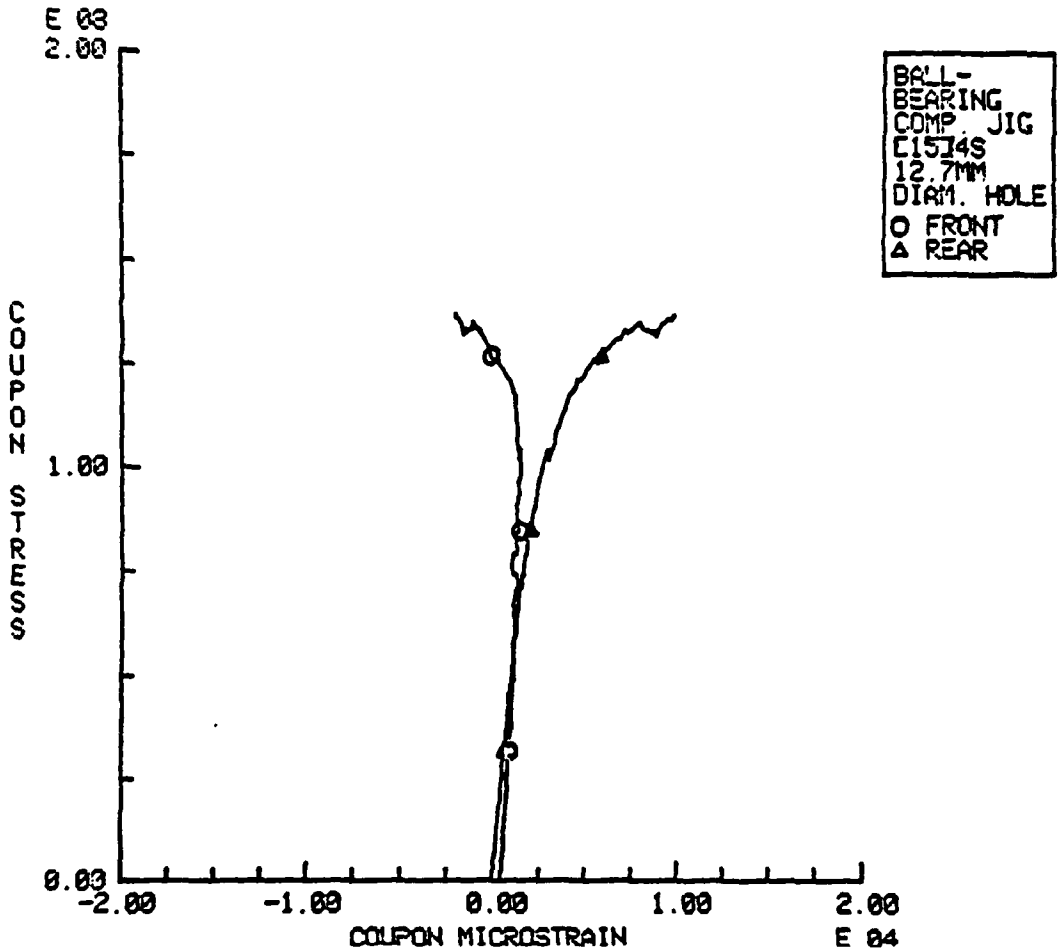

FIGURE 33 STRESS-STRAIN PLOTS FOR FRONT AND BACK SIDE OF COUPON IN RESTRAINING JIG

changed. Thus such an arrangement would violate one of the important assumptions.

The work has shown that the jig designed works well for obtaining elastic properties of composite coupons under compressive load but that fracture loads cannot be properly determined since local instabilities affect the stress distribution. However, this jig does represent improvement over other jigs as the steel balls which are free to rotate support the coupon without any important frictional loads. This work is fully reported by Dunmire in Reference 25.

A current investigation is underway which considers tubes as compressive specimens for laminated composites. A tube has a high moment of inertia and can thus resist Euler column buckling raising the critical stress above the in-plane compressive fracture stress. However, such considerations as shell buckling become important as local instabilities. The tubes being tested have length to radius ratios of about 5. Different stacking sequences and lamination angles are being tried.

3. LONGEVITY (FATIGUE)

The work at TELAC on the longevity of composite materials has been directed toward the study of damage modes and the accumulation of damage with repeated loading. The terminology "fatigue" and its connotations of S-N curves are not readily applicable to composites and thus, as suggested by Mar [26], the word "longevity" is purposefully used instead of "fatigue". The work to date has examined the growth of damage around notches under cyclic load. A notch is any macroscopic flaw purposefully introduced into the laminate. In these studies, the notch types considered have been holes and slits. The cyclic loads used have been tension-tension and compression-compression.

3.1 Split Propagation in Notched Unidirectional Coupons

Garcia [27] previously looked at the static failure of notched unidirectional composites. He found that the mode of failure was the propagation of a split from the edge of the notch parallel to the applied load. Splitting is a very important damage mechanism in many laminates and is defined as a crack running in the matrix parallel to the fiber. In a unidirectional specimen, the development of a split alleviates the stress concentration at the notch tip and eventually sepa-

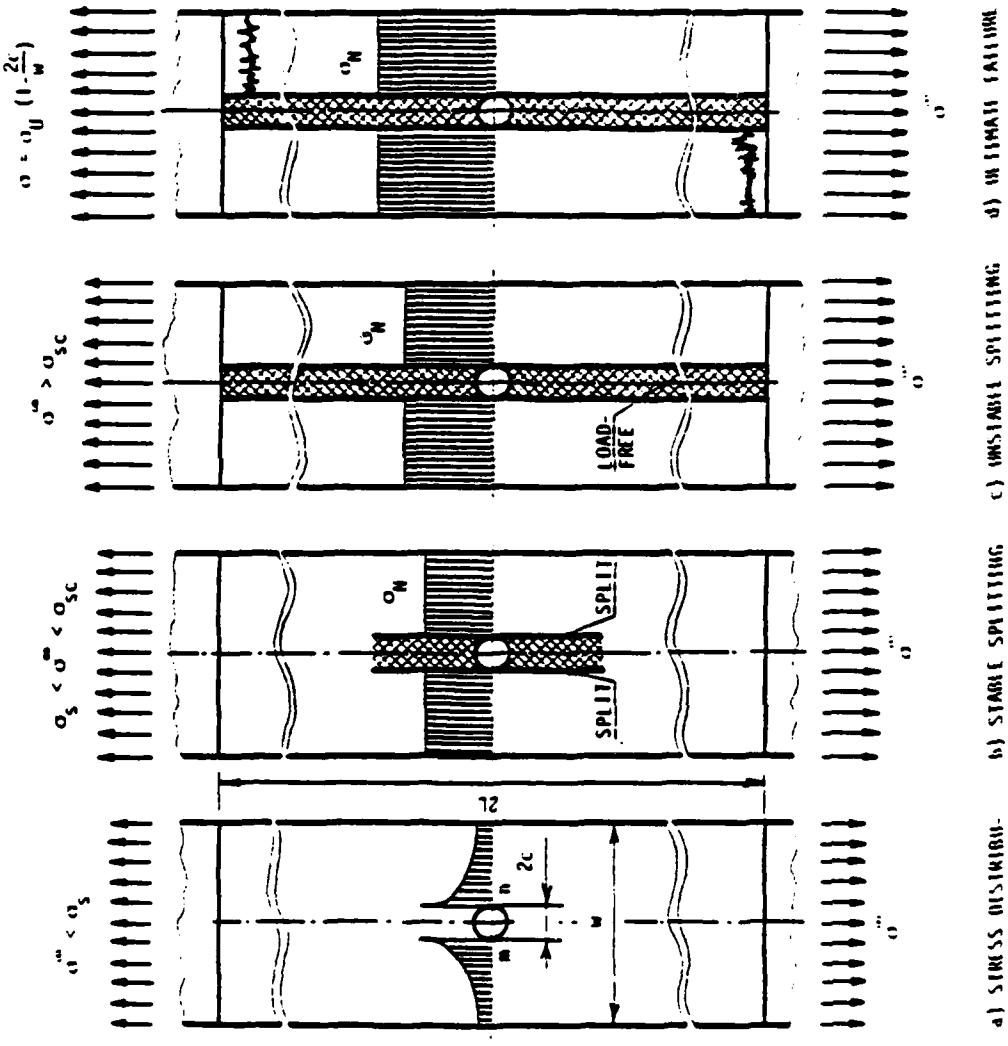

FIGURE 34 FAILURE MECHANISMS OF A UNIDIRECTIONAL COMPOSITE

rates the specimen into three sections, the middle of which does not carry any load as illustrated in Figure 34. The stress at which the split will propagate from the notch edge is known as the splitting stresse. The two undamaged portions of the specimen will then carry load until the ultimate virgin stress of the laminate is reached in each portion.

Lesieutre [28,29] later looked at the growth of these splits when similar coupons were loaded in cyclic tension-tension to a maximum stress below the static splitting stress. He found the split growth to correlate to the logarithm of the number of cycles and that this correlation depended on maximum cyclic stress and notch size. The latest investigation, conducted by Daken [30], looked at both the initiation and propagation of splits under tension-tension cycling in specimens with both slits and holes. A total of 120 unidirectional specimens were manufactured and tested. The specimens had slit and hole sizes of 3.175 mm, 6.35 mm, and 9.525 mm. Five specimens of each notch type and size were first tested monotonically to failure to determine the splitting stresses. The remaining specimens were tested in tension-tension fatigue at a stress ratio of .1 with three different maximum stress levels. The maximum stress levels were percentages of the static splitting stresses: 80%, 70%, and 60%. Five specimens of each notch type and size were tested for each stress level. The test program is summarized in Table 18.

TABLE 18

TESTING PROGRAM FOR SPLITTING INVESTIGATION

a. Static

Flaw Type	Hole			Slit		
Flaw Size	1/8"	1/4"	3/8"	1/8"	1/4"	3/8"
Number of Specimens	5	5	5	5	5	5

Total of 30 specimens

b. Cyclic

Flaw Type		Hole			Slit		
Flaw Size		1/8"	1/4"	3/8"	1/8"	1/4"	3/8"
Stress Level	0.8	5	5	5	5	5	5
	0.7	5	5	5	5	5	5
	0.6	5	5	5	5	5	5

Total of 90 specimens

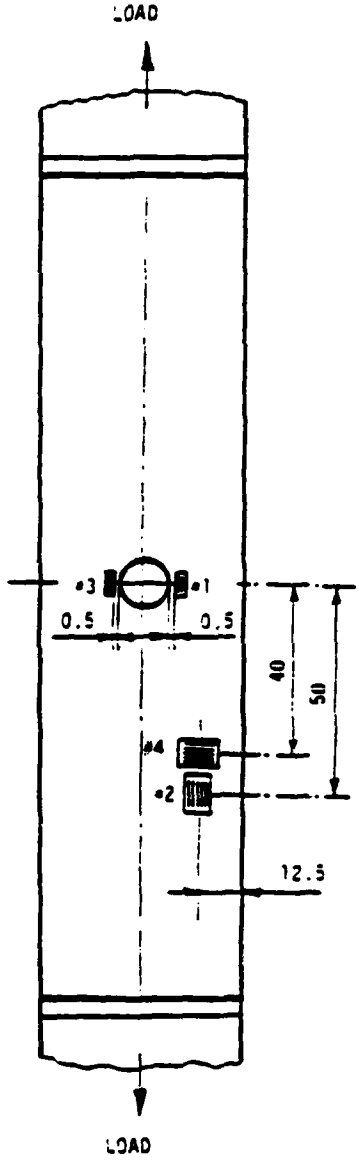

FIGURE 35 PLACEMENT OF STRAIN GAGES FOR STATIC SPLITTING STRESS MEASUREMENT

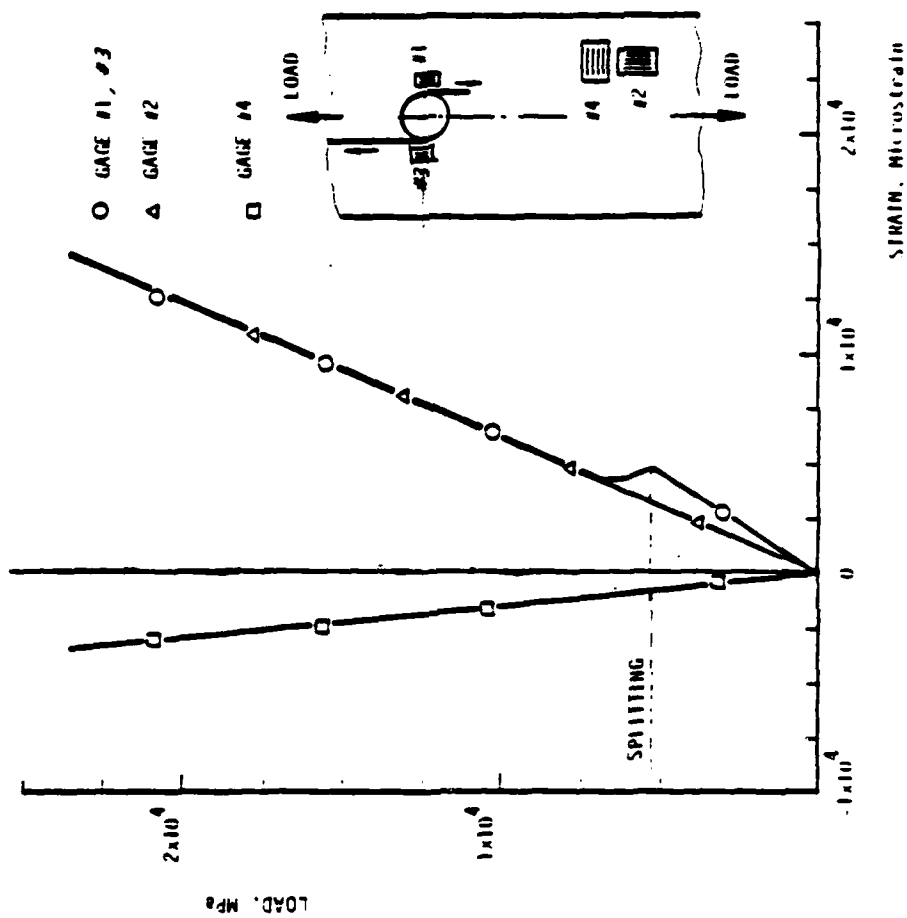

FIGURE 36 TYPICAL LOAD-STRAIN CURVES FROM UNIDIRECTIONAL TENSILE TEST

In the static tests, splitting stresses were measured by the judicious placement of strain gages around the notch as shown in Figure 35. When the split initiates, the stress concentration at the notch edge is relieved and the strain concentration detected by the gage at the notch edge is thus relieved. This results in the load-strain curve such as in Figure 36. The splitting stresses determined in this matter are summarized in Table 19 for specimens with slits, and in Table 20 for specimens with holes. Included in these tables are the net fracture stresses for these specimens. When this fracture stress is based on the net area, we find that the final fracture stress is the ultimate fracture stress of the virgin unidirectional material. The ultimate fracture stress of Hercules AS1/3501-6 graphite/epoxy is 1661 MPa. The results in Tables 19 and 20 fall in a band around this value.

It can be seen that the splitting stress depends on both the notch size and shape. The notch size effect has been correlated using the basic Linear Elastic Fracture Mechanics Equation [31]. The use of this equation yielded excellent correlation in these cases. It appears reasonable to expect that the LEFM equation would apply since splitting is a phenomenon which occurs only in the matrix which is an isotropic, homogenous medium. The consideration of notch shape shows that the splitting stresses of the specimens with slits were less than those with a corresponding size hole. Since slits intro-

TABLE 19

SPLITTING STRESSES AND FRACTURE STRESSES
FOR SPECIMENS WITH SLITS LOADED MONOTONICALLY TO FAILURE

Average Slit Length	Splitting Stress [MPa]	Net Fracture Stress [MPa]
3.277 mm	321 (11.5%)	1604 (11.1%)
6.416 mm	238 (1.3%)	1580 (6.8%)
9.164 mm	201 (4.9%)	1646 (7.5%)

Mean (Coefficient of Variation)
5 specimens of each type

TABLE 20

SPLITTING STRESSES AND FRACTURE STRESSES
FOR SPECIMENS WITH HOLES LOADED MONOTONICALLY TO FAILURE

Nominal Hole Diameter	Splitting Stress [MPa]	Net Fracture Stress [MPa]
3.175 mm	399 (6.1%)	1843 (12.8%)
6.35 mm	281 (7.5%)	1802 (8.7%)
9.525 mm	239 (12.9%)	1597 (5.5%)

Mean (Coefficient of Variation)
5 specimens of each type

duce a higher stress concentration then holes, it is reasonable to expect that the critical stress intensity factor will be reached at lower applied stress levels as the data suggests.

The main objective of the cyclic tests was to measure the split size versus number of cycles. Several Non-Destructive Evaluation techniques can be used and were considered for this purpose. However, a simple method was the only one which satisfied the criteria that the method be accurate, repeatable, safe, chemically non-interacting with graphite/epoxy, time efficient, and economic. The method, previously used by Lesieutre [28], is known as the "chalk-dust tracing" method. This method involves covering one of the specimen faces with a layer of chalk dust by rubbing a stick of soft white chalk against the specimen's surface. As the split propagates, the relative motion of the splits' surfaces during cyclic loading causes the chalk particles to pop out. This popping out leaves a clearly visible trace over the entire cracked length. The trace was enhanced by illuminating the specimen with a side light source.

All tests were conducted in load control at a stress ratio of 0.1. The frequency of the applied load was adjusted for each notch size and type dependent on the maximum cyclic stress in order to maintain a constant load rate for all tests. A base frequency of 30 Hz was used for specimens with a 3.175 mm diameter hole cycled with a maximum stress of 80% of the static

splitting stress. The tests were halted at predetermined intervals to mark the split size at each interval. These sizes were measured when the test was completed. The halts were spaced in five even intervals over each logarithmic decade. In all cases the tests were continued to 600,000 cycles or until the branches of the split reached a loading tab, whichever occurred earlier.

Splits originated from both sides of the notches in several different modes. These modes are represented in Figure 37. The experiments showed that the four branches of splits did not grow at similar rates as shown by a typical plot in Figure 38. However, the total length of the two splits on the right side of the notch was approximately the same as the total length of the two splits on the left side of the notch for most cases. Both lengths were used, however, in data reduction and correlation.

The split length was correlated with the number of cycles by using an equation of the form:

$$2a = -A + B \ln (N) \qquad (3.1)$$

where 2a is the current split length and N is the number of load cycles. This equation was applied to the experimental data using the lognormal mean of the individual split lengths as 2a. The results of performing a linear regression on the

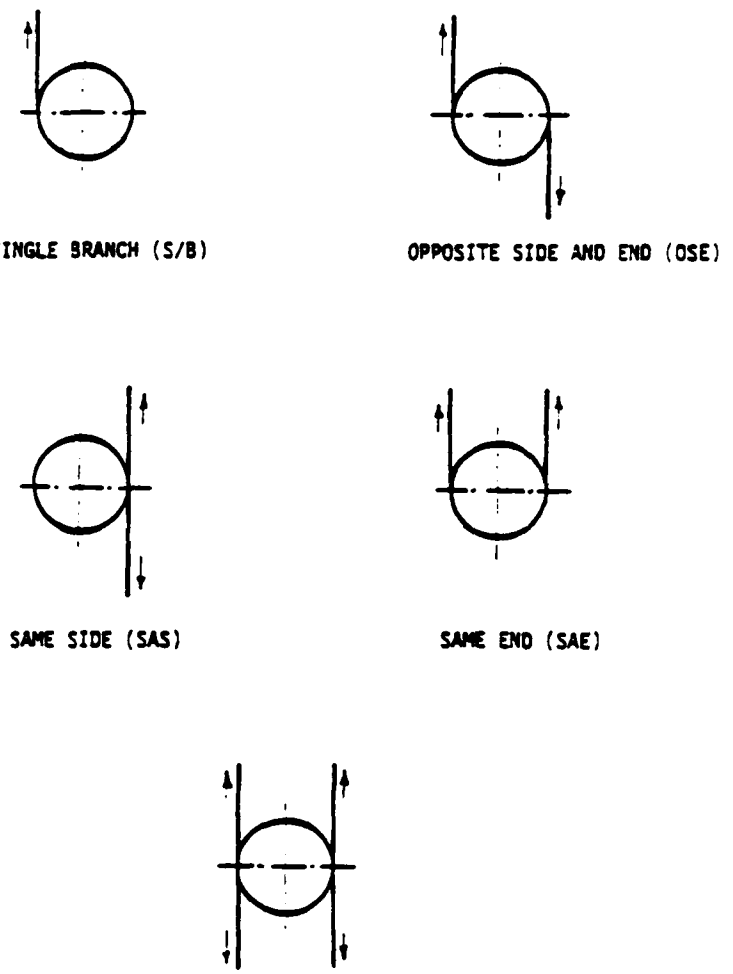

FIGURE 37 MODES OF SPLITTING INITIATION

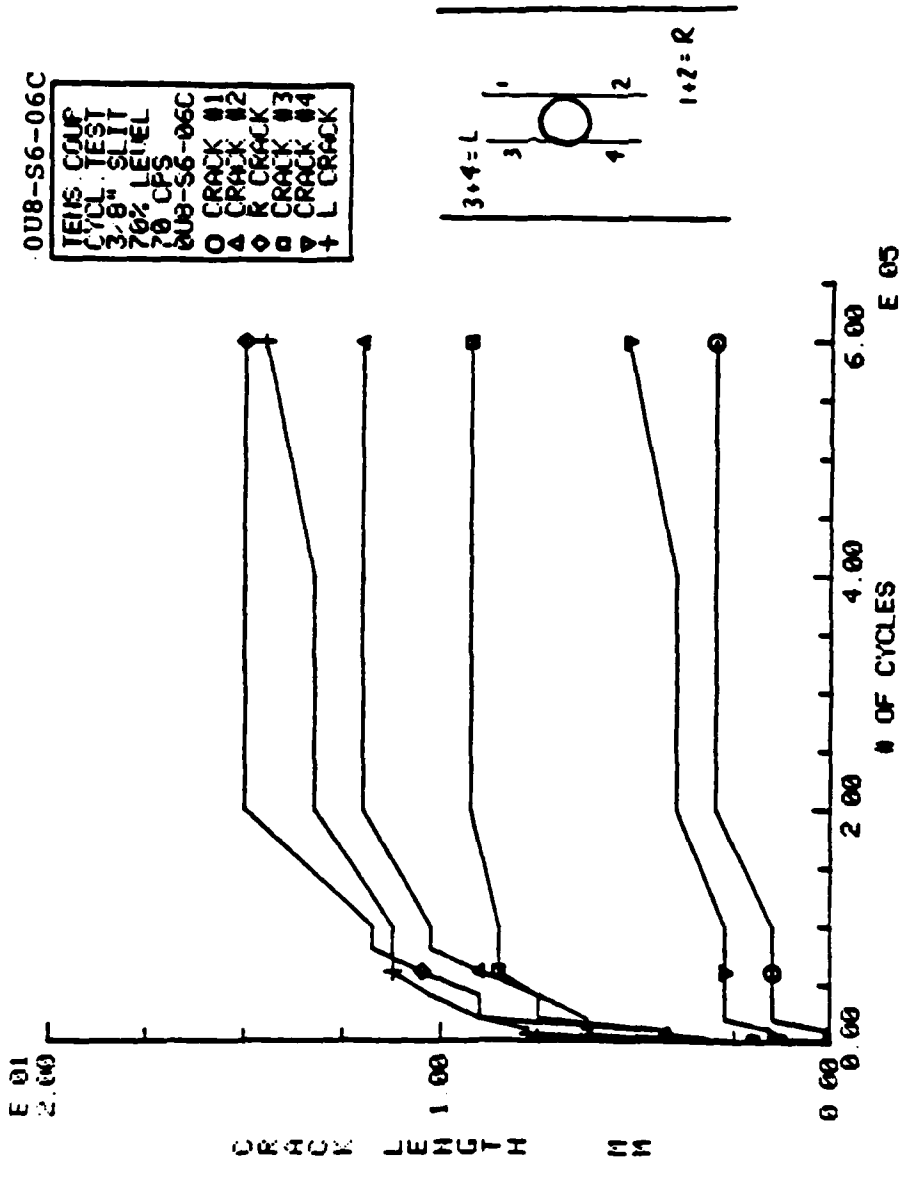

FIGURE 38 TYPICAL SPLIT GROWTH CURVE

data are summarized in Table 21. A typical plot of experimental split growth data on a semilog plot is presented in Figure 39 along with the resulting line using the growth equation shown above.

These results show some important trends. In general, the larger the hole size, the faster the crack propagates (as represented by a higher value of the constant B). In addition, the lower the maximum stress, the lower the value of B and thus the lower the growth rate. The results for specimens with slits are a bit more confusing. Once again, for a given slit size the lower the maximum cycling stress, the lower the split growth rate. However, the split growth rate does not seem to vary in any consistent way with nominal slit size.

Two other important numbers can be obtained once the constants in Table 21 have been determined. Referring to equation 3.1, the cycle at which the slit initiated can be determined by setting 2a equal to zero and solving for the cycle N. This number is indicated by N_o and is presented in Table 22. In addition, the initial rate of crack propagation can be determined by differentiating equation 3.1 and using the crack initiation cycle and thus obtaining the initial crack propagation rate. This is also summarized for all the cases in Table 22.

Once again, two general trends are apparent for both the specimens with holes and those with slits. The larger the ini-

TABLE 21

RESULTS OF LINEAR REGRESSION (A = INTERCEPT, B = SLOPE)
FOR SPLIT PROPAGATION RATE

Notch Type		Holes			Slits		
Stress Level	Nominal Notch Size [mm]	A [mm]	B [mm/cycle]	R^2	A [mm]	B [mm/cycle]	R^2
80%	3.175	28.9	5.66	.960	37.1	10.63	.990
	6.35	30.7	9.48	.993	10.8	9.64	.989
	9.525	32.2	12.67	.961	22.2	4.54	.967
70%	3.175	52.0	7.32	.979	16.0	3.50	.971
	6.35	61.7	7.80	.996	11.2	2.80	.987
	9.525	127.8	16.48	.900	14.2	3.39	.988
60%	3.175	13.1	2.13	.953	8.7	1.73	.966
	6.35	7.1	2.09	.810	5.1	0.92	.873
	9.525	52.9	5.30	.983	7.4	1.25	.988

R^2 = Correlation Coefficient
5 specimens of each type

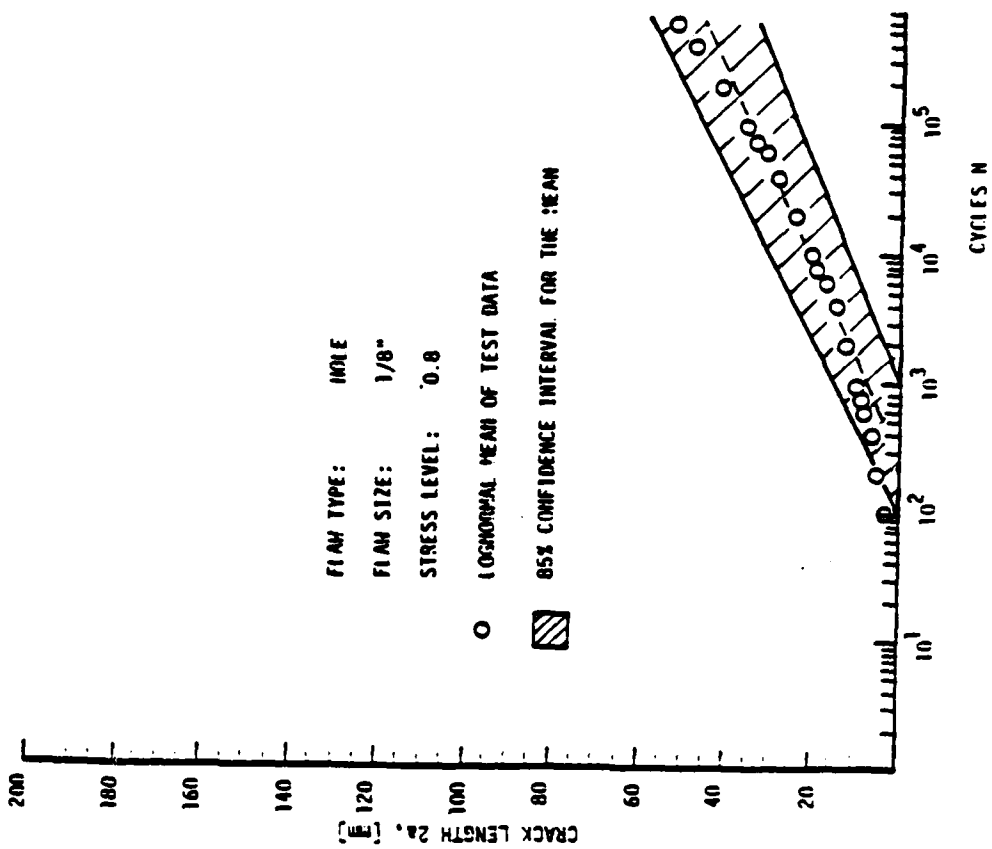

FIGURE 39 PLOT OF SPLIT GROWTH DATA VERSUS LOG CYCLES ALONG WITH CORRELATION

TABLE 22

SPLIT INITIATION CYCLES AND INITIAL PROPAGATION RATES
DETERMINED FROM LINEAR REGRESSION PARAMETER

Notch Type		Holes		Slits	
Stress Level	Nominal Notch Size [mm]	N_o [Cycles]	$\left(\frac{da}{dn}\right)_o$ [mm/cycle]	N_o [Cycles]	$\left(\frac{da}{dn}\right)_o$ [mm/cycles]
80%	3.175	233	0.00339	61	0.322
	6.35	30	0.365	9	3.210
	9.525	1,020	0.975	191	0.0314
70%	3.175	1,307	0.00604	176	0.0365
	6.35	4,511	0.00287	131	0.0519
	9.525	6,120	0.00710	167	0.0514
60%	3.175	1,547	0.00440	15,527	0.0116
	6.35	6,543	0.0696	5,680	0.00365
	9.525	36,139	0.00025	780	0.00327

tial flaw size, the earlier split initiation takes place. For example, at a maximum cyclic stress level of 80% of "static splitting stress" it takes 167 cycles for splitting to initiate in specimens with a 3.175 mm hole while it takes only 13 cycles for initiation in specimens with a 9.525 mm hole. Again, this trend is not as consistent in the slit specimen data. The second trend is that the lower the maximum cyclic stress the longer it takes for split initiation to occur. Similar trends can be observed for the initial split propagation rate: generally, the larger the initial notch, the larger the initial crack propagation rate; and the higher the maximum cyclic stress level the higher the initial split propagation rate.

The data also shows that the initial split propagation rate is larger and the split initiates earlier when the notch is a slit rather than a circular hole. This is in line with the data from the static tests which shows that specimens with slits had a lower splitting stress than specimens with holes of the same size. These phenomena can be attributed to the fact that the splitting damage initiates from the microcracks existing at the flaw tips. The stress field around any of these microcracks is determined by the type of the macroscopic notch. Thus the more severe the macroscopic stress concentration, the lower the splitting stress in static loading, the earlier the split initiates under cyclic load, and the faster the initial growth rate. The data does show that the growth rate of the

split slows down as the number of accumulated load cycles increases.

This investigation is described fully by Daken [30]. In this report, he also suggests further experiments which will help to increase the understanding of this phenomena of splitting in unidirectional composites. Of special interest is the recommendation that similar experiments be conducted on unidirectional laminates which are off-axis to the applied load.

3.2 Damage Initiation and Propagation in Composite Laminates under Compression-Compression Cyclic Load

In the past, several investigations have been conducted at TELAC into the damage initiation and propagation around a hole in graphite/epoxy laminates subjected to compression-compression cyclic loads. These tests have been conducted on honeycomb sandwich beams in both 4-point bending and axial column configurations. Two of these previous investigations are of interest here: Graves [32] and Fanucci [33]. Both looked at the damage propagation from holes in [+-45/0]s laminates, among others. Graves used a four-point bend specimen with a 6.35 mm diameter hole and determined damage in the form of delamination by tactile feel and close observation while the specimen was under load. Fanucci used an axial col-

umn specimen with a 12.7 mm diameter hole and determined damage through the use of Moire interferometry.

Different modes of damage propagation were observed in the two investigations. Graves observed the delamination to propagate in the direction of the applied load within the width of the hole. A typical representation of this is shown in Figure 40. Fanucci found that delamination propagated from 45° points on the hole as shown in Figure 41.

An investigation was undertaken to determine the reason for the difference in damage (delamination) propagation. There were differences in specimen type (four-point bend vs. axial column), damage detection method (tactile vs. Moire interferometry), and hole diameter (6.35 mm vs. 12.7 mm). In this investigation, the specimen type and damage detection method employed by Fanucci were used while the hole size was the 6.35 mm used by Graves. The column sandwich beam specimen is shown in Figure 42. A total of fifteen of these specimens were built with [+-45/0]s graphite/epoxy faces. Five of these were tested under static load. The results of this part of the investigation are discussed later. The remaining ten specimens were tested under compression-compression cyclic loading on an MTS 810 test machine. The tests were conducted at a frequency of 6 Hz with a minimum stress of 280 MPa (approximately 80% of static compressive ultimate) and a stress ratio of 10.

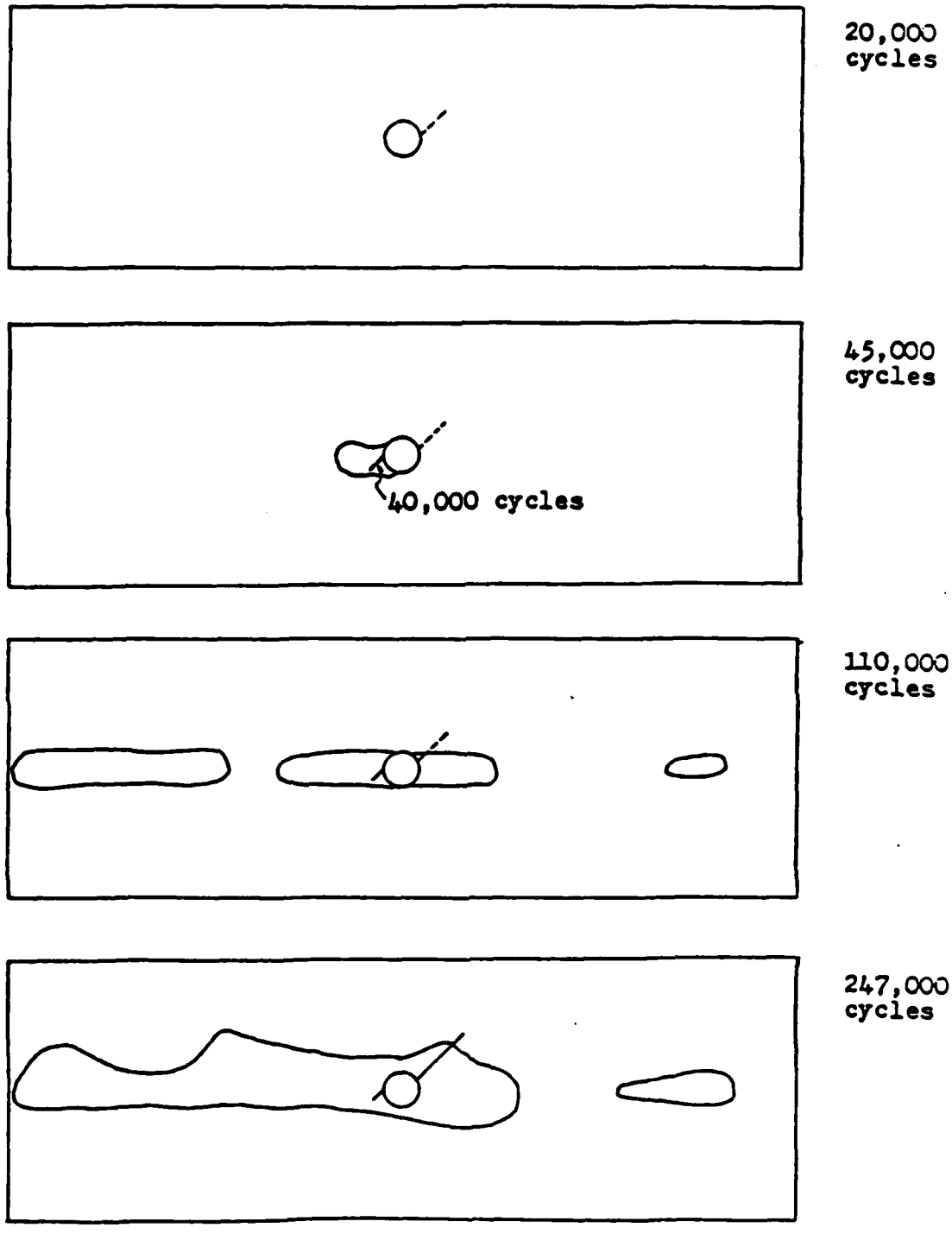

FIGURE 40 DAMAGE PROPAGATION OBSERVED BY GRAVES (REFERENCE 32) FOR [±45/0]$_s$ LAMINATES WITH 6.35 mm HOLE UNDER COMPRESSION-COMPRESSION CYCLIC LOAD

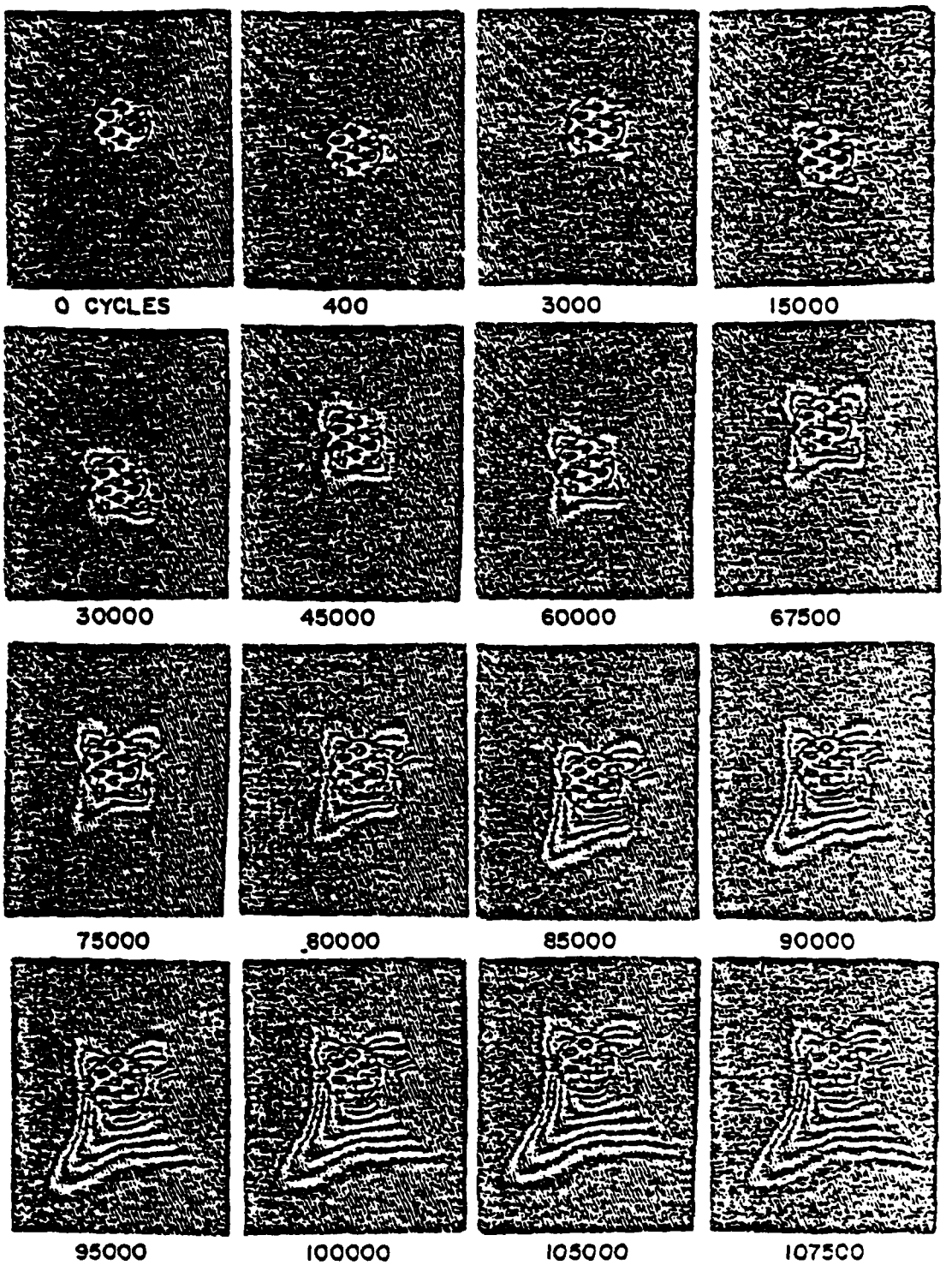

FIGURE 41 DAMAGE PROPAGATION OBSERVED BY FANUCCI (REFERENCE 33) FOR $[\pm 45/0]_s$ LAMINATES WITH 12.7 mm HOLES UNDER COMPRESSION-COMPRESSION CYCLIC LOAD

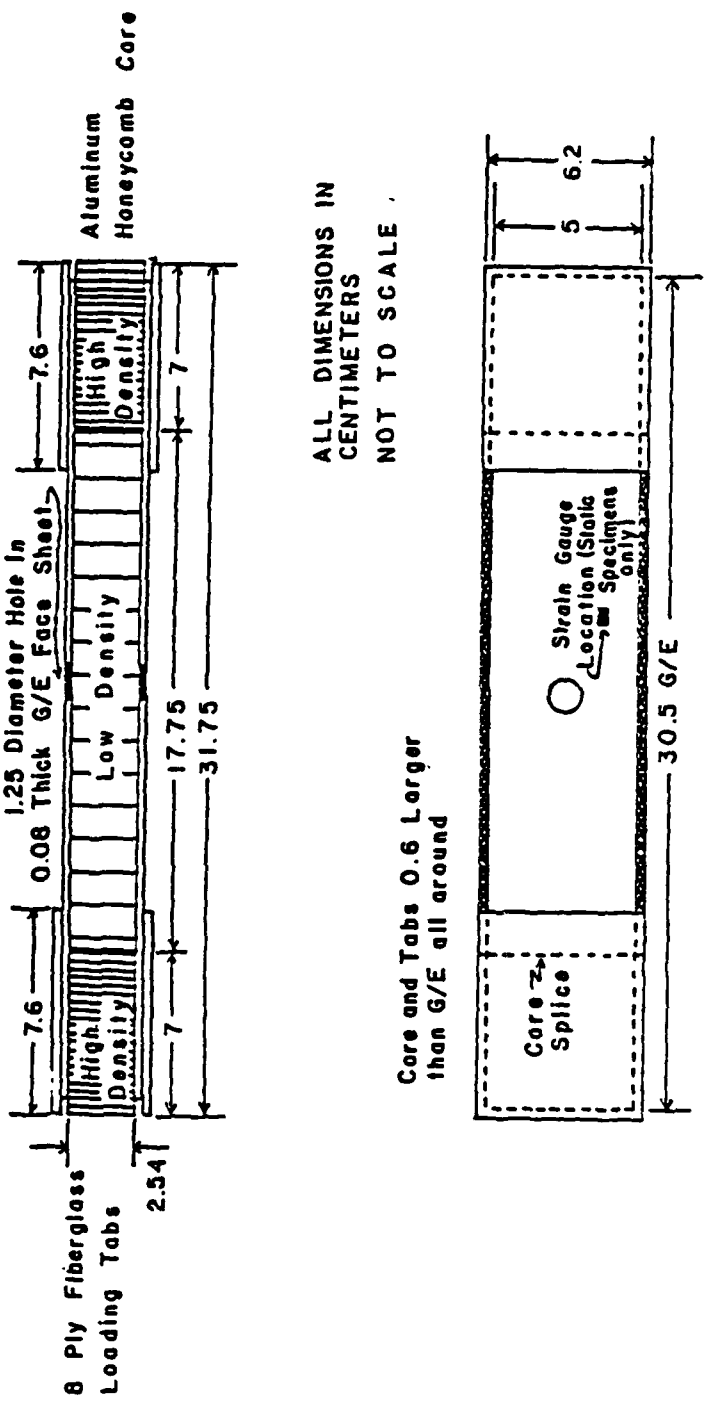

FIGURE 42 PHYSICAL CHARACTERISTICS OF COLUMN SANDWICH BEAM SPECIMEN

The damage was observed by using an out-of-plane Moire inteferometry technique refined at TELAC by Fanucci [23]. The technique involves placing a glass grid with 100 vertical lines to the inch very close (within one millimeter) to the surface of the specimen. The specimen is coated with a silver paint to enhance the photographs and observations. A collimated light source shines from the side casting shadows of the grid lines on the specimen's surface. Any out-of-plane (as referenced to the surface of the laminate) distortion of the laminate will distort the shadow pattern, causing interference fringes. These fringes are photographed while the specimen is held at a load midway between the maximum and minimum loads. Photographs were taken at constant intervals on a log time scale.

The results show that the damage propagation for these specimens was consistent with that observed by Graves (see Figure 40) as delamination grew and extended parallel to the applied load in a width equal to the hole diameter. This shows that the difference in damage propagation observed by Graves and Fanucci was not a result of specimen type but is in fact due to the difference in initial hole size. Thus, the damage propagation, in the form of delamination, can change for the same laminate depending upon the initial notch size.

It has been suggested by Fanucci and other authors that the delamination growth is due to interlaminar stresses which are present at free edges such as those at a hole. These

interlaminar stresses can change with notch size and shape thus indicating that delamination growth would be changed. Further research is now being conducted to look at the effect of thickness on this damage growth. As described in section 2.1, interlaminar stresses exist in an edge zone region the size of one laminate thickness. Thus, as the ply and laminate thicknesses increase, the size of the edge zone increases. Laminates with "double-ply" thicknesses (as described in section 2.1) are being tested to determine the influence of thickness on damage initiation and growth.

A side part of this reported investigation was to look at the difference in static compressive fracture stress between [+-30/0]s and [+-45/0]s laminates. Earlier results from Fanucci showed that the former laminate failed at a slightly lower stress than the latter. More data was needed for this to be conclusive. Axial column beams, as previously described, were tested in static compression. The results showed that the [+-30/0]s laminates failed at an averge stress of 300 MPa with a coefficient of variation of 7.2%. The [+-45/0]s laminates failed at an average stress of 355 MPa with a coefficient of variation of 5.3%. This is in line with the results found by Fanucci and with predictions based on the Tsai-Wu stress interaction criterion discussed in section 2.1. The stress interaction criterion predicts that the [+-30/0]s laminates will fail at a slightly lower stress than the [+-45/0]s lami-

nate as observed. However the Tsai-Wu criterion predicts a higher value than the experimental data with a predicted failure stress of 439 MPa for the [+-30/0]s laminate and 458 MPa for the [+-45/0]s laminate. It is important to note that these are in-plane fracture predictions and do not account for out-of-plane failures.

4. DYNAMICS AND AEROELASTICITY

The vibration of composite laminated plates present the concern of coupling between bending and twisting. Research into the flexure and vibration of plates at TELAC has looked into the consequences of this coupling. This coupling can be used to advantage by the designer in the design of aeroelastic structures. Research has also been concentrated on the effects of bending-torsion coupling on flutter and divergence properties of graphite/epoxy wings at various sweep angles.

4.1 Aeroelastic Flutter and Divergence of Rectangular Wings

An experimental and analytical investigation was made into the aeroelastic and divergence characteristics of six rectangular graphite/epoxy plate-like wings with styrene aerodynamic fairings. Four different laminates were used: [0x2/90]s, [+-45/0]s, [+45x2/0]s, and [+30x2/0]s. However, the latter two laminates could be reversed to the wind direction yielding the two additional configurations of [-45x2/0]s and [-30x2/0]s. The wings constructed with these laminates displayed unique aeroelastic properties due to the differing degrees of bending-torsion coupling. The experimental work included vibration tests, static load tests, and wind tunnel tests. The wind tunnel tests yielded data on divergence, classic

bending-torsion flutter, torsional stall flutter, and bending stall flutter.

Cantilever plates, of the laminates previously mentioned, were first tested in free vibration. The general plate layout and the sign convention used for the ply angle are shown in Figure 43. Later the wings made from these plates were also tested in this manner. The static deflections of these wings resulting from static loads were also determined. The experimental results from the free vibration (frequencies and mode shapes) and the static deflection tests (flexibility influence coefficients) were used to verify the analytical results.

The analysis used an assumed modes energy method for formulating the mass and stiffness matrics. Incompressible aerodynamic forces were calculated using the Vortex Lattice method for steady airflow and both Strip Theory and the Doublet Lattice method for unsteady airflow. the five assumed modes (two bending, two torsion, and one chordwise bending) produced good agreement between analysis and experiment for the lowest three natural frequencies. The divergence correlated remarkably well as shown in Table 23.

The flutter results were in good general agreement especially between experiment and Strip Theory analysis. This is shown in Table 24. The experimental data for the plates and wings are plotted in Figures 44 and 45 respectively. It is suggested

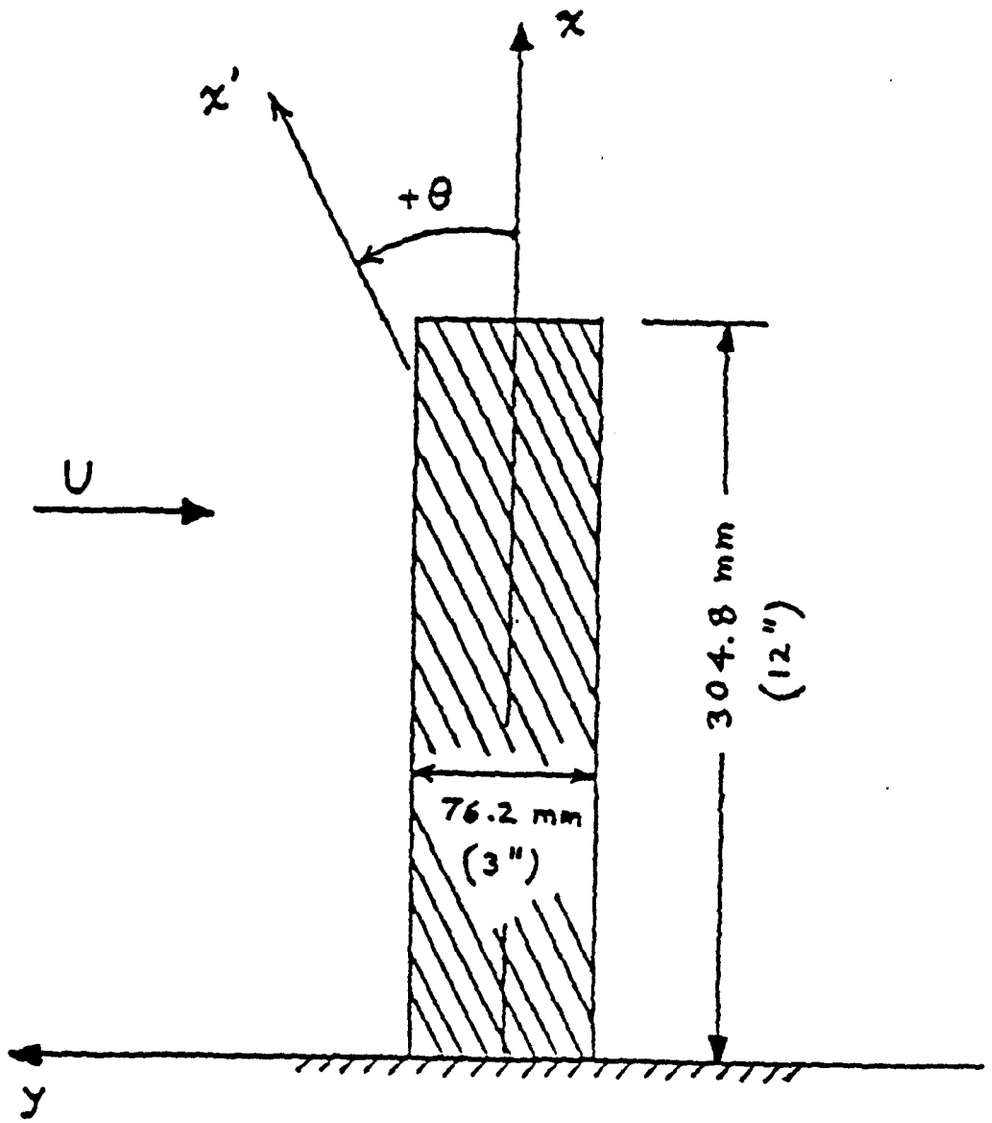

FIGURE 43 PLATE LAYOUT AND SIGN CONVENTIONS

TABLE 23

DIVERGENCE VELOCITIES IN FT/SEC

	Plate		Wing	
	Analysis	Experiment	Analysis	Experiment
$(0_2/90)_S$	92.27	90.0	99.55	---
$(\pm 45/0)_S$	∞	---	∞	---
$(45_2/0)_S$	∞	---	∞	---
$(30_2/0)_S$	∞	---	∞	---
$(-45_2/0)_S$	42.53	41.0	47.81	46.8
$(-30_2/0)_S$	44.42	38.5	48.81	46.1

TABLE 24

FLUTTER VELOCITIES IN FT/SEC

	Plate			Wing	
	Analysis		Experiment	Analysis	
	2-D	3-D		2-D	3-D
$(0_2/90)_S$	70.2	73.9	85.0	75.5	83.1
$(\pm 45/0)_S$	122.8	115.5	---	126.7	121.0
$(45_2/0)_S$	92.9	106.0	91.0	102.4	114.3
$(30_2/0)_S$	92.3	101.8	89.0	99.6	112.5
$(-45_2/0)_S$	105.0	99.0	---	112.1	111.7
$(-30_2/0)_S$	119.4	100.3	---	122.9	104.9

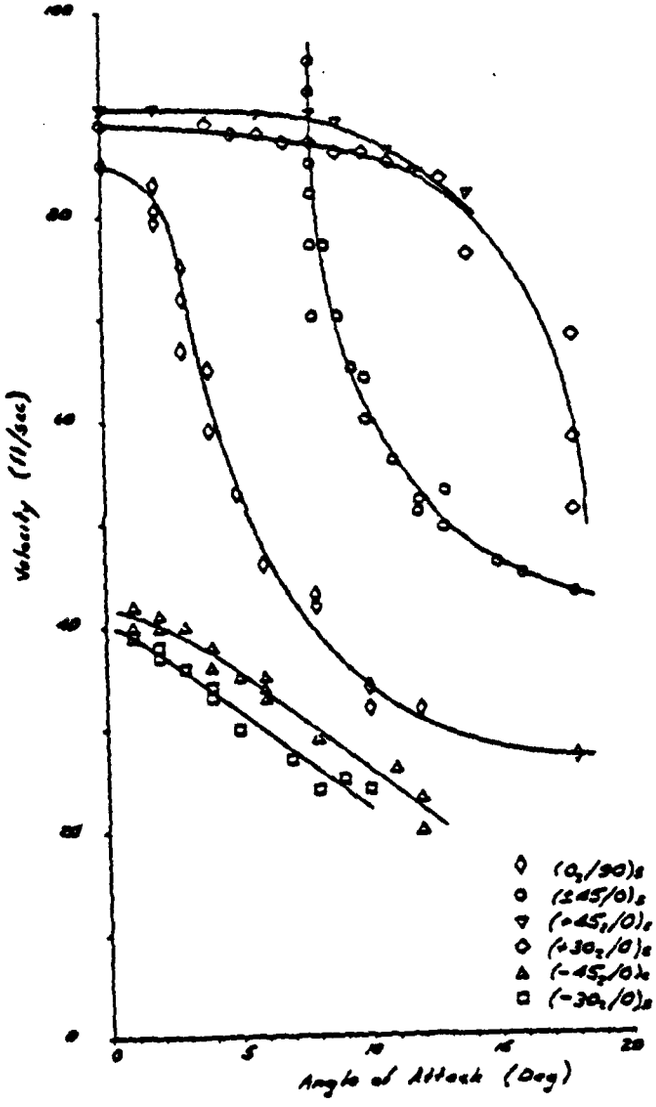

FIGURE 44 PLATE FLUTTER

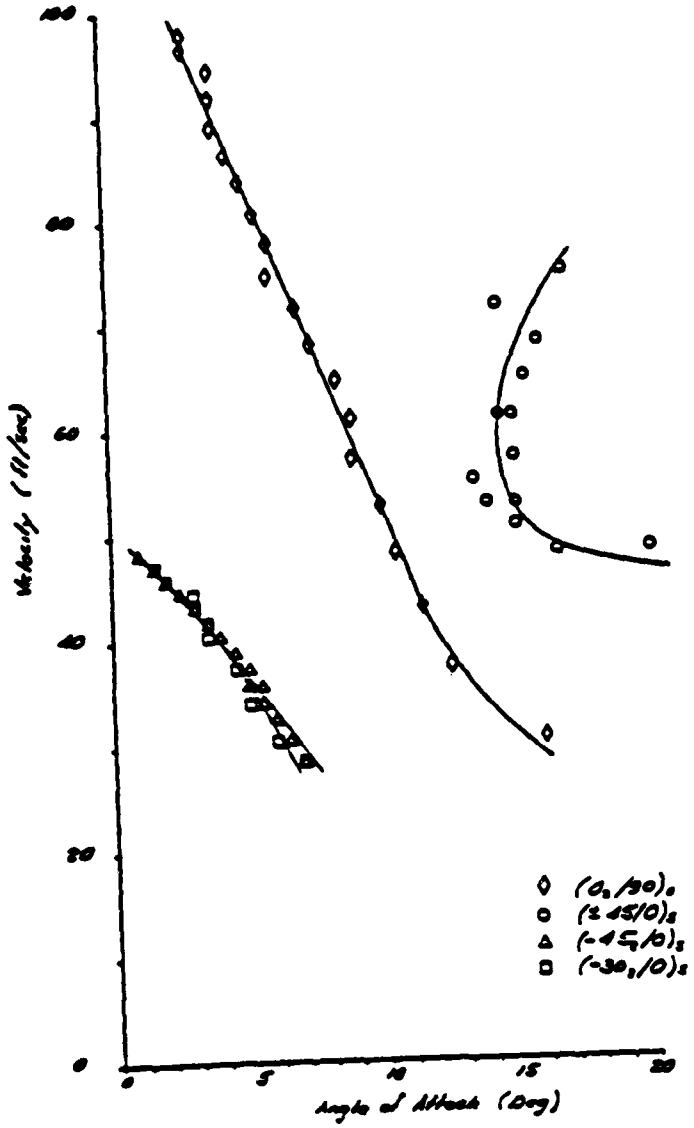

FIGURE 45 WING FLUTTER

that more panels in the Doublet Lattice Method analysis may have imporved the agreement with the Strip Theory analysis.

This work is more fully described by Selby in Reference 34.

4.2 Aeroelastic Properties of Straight and Forward Swept Graphite/Epoxy Wings

Experimental aeroelastic tests were conducted on a series of thirteen wings manufactured from Hercules AS1/3501-6 graphite/epoxy with different ply configurations at 0° and 30° forward sweep. These thirteen different laminates represented a wide range of bending-torsion coupling. These laminates are shown in Table 25 ranked according to their coupling. The 0° sweep configurations complemented some earlier studies at TELAC by Hollowell and Dugundji [35] and that by Selby [34] reported above.

The present study explored the nonlinear as well as linear aspects of flutter. The specimens which were constructed were sufficiently strong such that when divergence or flutter occurred the specimens were not destroyed but rather went into steady-state limit cycles which were limited in amplitude by the nonlinear airforces (stalling). As such, basic data on nonlinear stall flutter and divergence, as well as the more conventional linear flutter and divergence characteristics, was obtained.

TABLE 25

DIFFERENT LAMINATE LAYUPS USED FOR THE TEST WINGS

$[0_2/90]s$

$[+15_2/0]s$	$[\pm 15/0]s$	$[\mp 15/0]s$	$[-15_2/0]s$
$[+30_2/0]s$	$[\pm 30/0]s$	$[\mp 30/0]s$	$[-30_2/0]s$
$[+45_2/0]s$	$[\pm 45/0]s$	$[\mp 45/0]s$	$[-45_2/0]s$

increased negative bending-torsion coupling ← 0 → increased positive bending-torsion coupling

The experiments were conducted in the Acoustic Wind Tunnel of M.I.T.'s Department of Aeronautics and Astronautics with a maximum airspeed of 30 m/s. All the tests were monitored using videotape cameras, photographs, and strain gages in an attempt to obtain the static deflection and angles under airloads as well as the vibration amplitudes and frequencies. The root angle of attack could be readily changed as well as the wind velocity, so that nonlinear characteristics could be explored. Static tests were also performed to measure the static deflections of the wings under loads of pure force and pure moment. Loads were applied in even increments with measurements taken at each increment. These tests were performed before the wind tunnel tests so that any structural nonlinearities could be determined.

Theoretical analyses of the results were made using linear two-dimensional strip theory for the flutter behavior, and linear three-dimensional Weissinger L-Method theory for the divergence. An attempt was made to calculate the nonlinear steady airload, deflection, and twist behavior of the wing using rough approximation to the nonlinear lift and stalling characteristics of the wing.

The static deflection and twisting characteristics of these laminates under static applied forces and moments were well-predicted by a linear five-mode Rayleigh-Ritz analysis for small amplitudes as shown in Figure 46 for the [+-45/0]s lami-

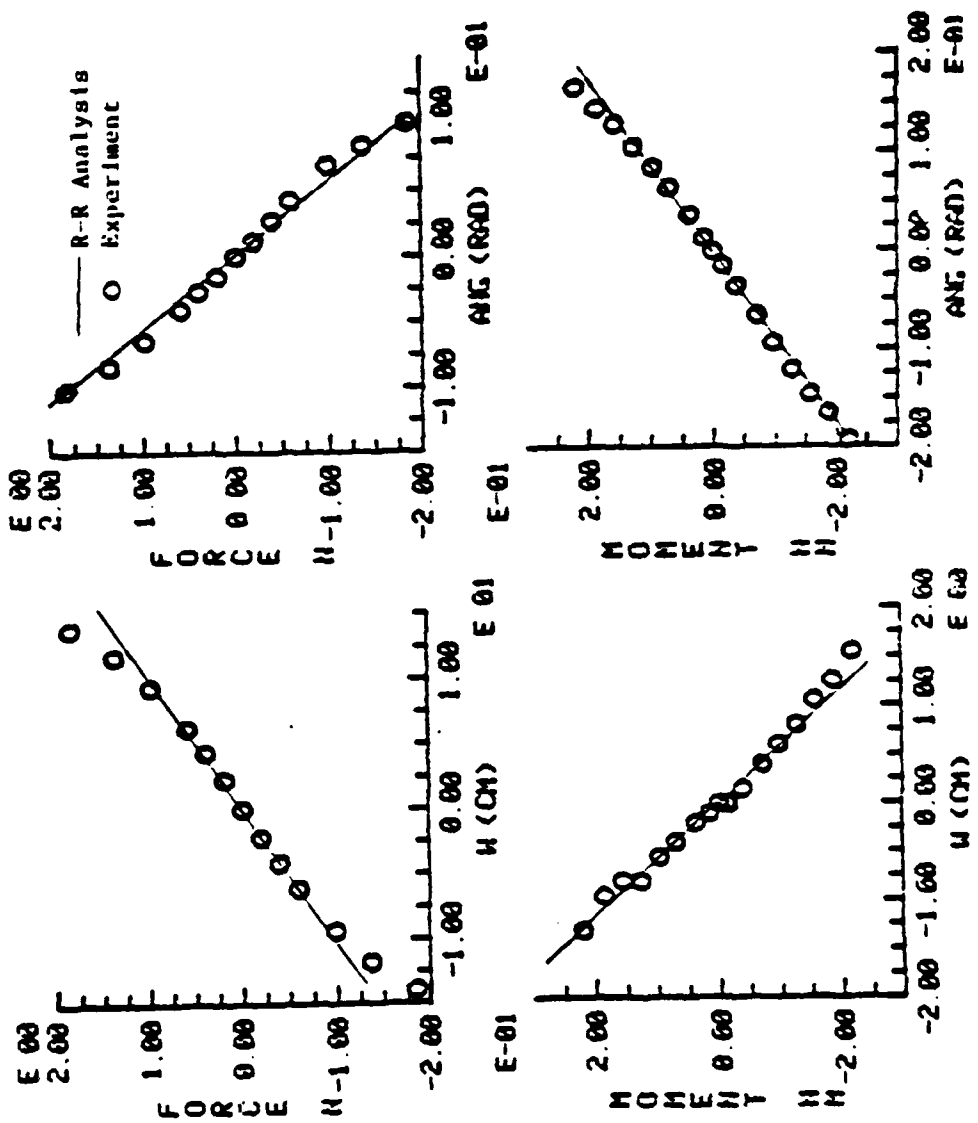

FIGURE 46 EXPERIMENTAL AND THEORETICAL STATIC DEFLECTIONS FOR $[\pm 45/0]_s$ WING

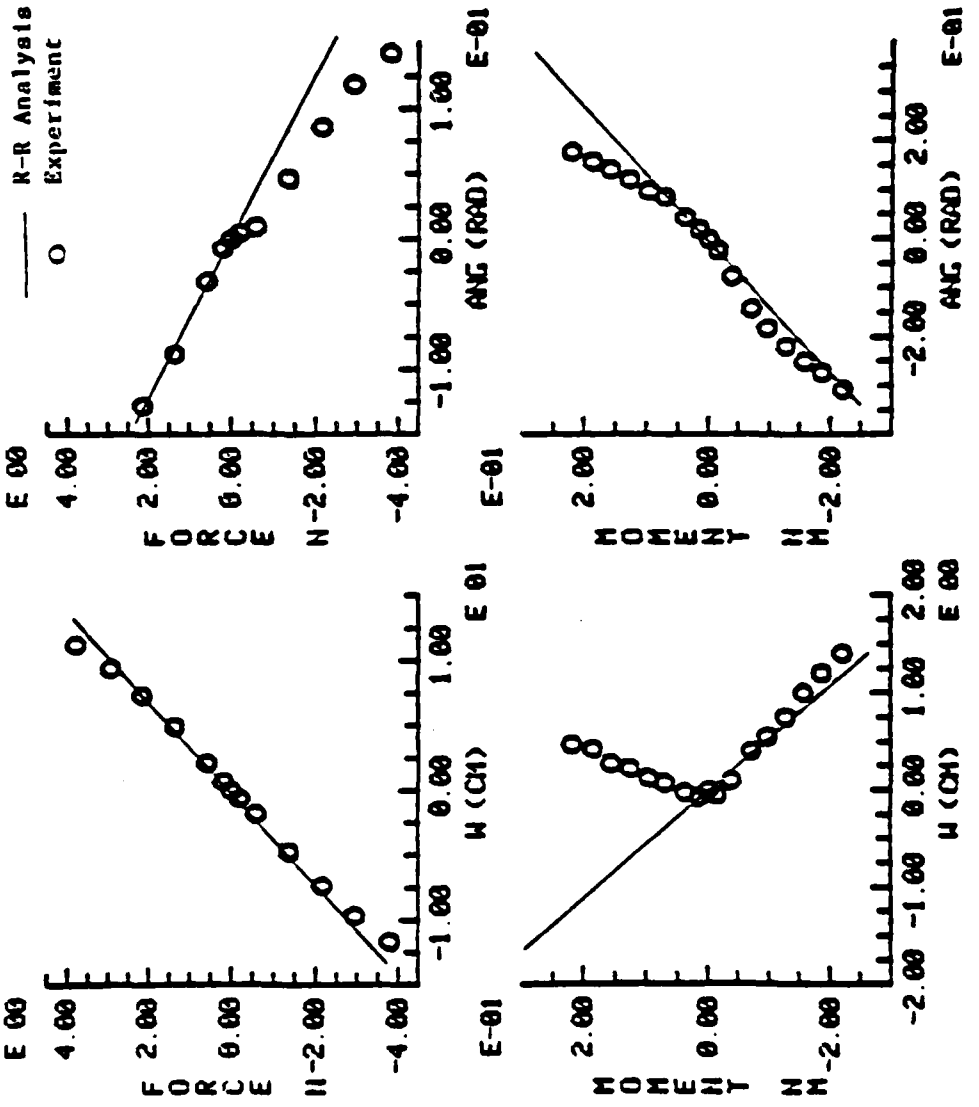

Figure B.3 [±15/0]s layup wing, static deflection.

FIGURE 47 EXPERIMENTAL AND THEORETICAL STATIC DEFLECTIONS FOR $[\pm 15/0]_s$ WING

nate. However, occasional buckling occurred especially for low ply angles. In these cases, the experimental data diverged from the results of the Rayleigh-Ritz analysis as shown in Figure 47 for the [+-15/0]s laminate.

The flutter and divergence characteristics of the wings at low root angle of attack are summarized in Figure 48. For negative ply angle and forward sweep, Λ, of -30°, divergence dominates the aeroelastic behavior. When the angled ply has a positive orientation, the divergence speed of the forward swept wing increases and a higher flutter speed limits the flight speed. However, increasing the ply angle to 45° again results in a low divergence speed. The linear five-mode flutter and divergence analyses gives good correlation with these experimental results as can be seen in Figure 48.

The typical nonlinear effects of high angle of attacks on the flutter and divergence behavior of these wings is indicated in a representative plot of velocity versus angle of attack for all laminates with ply angles of 15° shown in Figure 49. The frequency of the resulting vibration is also shown on these curves. For all the different laminates, four different types of aeroelastic phenomena were observed: divergence and bending-torsion flutter at low tip angles of attack and torsional stall flutter and bending stall flutter at high tip angles of attack. The sharp drop in torsional stall flutter seen in these experiments versus angle of attack has also been

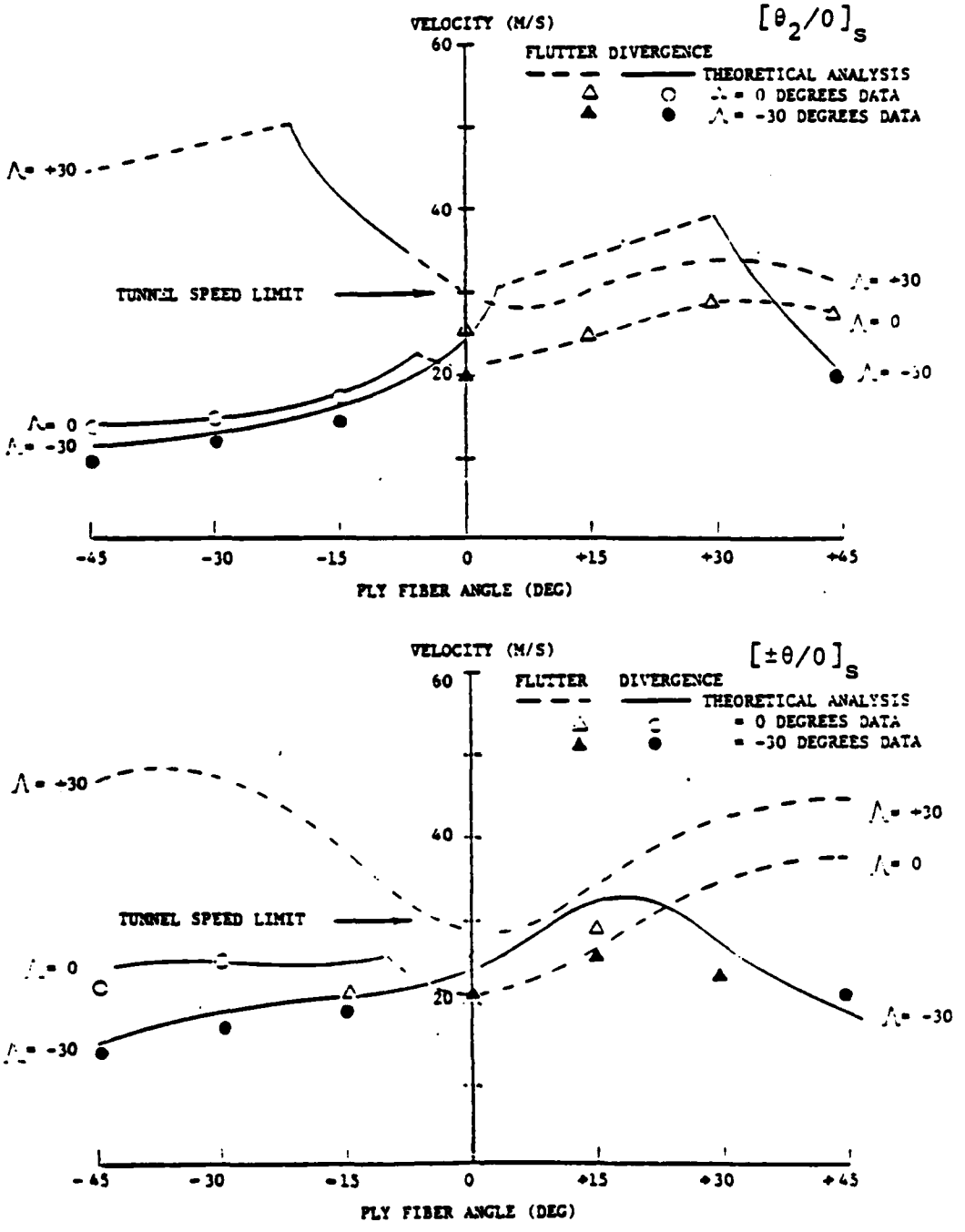

FIGURE 48 THEORETICAL AND EXPERIMENTAL EFFECTS OF PLY ANGLE ON FLUTTER AND DIVERGENCE SPEEDS

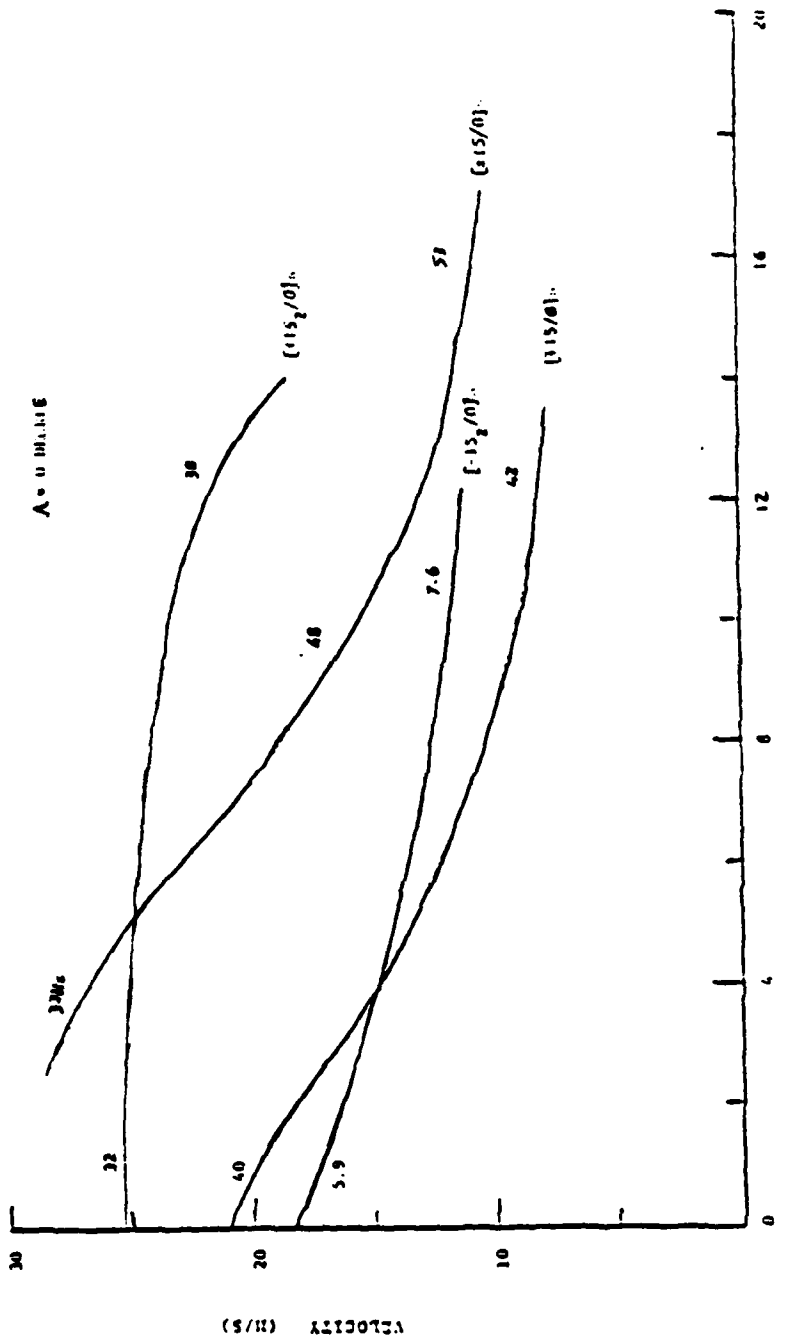

Figure D.2 Λ=0, 15 degree ply fiber angle layup wings, flutter boundary curves.

FIGURE 49 FLUTTER BOUNDARY CURVES FOR ZERO SWEEP ANGLE FOR LAMINATES WITH PLY ANGLES OF 15°

seen for isotropic wings. The bending stall flutter is a phenomena previously observed [35].

The nonlinear static equilibrium and twist angles due to nonlinear airloads were obtained from visual inspection of the videotapes and photographs taken of the tests. This data shows a highly nonlinear relation with root angle of attack as shown for the [-15x2/0]s configuration in Figure 50. The analytical calculations using rough nonlinear theory give good correlation with the experimental data as shown for the one particular laminate in Figure 50.

Theoretical calculations were performed for a linear flutter analyses of all the wings resulting in V-g and V-omega diagrams and divergence conditions are obtained based on a two-dimensional strip theory. Typical results are shown in Figure 51 for laminates with a ply angle of 15°.

This work is more fully described by Lansberger in Reference 36.

Work is now being conducted on built-up wings with the same tests and analyses to be performed as discussed above. These wings are constructed of graphite/epoxy skins bonded to thin aluminum rib and spar structures which approximate a box beam configuration.

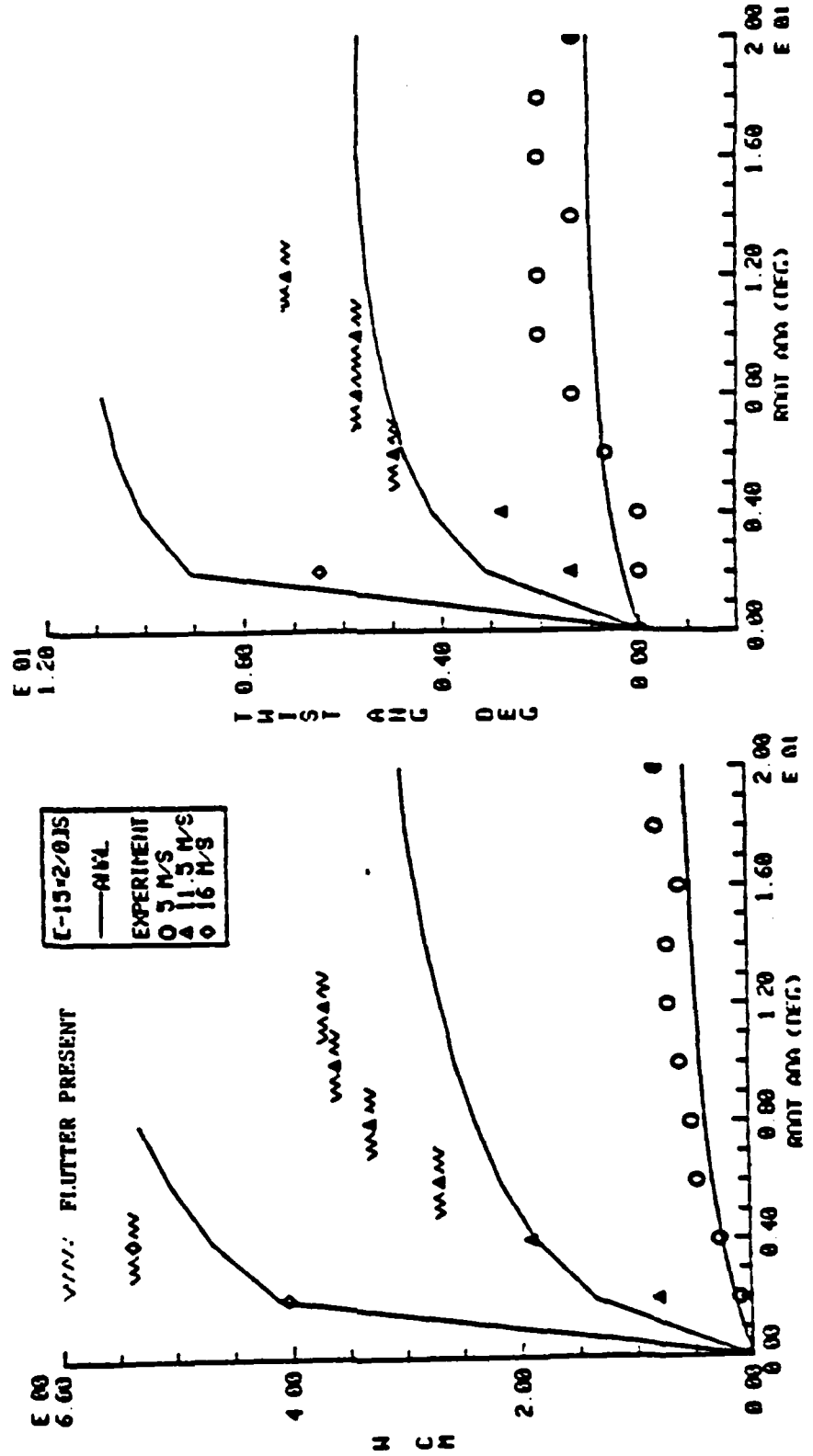

FIGURE 50 EXPERIMENTAL AND PREDICTED STEADY AIRLOAD DEFLECTIONS VERSUS ANGLE OF ATTACK FOR $[-15_2/0]_s$ WING

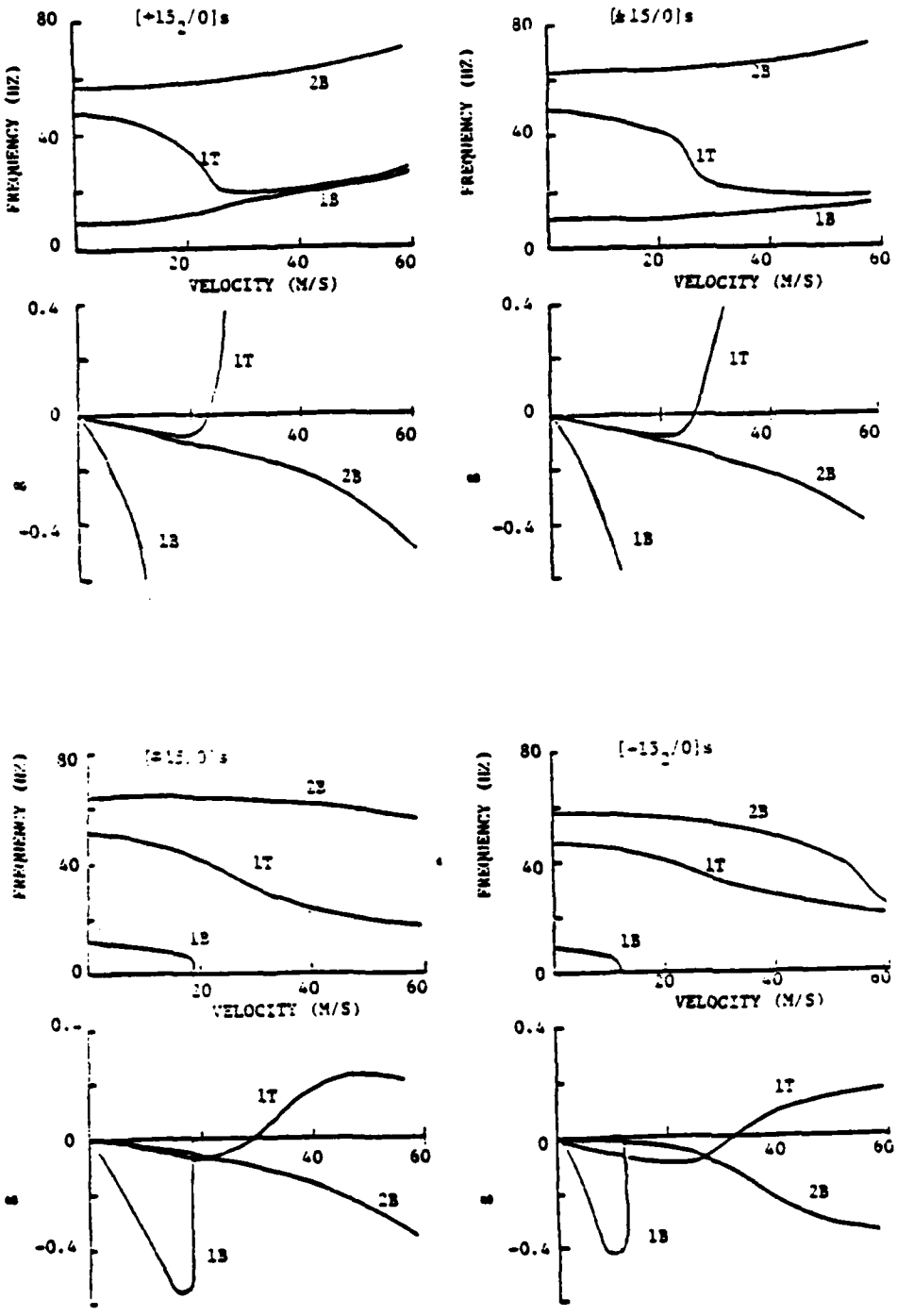

FIGURE 51 FLUTTER ANALYSIS DIAGRAMS FOR THE FOUR WINGS WITH A 15° FIBER ANGLE

REFERENCES

1. Garcia, Jose I., "Static Tensile Behavior of [0x6], [0/+-5]s, [0/+-10]s, and [0/+-15]s Graphite/Epoxy Laminates with Holes", M.I.T. Department of Aeronautics and Astronautics, S.M. Thesis, June, 1980.

2. Garcia, Jose I., "Fracture of [+-5/0]s, [+-10/0]s, and [+-15/0]s Graphite/Epoxy Coupons under Tension", TELAC Report 80-9, August, 1980.

3. McManus, Hugh L.N., "Failure Modes in a Family of Graphite/Epoxy Laminates", M.I.T. Department of Aeronautics and Astronautics, S.M. Thesis, May, 1981.

4. Soderquist, Joseph R., "Off-Axis Tension Tests of TELAC Material, [θx6]", TELAC Report 81-7, May, 1981.

5. Lagace, Paul A., "Static Tensile Fracture of Graphite/Epoxy", M.I.T. Department of Aeronautics and Astronautics, Ph.D. Thesis, April, 1982.

6. Tsai, S.W., and Wu, E.M., "A Generalized Theory of Strength for Anisotropic Materials", Journal of Composite Materials, Vol. 5, 1971, pp. 58-80.

7. Bar-Yoseph, Pinchas, and Pian, Theodore H.H., "Calculation of Interlaminar Stress Concentration in Composite Materials," Journal of Composite Materials, Vol. 15, 1981, pp. 225-239.

8. Lagace, Paul A., "Delamination Fracture under Tensile Loading", presented at Sixth Conference on Fibrous Composites in Structural Design, New Orleans, Louisiana, January, 1983.

9. Rizzo, R.R., "More on the Influence of End Constraints of Off-Axis Tensile Tests", Journal of Composite Materials, Vol. 3, 1969, pp. 202-219.

10. Brewer, John C., "Comparison of Tapered Graphite/Epoxy Coupons with Standard TELAC Graphite/Epoxy Coupons", TELAC Report 82-15, April, 1982.

11. Vizzini, Anthony J., and Lagace, Paul A., "TELAC Computing Facility: Software Description", in preparation.

12. Dodson, Carroll L., and Fujii, Eric, "Effects of Loading into the Nonlinear Region of Graphite/Epoxy Laminates", TELAC Report 82-6, May, 1982.

13. Trop, David, and Chin, David A., "Nonlinear Stress-Strain Behavior in Graphite/Epoxy Laminates", TELAC Report 82-7, May, 1982.

14. Chang, Ya-Pei A., and deLuis, J., "Determination of the Mechanical Properties of Graphite/Epoxy Fabric Prepreg Composite", TELAC Report 82-5, May, 1982.

15. Mar, James W., and Lin, Kuen Y., "Fracture of Boron/Aluminum Composites with Discontinuities", Journal of Comosite Materials, Vol. 11, 1977, pp. 405-421.

16. Mar, J.W., and Lin, K.Y., "Fracture Mechanics Correlation for Tensile Failure of Filamentary Composites with Holes, Journal of Aircraft, Vol. 14, 1977, pp. 703-714.

17. Fenner D.N., "Stress Singularities in Composite Materials with an Arbitrarily Oriented Crack Meeting an Interface", International Journal of Fracture, Vol. 12, 1975, pp. 705-721.

18. Mar, J.W., and Lagace, P.A., "Tensile Fracture of Graphite/Epoxy Laminates with Holes", Advances in Composite Materials, Proceedings of the 3rd International Conference on Composite Materials, Paris, France, 1980, pp. 130-145.

19. Lin, Kuen Y., "Fracture of Filamentary Composite Materials", M.I.T. Department of Aeronautics and Astronautics, Ph.D. Thesis, February, 1977.

20. Hoehn, George, "Fracture of Graphite/Epoxy Laminates with Slits", TELAC Report 81-13, September, 1981.

21. Brewer, John C., "Tensile Fracture of Graphite/Epoxy with Angled Slits", TELAC Report 82-16, December, 1982.

22. Graves, Michael J., "The Catastrophic Failure of Pressurized Graphite/Epoxy Cylinders", M.I.T. Department of Aeronautics and Astronautics, Ph.D. Thesis, September, 1982.

23. Fanucci, Jerome P., and Mar, James W., "Fatigue Damage Detection in Thin Composite Laminates using Out-of-Plane Moire Interferometry", Journal of Composite Materials, Vol. 16, March, 1982, pp. 94-102.

24. Tsai, Stephen W., and Hahn, H. Thomas, Introduction to Composite Materials, Technomic Publishing Co., Inc, 1980.

25. Dunmire, Christopher, J., "Development of a Compression Testing Method for Graphite/Epoxy Coupons", TELAC Report 82-17, October, 1982.

26. Mar, James W., "Fracture, Longevity, and Damage Tolerance of Graphite/Epoxy Filamentary Composite Material", presented at the AIAA/ASME/ASCE/AHS Structures, Structural Dynamics, and Materials Conference, Lake Tahoe, Nevada, May, 1983.

27. Garcia, Jose I., "Experimental Investigation of Splitting in Unidirectional Graphite/Epoxy Material", TELAC Report 79-5, May, 1979.

28. Lesieutre, George A., "Crack Growth in Four-Ply Unidirectional Graphite/Epoxy Laminates under Cyclic Loading", TELAC Report 80-6, May, 1980.

29. Mar, James W., "Fracture and Fatigue of Bi-Materials", AFWAL-TR-81-4077, January, 1982.

30. Daken, M. Hatem M.H., "Splitting Initiation and Propagation in Flawed Unidirectional Graphite/Epoxy Composite under Tension-Tension Cyclic Loading", M.I.T. Department of Aeronautics and Astronautics, S.M. Thesis, February, 1983.

31. Mar, James W., and Lin, K. Y., "Characterization of Splitting Process in Graphite/Epoxy Composites", Journal of Composite Materials, Vol. 13, October, 1979, pp. 278-287.

32. Graves, Michael J., "The Effects of Compression-Compression Fatigue on Balanced Graphite/Epoxy Laminates with Holes", M.I.T. Department of Aeronautics and Astronautics, February, 1979.

33. Fanucci, Jerome P., "Damage Initiation and Propagation during Compressive Fatigue of Flawed Graphite/Epoxy Composites", M.I.T. Department of Aeronautics and Astronautics, Ph.D. Thesis, June, 1981.

34. Selby III, Harry P., "Aeroelastic Flutter and Divergence of Rectangular Wings with Bending-Torsion Coupling", M.I.T. Department of Aeronautics and Astronautics, S.M. Thesis, February, 1982.

35. Hollowell, S.J., and Dugundji, J., "Aeroelastic Flutter and Divergence of Stiffness Coupled, Graphite/Epoxy Cantilevered Plates, Proceedings of the 23rd AIAA/ASME/ASCE/AHS Structures, Structural Dynamics, and Materials Conference, New Orleans, Louisiana, May, 1982.

36. Lansberger, Brian J., "Aeroelastic Properties of Straight and Forward Swept Graphite/Epoxy Wings", M.I.T. Department of Aeronautics and Astronautics, S.M. Thesis, February, 1983.

APPENDIX A

LIST OF REPORTS GENERATED UNDER CONTRACT

The following is a list of the reports which have been generated under this contract effort. Most of these were referenced in the main body of the report and are contained in the Reference section. However they are again listed here for convenience.

TELAC-81-13 Hoehn, George, "Fracture of Graphite/Epoxy Laminates with Slits", September, 1981.

TELAC-82-3 Selby III, Harry P., "Aeroelastic Flutter and Divergence of Rectangular Wings with Bending-Torsion Coupling", February, 1982. (S.M. Thesis)

TELAC-82-4 Lagace, Paul A., "Static Tensile Fracture of Graphite/Epoxy", April, 1982. (Ph.D. Thesis)

TELAC-82-5a Chang, Ya-Pei A., "Determination of the Mechanical Properties of Graphite/Epoxy Fabric Prepreg Composite", May, 1982.

TELAC-82-5b deLuis, Javier, "Determination of the Mechanical Properties of Graphite/Epoxy Fabric Prepreg Composite", May, 1982.

TELAC-82-6a Dodson, Carroll L., "Effects of Loading into the Nonlinear Region of Graphite/Epoxy Laminates", May, 1982.

TELAC-82-6b Fujii, Eric, "Effects of Loading into the Nonlinear Region of Graphite/Epoxy Laminates", May, 1982.

TELAC-82-7a Chin, David A., "Nonlinear Stress-Strain Behavior in Graphite/Epoxy Laminates", May, 1982.

TELAC-82-7b Trop, David, "Nonlinear Stress-Strain Behavior in Graphite/Epoxy Laminates", May, 1982.

TELAC-82-10 Graves, Michael J., "The Catastrophic Failure of Pressurized Graphite/Epoxy Cylinders", September, 1982. (Ph.D. Thesis)

TELAC-82-15 Brewer, John C., "Comparison of Tapered Graphite/Epoxy Coupons with Standard TELAC Graphite/Epoxy Coupons", April, 1982.

TELAC-82-16 Brewer, John C., "Tensile Fracture of Graphite/Epoxy with Angled Slits", December, 1982.

TELAC-82-17 Dunmire, Christopher J., "Development of a Compression Testing Method for Graphite/Epoxy Coupons", October, 1982.

TELAC-82-18 Trop, David, and Dunnmire, Christopher J., "Graphite/Epoxy Composite Material in Compression: Fatigue Damage Patterns versus Testing Method; And a Comparison of Fracture Strength for [+-45/0]s and [+-30/0]s Coupons with 1/2 inch Diameter Holes", December, 1982.

TELAC-83-4 Lansberger, Brian J., "Aeroelastic Properties of Straight and Forward Swept Graphite/Epoxy Wings", February, 1983. (S.M. Thesis)

TELAC-83-6 Hatem, M. Hatem M.H., "Splitting Initiation and Propagation in Flawed Unidirectional Graphite/Epoxy Composites under Tension-Tension Cyclic Loading", February, 1983. (S.M. Thesis)

In addition, the following articles and/or presentations were made on work supported under this contract:

Fanucci, Jerome P., and Mar, James W., "Fatigue Damage Detection in Thin Composite Laminates using Out-of-Plane Moire Interferometry", Journal of Composite Materials, Vol. 16, March, 1982, pp. 94-102.

Hollowell, S.J., and Dugundji, J., "Aeroelastic Flutter and Divergence of Stiffness Coupled, Graphite/Epoxy Cantilevered Plates", Proceedings of the 23rd AIAA/ASME/ASCE/AHS Structures, Structural Dynamics, and Materials Conference, New Orleans, Louisiana, May, 1982.

Lagace, Paul A., "Delamination Fracture under Tensile Loading", presented at Sixth Conference on Fibrous Composites in Structural Design, New Orleans, Louisiana, January, 1983.

APPENDIX B

PERSONNEL

The following personnel have been associated with the present program during the past year:

Staff

Prof. James Mar (Laboratory Head)
Asst. Prof. Edward Crawley
Prof. John Dugundji
Asst. Prof. Paul Lagace
Prof. Theodore Pian
Mr. Albert Supple

Graduate Students

Hatem Daken (Egyptian Government)
Marc Gronet
Capt. B.J. Lansberger (USAF)
Stephen Nolet
Harry Selby (Lockheed Georgia)
Anthony Vizzini

Undergraduate Students
(part time, varying lengths of time)

Karen Archard	Ya-Pei Chang	Carroll Dodson
Keith Ashelin	David Chin	Chris Dunmire
John Brewer	John Chisholm	Eric Fujii
Jim Butler	Robert Dare	George Hoehn
Scott Causbie	Javier deLuis	David Trop

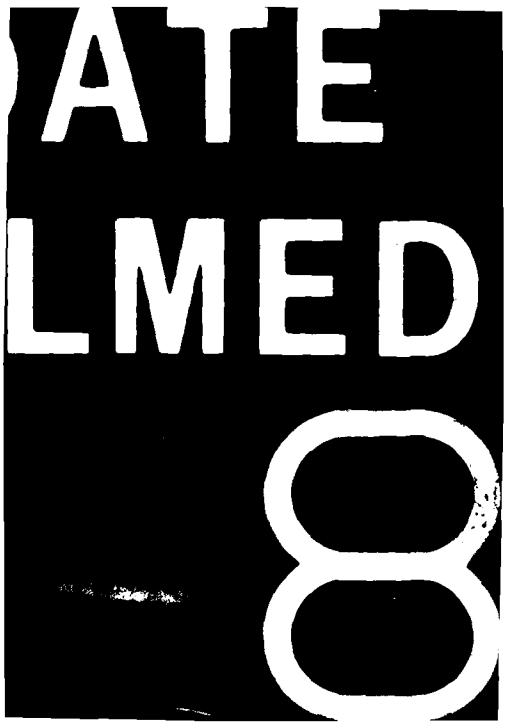
ATE
LMED
8